ABSTRACT

Title of Document: CONSTRAINTS ON THE DEPOSITIONAL AGES OF LESSER HIMALAYAN ROCKS IN CENTRAL NEPAL AND THEIR STRUCTURAL IMPLICATIONS

Katherine Burgy, Master of Science, 2009

Directed by: Dr. Aaron Martin, Department of Geology

The lack of good exposures and paucity of datable horizons in central Nepal has hindered the ability of geologists to piece together a relatively cohesive and straightforward stratigraphic succession within the Lesser Himalaya. U-Pb isotopic analyses of detrital zircons from the Modi Khola valley indicates maximum depositional ages of ~1875 Ma for the Kuncha Formation, ~1800 Ma for the Fagfog Formation, and ~ 1780 Ma for the Kushma Formation. The intrusive 1831 ± 17 Ma Ulleri augen gneiss provides a minimum depositional age bound for the Kuncha. Combined, these data suggest the Kuncha Formation is the oldest member of the Lesser Himalayan series in central Nepal. Additionally, $\delta^{13}C$ data suggest the Malekhu Formation of the Lakharpata Group was deposited before ca. 1250 Ma. A field mapping comparison based on the redefined stratigraphy indicates the Ramgarh thrust is located >10 km farther south than previously mapped, potentially reducing regional shortening estimates.

CONSTRAINTS ON THE DEPOSITIONAL AGES OF LESSER HIMALAYAN ROCKS IN CENTRAL NEPAL AND THEIR STRUCTURAL IMPLICATIONS

By

Katherine Burgy

Thesis submitted to the Faculty of the Graduate School of the
University of Maryland, College Park, in partial fulfillment
of the requirements for the degree of
Master of Science
2009

Advisory Committee:

Assistant Professor Aaron Martin, Chair

Associate Professor Alan J. Kaufman

Professor Roberta Rudnick

Acknowledgements

First and foremost I would like to thank my advisor, Aaron Martin, for having faith that a person who had never traveled outside of the U.S. could handle five weeks in central Nepal and come away with good data. Also thank you for the many thoughtful discussions and revisions of this work. I hope you consider your first foray into advising a Master's student successful. Thanks also go to my committee members, Jay Kaufman and Roberta Rudnick, for their invaluable insights and suggestions.

Namaste to our colleagues and friends in Nepal. To Tank and Shialashree Ojha who made our trip as smooth as possible, thank you! Thanks also to Dilbadur for guiding me on my first "solo" mapping days, and for understanding that sometimes a girl just needs tea and cookies. You made Nepal a warm and welcoming place for me.

For data analysis I am indebted to the people at the University of Arizona LaserChron Center, especially Victor Valencia and George Gehrels. At Maryland, thank you to Brendan Williams, Craig Hebert, and Phil Piccoli.

My fellow graduate students also deserve recognition for taking this journey with me and for reminding me of important deadlines. Special thanks to Rachel Potter, Lisa Schleicher-Walsh, and Kate Scheiderich.

Thank you to my wonderful family for your love and for taking care of the critters while I was away. Thank you to Jess Hayden for "best friend" support always. Lastly, thank you to Nirmal Mehta for extraordinary technical and moral support. Without you I would still be working on the same Illustrator file. You should have been a geology major. Thank you all.

Table of Contents

List of Tables

List of Figures

Chapter 1 – Introduction to the Himalaya

1.1 Orogenesis

"Mountains are the beginning and end of all scenery" – John Ruskin, art critic and author

To geologists mountains are more than just majestic scenery; they represent a remarkable result of plate tectonics. Orogenesis, or mountain building, offers insight into the workings of the Earth; including past and present plate motions, crustal strength and deformation, and related magmatism and metamorphism. In addition, mountains influence regional and global climate by shifting air circulation patterns, leading to rain shadows and orographic effects. Mountains isolate plant and animal populations, leading to the development of new species and act as barriers to migration. Numerous human civilizations have also benefitted from the strategic advantages conferred by occupation of the topographic high ground.

1.2 The Himalaya

The word Himalaya comes from the Sanskrit *hima* or "snow" and *ālaya* or "abode", in other words "place where there is snow". Bounded to the north by the Tibetan Plateau and to the south by the Indian subcontinent, the range extends from ~ 76° to ~91°E longitude, and is home to eight of the ten highest peaks in the world including Mt. Everest and K2 (Fig. 1.1; Hodges, 2000). Additionally, the range partially or entirely encompasses the countries of Nepal, Tibet, China, India, Pakistan, and Bhutan.

The Himalaya are considered the "type" example of a continent-continent collision. Beginning around 55-50 Ma ago and continuing to the present day, the collision of the Indian and Eurasian plates has accommodated a minimum of 2500 km of convergence (Achache et al., 1984; Patriat and Achache, 1984; Besse et al., 1984; Besse and Courtillot, 1988; Rowley, 1996; Guillot et al., 2003; DeCelles et al., 2004; Leech et al., 2005; Leech et al., 2007). Of this, approximately 800-1200 km are thought to be accommodated by the Himalayan fold and thrust belt (Lyon-Caen and Molnar, 1985; Lillie et al., 1987; Srivastava and Mitra, 1994; Bilham et al., 1997; Powers et al., 1998; Larson et al., 1999; Lavé and

Avouac, 2000; DeCelles et al., 2002). The fold and thrust belt includes mostly south-vergent thrusts and associated folds, which consist of lithified sediments accumulated on the northern margin of India prior to collision (DeCelles et al., 2001).

Regional balanced cross sections across the fold and thrust belt reveal minimum shortening estimates, however they do not include the shortening contributions of penetrative strain or small scale folds and faults, which would increase total shortening estimates considerably (DeCelles et al., 2002). The western portion of the Himalaya, including Pakistan, western Nepal, and northwestern India, appear to have accommodated the most shortening, on the order of 353-743 km from the South Tibetan Detachment System (STDS) to the Main Frontal thrust (MFT) (Coward and Butler, 1985; Srivastava and Mitra, 1994; DeCelles et al., 1998; DeCelles et al., 2001; DeCelles et al., 2002; Robinson et al., 2006). In central Nepal, Schelling (1992) estimates 210-280 km of shortening between the STDS and the Main Frontal thrust. In the eastern portion of the Himalaya, estimates of shortening range from 185-245 km between the STDS and MFT, and up to 323 km from the Indus-Yalu suture to the MFT (Schelling and Arita, 1991; Hauck et al., 1998).

Figure 1.1– The Himalaya from space. Image from NASA World Wind.

In Nepal, where the focus of this research is located, the fold and thrust belt is divided into four tectonostratigraphic units from south to north, the Subhimalayan (SH), Lesser Himalayan (LH), Greater Himalayan (GH), and Tibetan Himalayan (TH) zones, all of which are bounded by faults (Heim and Gansser, 1939). These tectonostratigraphic, or geologic, units should not be confused with the physiographic provinces of the Himalaya by the same name (Fig. 1.2). This paper will refer only to tectonostratigraphic divisions. The fold and thrust belt region has received a great deal of attention because it can potentially answer many of the questions geologists have about the Himalaya and mountain building in general.

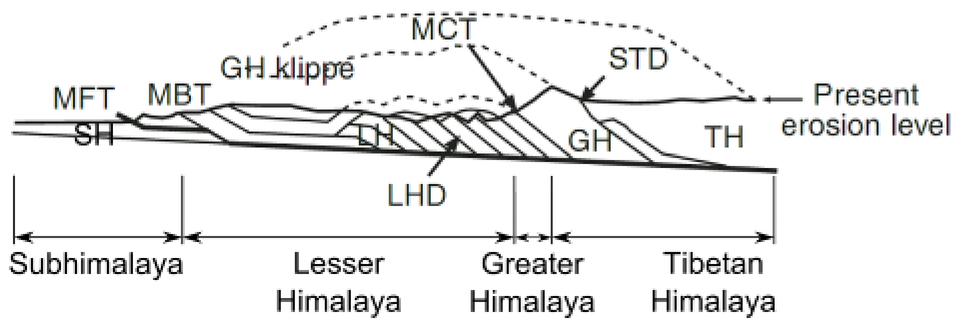

Figure 1.2 – Geologic cross section of the Himalaya with the tectonostratigraphic units marked on the cross section and physiographic provinces delineated below. TH – Tibetan Himalaya, GH – Greater Himalaya, LH- Lesser Himalaya, LHD – Lesser Himalayan Duplex, SH – Subhimalaya, STD – South Tibetan Detachment, MCT – Main Central thrust, MBT – Main Boundary thrust, MFT – Main Frontal thrust. Modified from Robinson et al., 2006.

1.3 Fold and Thrust Belt Formation

"It is a truism in structural geology that broad, thin-skinned fold and thrust belts are easy to find, but difficult to explain mechanically" – William Chapple, Geologist

Early workers recognized fold and thrust belts as areas of extensive crustal shortening and their geometries and kinematics became the focus of extensive research (Armstrong and Oriel, 1965; Bally et al., 1966; Dahlstrom, 1970; Elliott 1976 a, b; Chapple, 1978; Bombolakis, 1986; Butler, 1987). Chapple was one of the first to enumerate several defining characteristics of fold and thrust belts as we know them today. He described a wedge shaped region of deformation, thicker at the back (hinterland) and thinner at the toe (foreland), which was bounded at its base by a relatively weak geologic layer. He noted that shortening and thickening occurred throughout the wedge, primarily towards the back-end of the wedge. Chapple posited that material within the wedge maintained cohesion and that displacement on the thrust faults was relayed to successive, adjacent faults. The driving force responsible for the development of the fold and thrust belt was a "compressive flow" or "push from behind", as opposed to gravity driven "gliding" or other previously proposed mechanisms (Elliott 1976 a,b).

Additional work revealed other common characteristics of fold and thrust belts including a positive, linear relationship between fault displacement and fault length, and foreland propagation of in-sequence thrusting, although there are cases of out-of-sequence thrusting as well (Armstrong and Oriel, 1965; Bally et al., 1966; Elliott 1976 a, b; Goff and Wiltschko, 1992; Pearson and DeCelles, 2005; Robinson et al., 2006; Robinson, 2008). A regular decrease in spacing between thrust ramps toward the foreland has also been noted (Bombolakis, 1986; Goff and Wiltschko, 1992; Panian and Wiltschko, 2007).

To explain these observations, the critical taper theory was proposed by Davis et al. in 1983, and has subsequently been elaborated upon by numerous workers (Dahlen et al., 1984; Goff and Wiltschko, 1992; Makel and Walters, 1993; Horton, 1999; DeCelles and Mitra, 1995; Strayer, 2001; Bollinger et al., 2006). The theory accepts the basic geometry described by Chapple and explains the mechanics of wedge formation as analogous to a wedge of snow or dirt pushed along by a plow. At first, the material deforms internally until a wedge shape forms, and sliding begins along the base. At this point the wedge has attained a critical taper, where all points within the wedge are on the verge of failure under horizontal compression. As material is added or lost, or as internal factors such as pore fluid pressure change, the wedge geometry (α or β) responds through internal deformation or faulting to maintain its' critical state (Fig. 1.3; Davis et al., 1983; Horton et al., 1999).

How and where the first thrust fault in a thrust sheet forms is currently debated. Most modelers agree that maintenance of wedge geometry is likely the main controlling factor in thrust fault formation. However, a variety of factors can influence where the break occurs. Work by Goff and Wiltschko (1992) suggests that the weight of overlying thrust sheets stabilizes the footwall of the incipient thrust, i.e. that the length and mass of overlying thrust sheets have a direct effect on the location of the next thrust sheet. Therefore, rates of thrust fault emplacement and erosion might also contribute to variation in the spacing of thrust faults. It is easy to understand why the prediction of thrust sheet dimensions is difficult! Nevertheless, it is reasonable to assume there is some minimum thickness of a thrust sheet necessary for the rocks to remain cohesive during movement and to avoid complete erosion during the time it takes a thrust sheet to be emplaced.

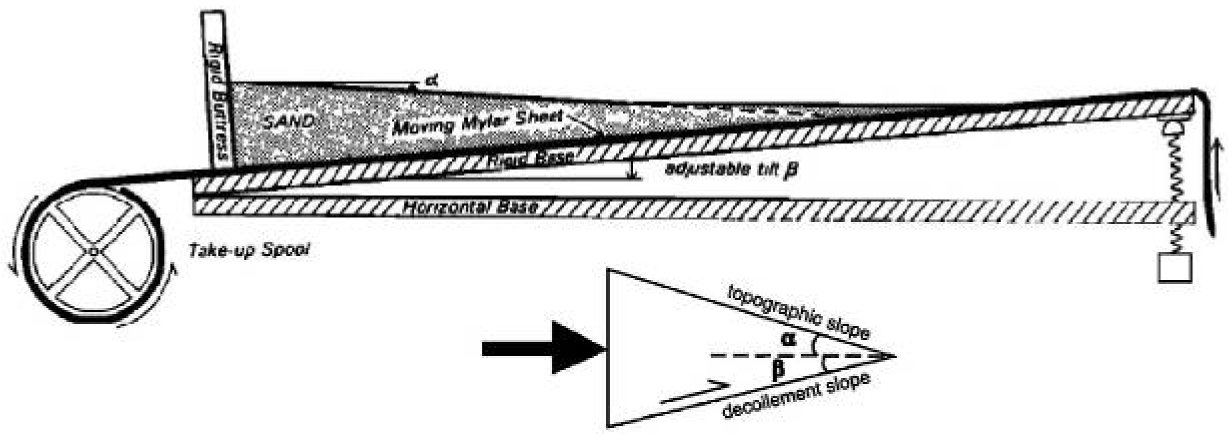

Figure 1.3 – Original model developed by Davis et al. (1983) that used sand and a moving mylar sheet to approximate wedge formation. Lower schematic shows an idealized critical taper (Horton, 1999).

1.4 Enduring Questions

By developing an extensive and cohesive understanding of the Himalayan fold and thrust belt, geologists can gain insight into the processes that shape the face of our entire planet. However, many questions remain incompletely answered, including: (1) How do mountain ranges fully accommodate shortening? Possible mechanisms include faulting, internal deformation, and extrusion of crust, but may likely be a combination of these and other mechanisms. (2) What is the order and timing of shortening events? Thrusting may occur in- or out- of- sequence. (3) How much shortening occurred and where? Regional shortening estimates vary and are dependent upon correct mapping of faults and geologic units. (4) Where are the major faults located, how much movement occurred on them, and are they still active? This information has ramifications for the area's geologic history.

In order to answer questions such as the ones listed above, fundamental information about the geology of the fold and thrust belt is needed. What are the ages of the geological units? How are the units related? The development of regional stratigraphy and subsequent field mapping provide the foundation of knowledge necessary to make interpretations of the larger "big picture" structures involved in mountain building. In this study, I examine Lesser Himalayan rocks in central Nepal to obtain depositional ages of the units. From these ages I evaluate the accuracy of the current stratigraphy and subsequently modify regional geologic maps, as necessary. This work relates to the broader questions about fold and thrust belts because the location of faults, hence the thicknesses of the overlying thrust sheets and the development of accurate cross- sections and regional shortening estimates, are dependent upon correct mapping based on accurate stratigraphy.

Of the two units that make up the Lesser Himalayan series, only the younger unit, the Tansen, is fossiliferous. The older Nawakot Unit lacks fossils that might indicate relative ages of its members, so other methods of dating are necessary. To this end, I use U-Pb isotopic analyses of detrital zircons sampled from several siliciclastic units to obtain maximum ages of deposition. These ages are further constrained by a cross cutting igneous unit of known age. I also use chemostratigraphic data (time series $\delta^{13}C$ variations), sampled from the stratigraphically highest carbonate within the Lesser Himalaya, to place a lower limit on deposition of the Lesser Himalayan sequence. The rearrangement of stratigraphy based on these analyses lead to a revision of current maps and fault placement, thus changing regional shortening estimates based on balanced cross-sections.

Chapter 2 – Geochemical Background of Isotopic Systems Utilized

2.1 Perspective

This work examines several geologic units from central Nepal whose lithologies range from clean quartzite and sandy phyllite to crystalline carbonate and calcareous shale. In order to constrain depositional ages of these units several methods were applied. A brief description of each isotopic system used in this research is covered below.

2.2 Carbon

The carbon cycle is a series of complex interactions between the biosphere, atmosphere, hydrosphere, and lithosphere. Of all the carbon available on Earth, 98.89 % is found in the form of carbon-12, while only 1.11% consists of the carbon-13 isotope. The ratio of the two isotopes in the Earth reflects global-scale oceanographic and climatic changes based upon isotopic fractionation (Prothero and Schawb, 2004).

Isotope fractionation includes equilibrium isotope effects, where the heavier isotope (in this case carbon-13) preferentially goes into the compound in which it is most strongly bound (Bigeleisen, 1965), and kinetic isotope effects, where the rate of a chemical reaction is sensitive to the atomic mass at a particular position of the reaction species (Hayes, 1983).

2.2.1 Delta Notation

Due to the fact that isotopic abundances may differ at or beyond the third significant figure, geologists have developed delta notation expressed in parts per mil or parts per thousand (‰), as the conventional way to communicate findings. Delta notation is given by the following equation (1):

$$\delta^{13}C = \frac{[(^{13}C/^{12}C)_{sample} - (^{13}C/^{12}C)_{standard})]}{(^{13}C/^{12}C)_{standard}} * 1000 \qquad (1)$$

The standard used for calibration has traditionally been the Pee Dee Belemnite (PDB). As there is no longer a supply of this material, alternative standards such as NBS-19 (this study) are used and then referenced to Vienna-PDB (V-PDB).

2.2.2 Carbon Cycling

While critical to life on the planet, the majority of carbon on the Earth's surface is actually sequestered in sedimentary rocks, namely carbonates and solid organic compounds (Fig. 2.1; Ripperdan, 2001). In ocean water carbon is largely present in the form of the bicarbonate ion (HCO_3^-). Carbonate minerals are formed by the combination of divalent cations, predominantly Ca^{2+}, with the carbonate ion (Hoefs, 2004):

$$Ca^{2+} + CO_3^{2-} = CaCO_3 \qquad (2)$$

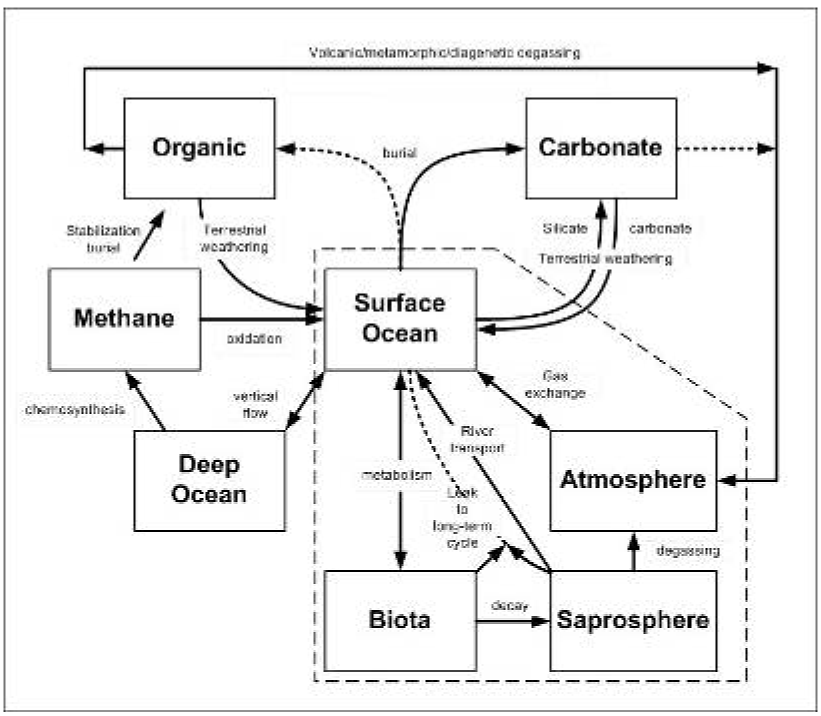

Figure 2.1 – Diagram of carbon cycling pathways. Modified from Ripperdan, 2001.

Short term cycling and fractionation of carbon isotopes is dominated by photosynthetic fractionation of CO_2, which preferentially incorporates ^{12}C into plant tissues (O'Leary, 1981; Farquhar et al., 1989). When photosynthesis occurs in the oceans, it may enrich the surrounding ocean water in ^{13}C. This kinetic isotope effect is the primary basis for the fractionation of carbon isotopes between the $C_{organic}$ (C_{org}) and $C_{carbonate}$ (C_{carb}) reservoirs (Kaufman and Knoll, 1995). The magnitude of fractionation between two compounds, A and B, can be described by a fractionation factor (α) in which:

$$\alpha_{A\text{-}B} = R_A/R_B \qquad (3)$$

where R is the ratio of numbers of any two isotopes in a compound A divided by the corresponding ratio in compound B (Hoefs, 2004, Kaufman, Pers. Comm.).

Long term cycling of carbon is based on the flux of carbon into the oceans from weathering and out gassing, and the corresponding outward flux through sedimentation and burial (Broeker, 1970; Hayes, 1983; Buick et al., 1995; Ripperdan, 2001). Most importantly, secular changes in the carbon isotope record reflect the relative proportions of C_{org} and C_{carb} being buried in marine sediments (Broeker, 1970; Hayes, 1983; Kaufman and Knoll, 1995; Veizer et al., 1999; Anbar and Knoll, 2002).

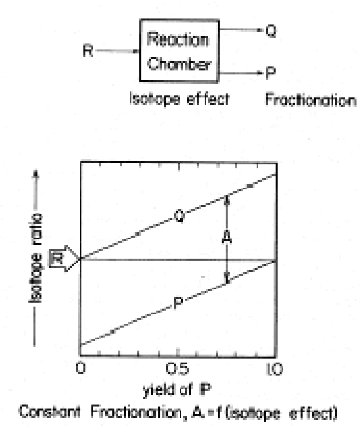

Figure 2.2 – Schematic of the open system ocean as a reactant chamber with input/reactant R, and outputs/ products Q and P, which in this diagram represent C_{carb} and C_{org} respectively. Bottom diagram demonstrates the isotopic fractionation (A) between Q, and P.

The open system behavior of the ocean can be described mathematically in the terms of carbon inputs and carbon outputs (Fig. 2.2; Hayes, 1983). If a steady state of inputs (reactant R in Fig. 2.2) and outputs (products Q and P in Fig. 2.2) is assumed, fractionation between outputs is controlled by the kinetic isotope effect:

$$R_{pe} = \alpha_{P/R} * R_{re} \tag{4}$$

$$R_{qe} = \alpha_{Q/R} * R_{re} \tag{5}$$

which when combined yield:

$$R_{pe}/R_{qe} = \alpha_{P/R} / \alpha_{Q/R} \tag{6}$$

where R_{pe} is the ratio of P at equilibrium, R_{qe} is the ratio of Q at equilibrium, $\alpha_{P/R}$ is the fractionation factor between P and R, $\alpha_{Q/R}$ is the fractionation factor between Q and R, and R_{re} is the ratio of reactant at equilibrium. Considering the law of conservation of mass:

$$n_iF_i = n_aF_a + n_bF_b \tag{7}$$

where n is the molar quantity of carbon in i, a, and b, and F is the fractional isotopic abundance or F = $[^{13}C/(^{13}C + ^{12}C)]$. Therefore:

$$F_i = f_aF_a + (1-f_a)F_b \tag{8}$$

where f_a is the fraction of input i that is going to product A (n_a/n_i), and ($1-f_a$) is equal to the fraction of input going to product B (n_b/n_i). Simultaneous solving of equations 6 and 8 yields:

$$\delta_p = \delta_r + (1-f_p)\varepsilon \tag{9}$$

and

$$\delta_q = \delta_r - f_p\varepsilon \tag{10}$$

where δ_r is the isotopic composition of carbon entering the ocean, δ_p is the isotopic composition of organic carbon, δ_q is the isotopic composition of carbonate, f_p is the fraction of organic carbon being buried in sediments, and $\varepsilon = [(\alpha_{P/R} / \alpha_{Q/R})-1)*10^3]$. The typical values of carbon entering and leaving the ocean are δ_r ~5.5‰ and ε ~25‰, respectively (Kaufman, Pers. Comm.). Ultimately, if burial of C_{org} increases, the long term carbon isotope record preserved in carbonates will record more positive values. If relatively less C_{org} is being buried in sediment, long term carbon isotope values of carbonates will be more negative.

Therefore, variation in the carbon isotope record is enhanced or attenuated by a variety of processes including: changes in biological productivity, changes in geologic preservation rates of organic carbon, atmospheric CO_2 sorption by weathering of continental materials, changes in CO_2 content in ocean water based on temperature changes, oceanic circulation, and volcanic out gassing (Ripperdan, 2001). Typical values of some carbon reservoirs can be seen in Figure 2.3.

Additional variations in the carbon record are caused by complicating factors such as: non-equilibrium processes at the depositional interface, preservational bias, local ^{13}C heterogeneities from organic matter, and post-depositional diagenesis, including the liberation of volatiles with increasing temperature and the infiltration of externally derived fluids (Valley, 1986; Kohn and Valley, 1994; Ripperdan, 2001).

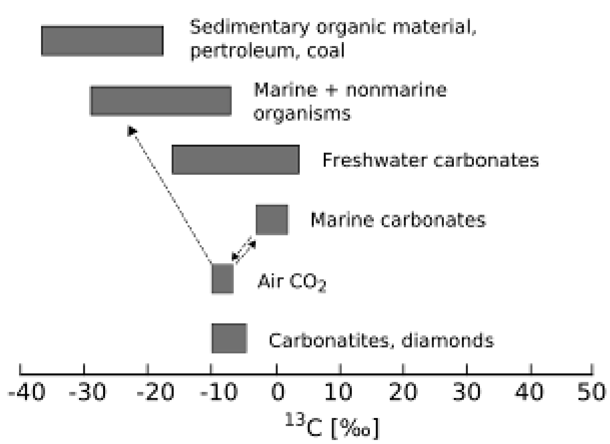

Figure 2.3 – Typical $\delta^{13}C$ values of some carbon reservoirs in ‰$_{V\text{-}PDB}$ (Hoefs, 2001).

Many researchers, working in sedimentary basins around the world, have developed a composite record of carbon isotopes through time. It appears that throughout Earth history, with one or two notable exceptions, variable and fluctuating carbon isotope values have been the norm. Though prior to 2.6 Ga the carbon isotope curve is essentially flat, workers note that significant positive and negative excursions similar to modern day values were seen (Schidlowski et al., 1983; Karhu and Holland, 1996; Lindsay and Brasier, 2002). From ~1.8 to 1.0 Ga another relatively quiescent interval in the carbon record occurs, with isotopic values typically near 0 ± 2‰ (Knoll et al. 1995, Buick et al. 1995; Kaufman, 1997; Des Marais, 1997). Towards the end of the Mesoproterozoic and the beginning of the Neoproterozoic, researchers observe a general trend of increasing fluctuations in carbon isotopes (Kah et al., 1999; Kumar et al., 2002), which gradually increase in amplitude up to 10‰ and greater, most often associated with widespread glaciations (Kaufman and Knoll, 1995; Kaufman et al., 2006; Kaufman et al., 2007; Tewari and Sial, 2007). The wildly swinging values of the Neoproterozoic eventually give way to more moderate fluctuations of the Phanerozoic (Zachos et al., 2001; Tewari and Sial, 2007). Several authors attribute the large fluctuations in the isotopic carbon record to tectonism and the formation or break up of supercontinents and a web of closely linked phenomena including carbon sequestration, rising atmospheric oxygen levels, and glaciations (Derry et al., 1992; Kaufman and Knoll, 1995; Berner, 2001; Ripperdan, 2001; Anbar and Knoll, 2002; Lindsay and Brasier, 2002; Kaufman et al., 2007).

2.3 Oxygen

Typically measured simultaneously with carbon isotopes and expressed in the same delta notation, oxygen isotopes provide important chemostratigraphic information to geologists. Changes in atmospheric oxygen are intimately related to the carbon cycle, including the biologic and tectonic processes of photosynthesis, sedimentation/burial of organics, weathering, and erosion (Berner et al., 2001). The formation of supercontinents leads to the burial of large amounts of organic carbon, which in turn leads to an increase in atmospheric O_2 levels (Lindsay and Brasier, 2002). Increases in atmospheric oxygen, in turn, affect the oxygen content of ocean waters.

In addition, Urey (1947) and Emiliani (1955) determined that oxygen isotopes (^{16}O= 99.756% and ^{18}O = 0.205%) fractionate based on temperature. Later work indicated that ice volume (glaciation) plays a larger role in changing the isotopic ratios of oxygen in seawater (Prothero and Schwab, 2004). In this system, ^{16}O rich water is preferentially evaporated, which is then precipitated from clouds. Due to global atmospheric circulation patterns, these clouds move out from the equator towards the poles. During glaciated periods, this water is captured on land and fails to return to the oceans. The oceans thus become progressively enriched in ^{18}O over time (Fig. 2.4; Alley and Cuffey, 2001). These findings make oxygen isotopes indicators of paleo-ice volume.

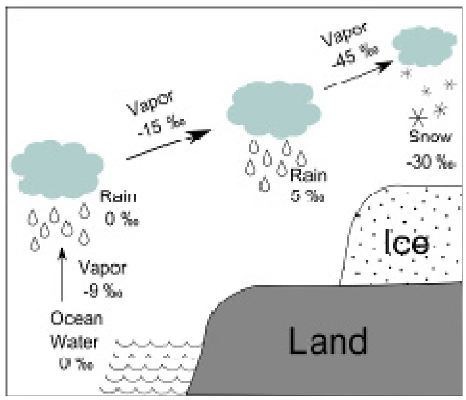

Figure 2.4 – Schematic of oxygen isotope fractionation during evaporation and precipitation. Values given are only illustrative. Modified from Alley and Cuffey, 2001.

A globally correlated curve of isotopic oxygen values throughout time has been developed. However, while $\delta^{13}C$ values have been shown to be relatively resistant to diagenetic changes, oxygen isotopes are much more easily altered (Hudson, 1977; Tucker, 1983; Burdett et al., 1990; Kaufman et al., 1991). This is likely due to the nature of most meteoric and metamorphic fluids, which have relatively little carbon to exchange with the rocks, but plenty of oxygen. The oxygen atoms are supplied from the fluid. Work by Baumgartner and Valley (2003) reveal that as metamorphism increases, the $\delta^{18}O$ values of carbonates decrease due to a variety of volatization reactions. Similarly, Alley and Cuffey (2003) found that most meteoric fluids are relatively depleted in ^{18}O, which would in turn result in lower measured $\delta^{18}O$ values. Furthermore, Jacobsen and Kaufman (1999) demonstrate that a much larger (factor of 10 or greater) water to rock ratio is necessary in order to reset ^{13}C values versus ^{18}O values (Fig. 2.5). Typical values of some oxygen reservoirs are seen in Fig. 2.6.

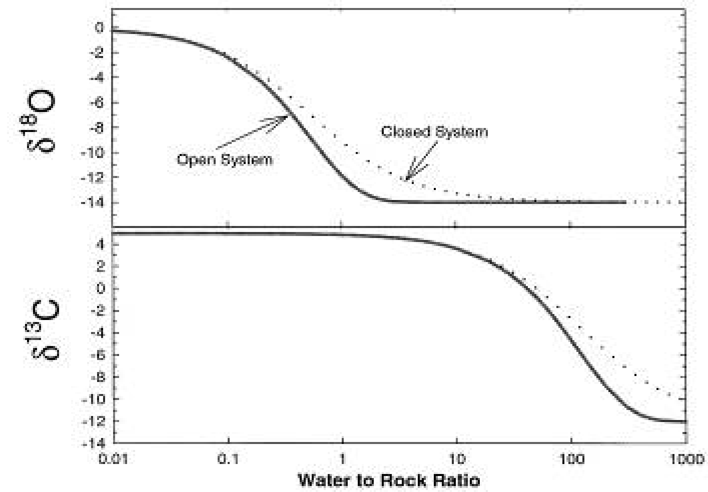

Figure 2.5 – $\delta^{18}O$ and $\delta^{13}C$ values with increasing water to rock ratio for both closed and open systems. Modified from Jacobsen and Kaufman, 1999.

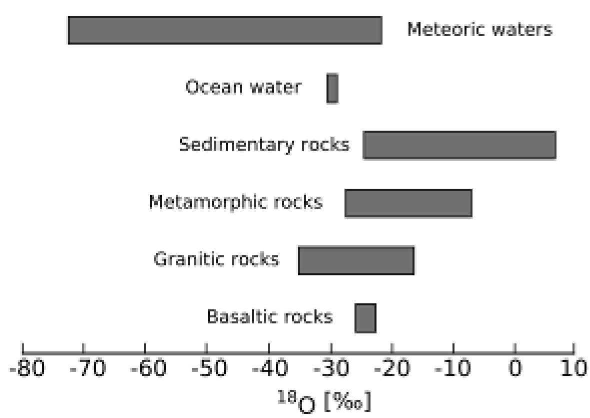

Figure 2.6 – Typical $\delta^{18}O$ values of some oxygen reservoirs in ‰$_{V\text{-}PDB}$ (Hoefs, 2001).

2. 4 Uranium-Lead

The uranium-thorium-lead system is one of the more complicated systems in radiogenic isotopes. The system includes three radiogenic parent isotopes which decay to three different daughter products, as well as emit alpha (α or ^{4}He), beta (β^-), and antineutrino ($\bar{\nu}$) particles (Fiorentini et al., 2007). For U-Pb dating, the ^{238}U and ^{235}U pathways are used:

$$^{238}U = 8\ ^4He + 6\beta^- + 6\bar{\nu} + {}^{206}Pb \qquad (11)$$

$$^{235}U = 7\ ^4He + 4\beta^- + 4\bar{\nu} + {}^{207}Pb \qquad (12)$$

The system also has one stable isotope of lead, ^{204}Pb. This isotope is used as the denominator in the decay equations written below as (Hole, 1998):

$$^{206}Pb/^{204}Pb = {}^{206}Pb/^{204}Pb_i + {}^{238}U/^{204}Pb \ * (e^{\lambda 1t} - 1) \qquad (13)$$

$$^{207}Pb/^{204}Pb = {}^{207}Pb/^{204}Pb_i + {}^{235}U/^{204}Pb \ * (e^{\lambda 2t} - 1) \qquad (14)$$

where ^{206}Pb/^{204}Pb and ^{207}Pb/^{204}Pb are the isotope ratios at the present, i denotes the initial lead isotope ratio at the time of sample formation, ^{238}U/^{204}Pb and ^{235}U/^{204}Pb are the isotope ratios at the present time, λ1 and λ2 are decay constants, and t is the time elapsed since the closure temperature of the mineral was reached (Hole, 1998). The decay constants used are:

$$\lambda 1 = 1.551 * 10^{-10} \qquad \text{half life} = 4.468 \text{ Ga} \qquad (15)$$

$$\lambda 2 = 9.848 * 10^{-10} \qquad \text{half life} = 704 \text{ Ma} \qquad (16)$$

These independent decay systems provide two independent geochronometers, which should provide two independent ages for a given sample. Ideally, these two ages coincide, which is termed concordant. If you rearrange equations 5 and 6 to:

$$^{206}Pb^*/^{238}U = e^{\lambda 1t} - 1 \qquad (17)$$

$$^{207}Pb^*/^{235}U = e^{\lambda 2t} - 1 \qquad (18)$$

where the * denotes the amount of radiogenic lead that has been produced by the sample, for a specified value of t, the amount of radiogenic lead of a sample can be calculated. If plotted on a ^{207}Pb*/^{235}U versus ^{206}Pb*/^{238}U graph, this would produce a curve known as the concordia (Fig. 2.7). However, because the elements are radioactive, crystal damage to the zircon containing the U and Pb is not uncommon.

Radiation damage can allow lead to be lost from the mineral, as the zircon crystal lattice preferentially incorporates uranium and excludes lead. Lead loss by diffusion during metamorphism or incorporation into igneous rocks can result in different ages for the ^{238}U and ^{235}U systems, which is called discordance (Lee et al., 1997). Several studies have also shown re-crystallization of zircons during metamorphism can lead to redistribution of Pb within the mineral, possibly to zones of lower uranium concentration (Mattinson et al., 1996; Hawkins and Bowring, 1997; Mezger and Krogstad, 1997; Pidgeon and Wilde, 1998; Carson et al., 2002a, b; Romer, 2003). When re-crystallized zones of high Pb are sampled, they plot above the concordia and are said to be reverse discordant.

Zircon ($ZrSiO_4$) is one the most common minerals dated using the U-Pb system. Zircon is a stable, tetragonal mineral at the Earth's surface. Its crystal lattice accepts uranium but excludes lead, and it has a closure temperature of ~1,000°C (Dahl, 1997; Lee et al., 1997; Hole, 1998; Cherniak and Watson, 2001; Finch and Hanchar, 2003; Schmitz and Bowring, 2003). Zircon is quite common in felsic and intermediate rocks, but its abundance is low in mafic and ultramafic rocks. In this study detrital zircons, those that are not primary but have been weathered from the original rocks in which they formed and reincorporated into younger sedimentary rocks, are dated using the U-Pb system to render populations of ages for a given formation. Based on the geologic principle of inclusions, the sedimentary unit containing detrital zircons of interest must be younger than the youngest zircon found within the rock. Therefore, the youngest robust ages of detrital zircons are interpreted to be the maximum depositional age of a given unit (Fedo et al., 2003).

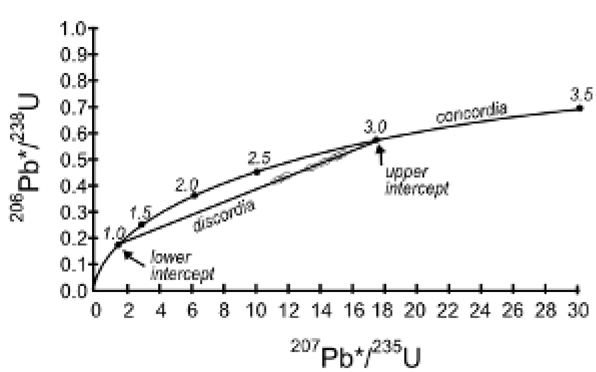

Figure 2.7 – Sample concordia plot (Hole, 1998).

Chapter 3 – Lesser Himalayan Rocks

3.1 Introduction

The Himalaya has been a natural focal point in the study of continent-continent collisional orogenies. Numerous theories and models have been developed to elucidate the processes responsible for the ongoing uplift and thickening of crust in the world's largest mountain range. While grand in scope, explanations ranging from the classic wedge shaped, forward-propagating thrust systems (Davis et al., 1983; DeCelles et al., 2001; Robinson et al., 2006; Kohn, 2008) to more avant-garde theories of crustal extrusion (Beaumont et al., 2001; Jamieson et al., 2004) are undeniably dependent upon accurate geometric and kinematic information to make correct predictions. Conversely, geometric and kinematic information gathered act as tests of the theoretical models.

The most basic and perhaps, therefore, the most important step towards creating these models is the development of an understanding of regional stratigraphy. In the Lesser Himalayan series of central Nepal (Fig. 3.1), the rocks have few fossils and are difficult to date and correlate regionally (DeCelles et al., 2001). Workers have thus conceptualized a variety of stratigraphic columns in order to evaluate field relations (Heim and Gansser, 1939; Pêcher, 1978; Hodges et al., 1996; Upreti, 1996; DeCelles et al., 2001; Martin et al., 2005; Pearson and DeCelles, 2005; Robinson et al., 2006). Through the use of U-Pb isotopic analyses of detrital zircons and time series $\delta^{13}C$ variations, this study aims to constrain depositional ages for several units in the Lesser Himalayan sequence, and as a result, will inform the regional stratigraphic succession and structural organization.

3.2 Geologic Setting

Although the Himalaya offers a spectacular opportunity to study the processes of mountain building, it also presents great challenges. Steep topography, abundant vegetation, and a paucity of datable horizons throughout much of the region are several obstacles to the identification and correlation of stratigraphic units across the range. This is evidenced by the multitude of monikers for individual formations and the proliferation of stratigraphic columns for the region that are not in agreement. Most problematic are the lack of definitive ages and relationships between units, which necessarily makes it difficult to establish links between units of eastern and central Nepal with that of the better exposed and documented units in western Nepal, and along the rest of the Himalayan arc (DeCelles et al., 2001; Robinson et al., 2006).

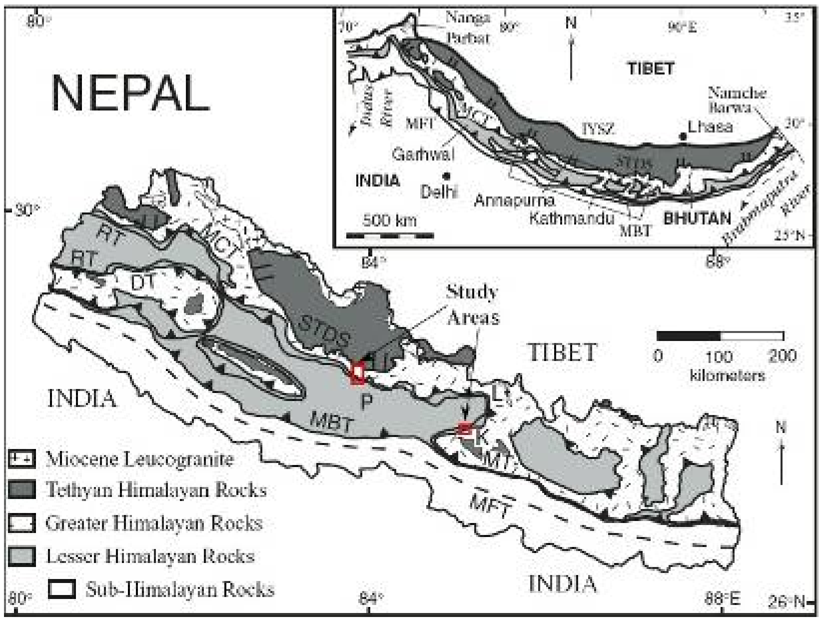

Figure 3.1 –Geologic map of Nepal with study areas outlined in red (Martin et al., 2005). K – Kathmandu, P- Pokhara, L- Langtang, IYSZ – Indus Yarling Suture Zone, STDS – South Tibetan Detachment System, MCT- Main Central thrust, RT – Ramgarh thrust, MT- Mahabarat thrust, DT – Dadeldhura thrust, MBT – Main Boundary thrust, MFT – Main Frontal thrust

The four main tectonostratigraphic units that constitute the Himalaya are, from south to north, the Subhimalayan (SH), Lesser Himalayan (LH), Greater Himalayan (GH), and Tibetan Himalayan (TH) zones, all of which are divided by faults (Fig. 3.1; Heim and Gansser, 1939). This work focuses solely on the Lesser Himalayan rocks, using the stratigraphic scheme of Upreti (Fig. 3.2a, b; 1996) as a basis for mapping.

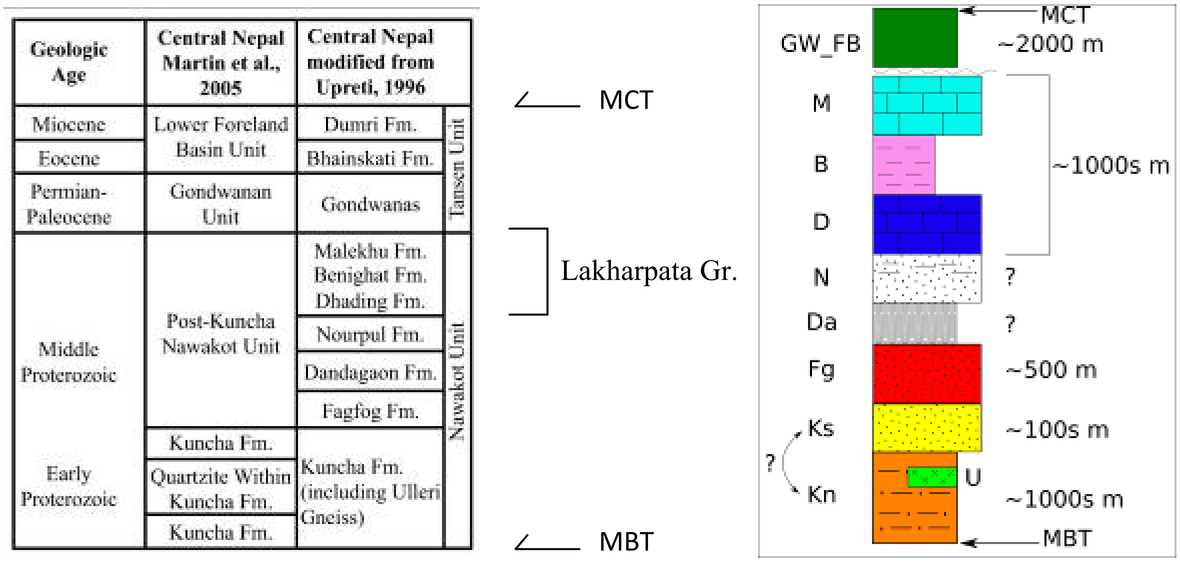

Figure 3.2a, b – a) Proposed stratigraphy of Lesser Himalayan rocks by (r) Martin et al. (2005) and (l) Upreti (1996). b) Schematic of stratigraphy used in this study, with approximate thicknesses labeled. Symbols (Kn) Kuncha Formation, (Ks) Kushma Formation, (Fg) Fagfog Formation, (Da) Dandagon Formation, (N) Norpul Formation, (D) Dhading Formation, (B) Benighat Formation, (M) Malekhu Formation, (GW_FB) Gondwana and Foreland Basin units, (MBT) Main Boundary thrust, (MCT) Main Central thrust. The Dandagon and Norpul formations are not recognized in the Modi Khola.

The Lesser Himalayan series is structurally bounded below by the Main Boundary thrust (MBT) and above by the Main Central thrust (MCT) (DeCelles et al., 2001). While there are several faults associated with the Lesser Himalayan series with displacements on the order of tens of kilometers, only the Main Central thrust and the Ramgarh thrust (RT) are considered in this study. The Ramgarh thrust is located within the Lesser Himalayan series, generally placing the oldest Proterozoic rocks against younger LH rocks or Miocene foreland basin deposits (Pearson and DeCelles, 2005). The MCT and RT are thought to accommodate over 140 km and 120 km of slip, respectively, making them the largest factors in regional shortening estimates.

Upreti (1996) designates the basal member of the Nawakot unit of the Lesser Himalayan sequence in central Nepal the Kuncha Formation. However, the base of this formation has not been described or located within Nepal. Largely composed of grey-green phyllites and phyllitic quartzites, the Kuncha Formation extends westward from central Nepal for over 300 km, and may be the lateral equivalent of the Ranimata Formation of western Nepal (DeCelles et al., 2001; Pearson and DeCelles, 2005). The Kuncha Formation has a thickness of several thousand meters and is intruded by the Ulleri augen gneiss, a granitic intrusion containing zircons that are 1831±17 Ma, providing a minimum age constraint for the formation (DeCelles et al., 2000). Not recognized as a separate unit by Upreti in central Nepal, the Kushma Formation is a several hundred meter thick unit of white to grey, fine to very fine grained, well sorted quartzite (DeCelles et al., 2001). In western Nepal, the Kushma Formation is stratigraphically below the Ranimata (Kuncha?) Formation (DeCelles et al., 2000; Pearson and DeCelles, 2005; Robinson et al., 2006) and the exact nature of the relationship between the Kuncha and Kushma formations in central Nepal, as well as the similarity in names, has caused considerable confusion. Martin et al. (Fig. 3.2; 2005) included the Kushma quartzite in the Kuncha Formation, however, a depositional age for either unit in central Nepal has not been determined and is a focus point of this research.

Moving upward in the section, the Fagfog Formation is an off-white to cream colored quartzite, with a large amount of ripples and trough cross bedding. In western Nepal it has a thickness of ~500 m and detrital zircons indicate an age younger than 1.68 Ga (DeCelles et al., 2000). The Dandagon Formation (or Galyang in western Nepal) is a green to grey phyllite that lacks any particularly useful diagnostic characteristics. This unit is stratigraphically below the much more distinctive Norpul (or Syangia) Formation. The Norpul Formation consists of pink/white quartzites and stunning reddish – purple phyllites and slates. Moving upwards again are the three members of the Lakharpata Group. In stratigraphic order; the ridge-forming, blue-gray Dhading dolomite, the black-gray Benighat slate, and the blue-gray Malekhu limestone. The lower portion of the Dhading Formation is described as a collection of gray slates and stromatolitic limestones, while the upper portion is characterized as more than 80% stromatolitic dolomite, interspersed with a few quartz sandstones and oolitic dolomites (Upreti, 1996). The Malekhu Formation consists of thinly bedded dolomites and shales, moving upward into thickly bedded dolomite, with the upper portion including intraformational pebble conglomerates and chert nodules as well. Stromatolite structures are not as pervasive in the Malekhu Formation.

Unconformably overlying the Lakharpata Group (and the Nawakot unit) is the Tansen Unit, consisting of the Gondwanan unit and the Bhainskati and Dumri formations. The Carboniferous to Paleocene Gondwanan sequence consists of sandstone, black shale, coal, lignite, and quartz pebble conglomerate (DeCelles et al., 2001). Bryozoa from the genera *Fenestrella, Polypora,* and *Acanthocladia* and spores of the genus *Vittatiana* have been used to ascertain relative ages of this sequence (Upreti, 1996). The Bhainskati and Dumri formations, which make up the Lower Foreland Basin Unit of Martin et al. (2005), consist of Eocene to Miocene black shale, fossiliferous (*Nummulites* and *Assilina*) limestone, and sandstone (Upreti, 1996).

The petrography and metamorphic history of the Lesser Himalayan rocks in central Nepal have been studied by numerous workers (Arita 1983; Upreti, 1996; Paudel and Arita, 2000; Catlos et al., 2001; Beyssac et al., 2004; Bollinger et al., 2004; Kohn, 2008). Work by Martin (2005) in the Modi Khola valley indicates a peak equilibrium assemblage of quartz + muscovite + biotite ± garnet ± plagioclase feldspar in the Lesser Himalayan series. Exceptions include one sample that lacks muscovite and one which has chlorite, but no biotite. Accessory minerals present in the rocks include allanite, apatite, hematite/magnetite, ilmenite, monazite, pyrite, thorianite, tourmaline, xenotime, and zircon. Therefore, the pelites in the hanging wall of the Ramgarh thrust in central Nepal are garnet zone.

Garnet-biotite and garnet-ilmenite cation exchange thermometry and GMBP barometry by Martin (2005) indicates that the Lesser Himalayan rocks between the Ramgarh thrust and the Main Central thrust underwent a peak temperature of 575°C and pressure at the peak temperature of 9 kbar (900 MPa). Work by Beyssac et al. (2004), using Raman spectroscopy of carbonaceous matter, yielded peak temperatures of 330°-540°C which agree within the uncertainty with the finding of Martin (2005). In the Marsyangdi river valley, several kilometers east of the Modi Khola valley, Catlos et al. (2001) found peak conditions of 450°-550°C and 6-8 kbar (600-800 MPa) using muscovite $^{40}Ar/^{39}Ar$ analyses and thermobarometric analyses of garnet bearing assemblages. Research thus suggests that the Lesser Himalayan rocks in central Nepal experienced metamorphism from greenschist to lower amphibolite facies.

The focus of this research is in the previously mapped Modi Khola valley in the Annapurna range of central Nepal (Fig. 3.1). The area has relatively good access and exposure of Lesser Himalayan rocks, and the structural top of the section has been well defined (Martin et al., 2005). A second study is located in the well-mapped Galcchi Bajar area of Trishuli River Valley, approximately 40 km west of Kathmandu, where the uppermost member (Malekhu Formation) of the Lakharpata Group is exposed (Fig. 3.3; Pearson and DeCelles, 2005). The lower carbonate member of the Lakharpata Group, the Dhading Formation, is poorly exposed in both areas and was thus not sampled.

With the aim of resolving some of the aforementioned stratigraphic ambiguities, dating of detrital zircons in quartzites from the Modi Khola valley and $\delta^{13}C$ stratigraphy of the Malekhu Formation in Galcchi Bajar are used to constrain the depositional ages of the units of the Lesser Himalayan sequence and subsequently the position of the Ramgarh thrust and other structures. As such, the three hypotheses that guide this research are as follows:

1) In the Lesser Himalayan rocks of the Modi Khola, the Kushma quartzite is older than the Kuncha Formation.
2) In the Lesser Himalayan rocks of the Modi Khola, the quartzite stratigraphically below the carbonates of the Lakharpata Group is the Fagfog quartzite.
3) The Malekhu Formation in the Lakharpata Group north of Galcchi Bajar was likely deposited before ~1250 Ma.

3.3 Methods

3.3.1 Field Mapping

Field mapping and sampling in the Modi Khola valley was conducted during May and June 2007. Carbonate samples were also collected in 2007 from the Trishuli River valley north of the town of Galcchi Bajar (Fig. 3.3). Detrital zircon samples were collected from type localities in central Nepal by Dr. Martin during the 2006 field season (Fig. 3.4). All field stations were marked using the Global Positioning System and recorded. Thin section samples were oriented using a Brunton compass. Samples were then stored individually to prevent cross-contamination.

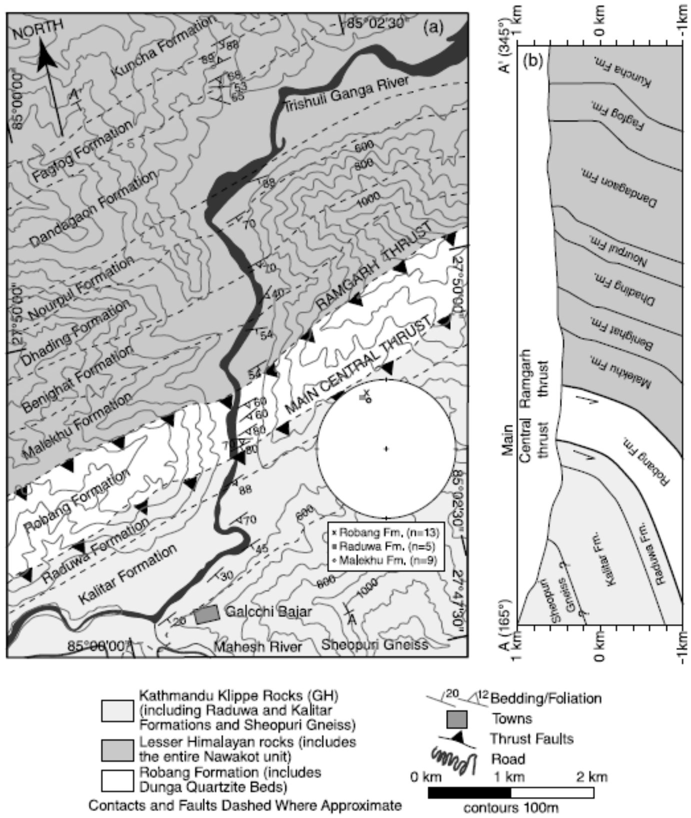

Figure 3.3 – Geologic map and cross section of the Trishuli river valley north of Galcchi Bajar (Pearson and DeCelles, 2005).

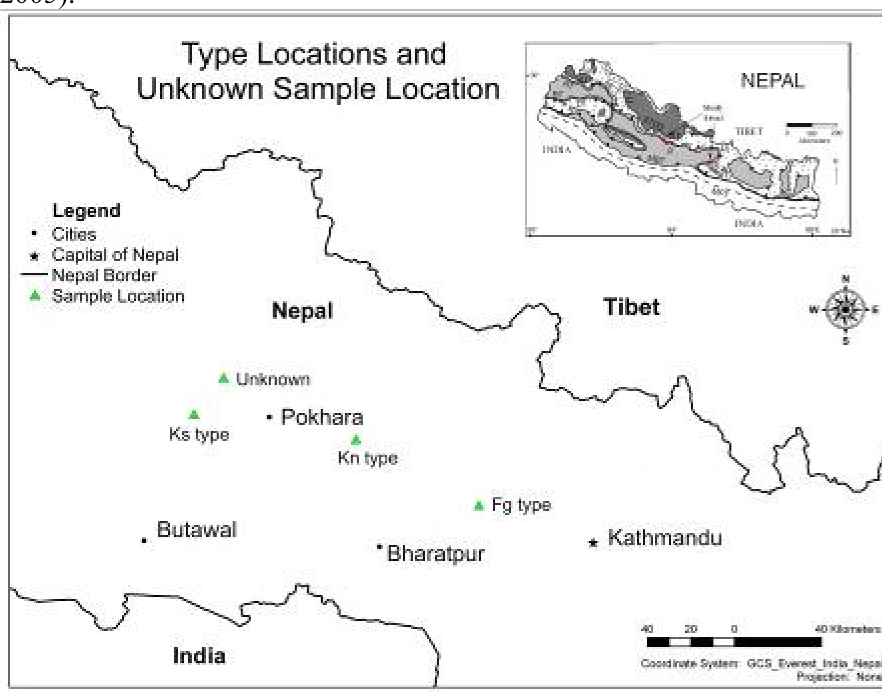

Figure 3.4 – Map of type localities in central Nepal where samples were taken during the 2006 and 2007 field seasons. The unknown sample is located within the Modi Khola valley, which is one of two study areas in this research. Inset map modified from Figure 3.1. Base map courtesy of Lisa Walsh (2008).

3.3.2 Malekhu Formation

Previously mapped by Pearson and DeCelles (Fig. 3.3; 2005), the Trishuli River north of Galcchi Bajar has relatively good rock exposure and is easily accessible, providing an ideal location for measuring and sampling the Malekhu Formation. Carbonate samples were collected at 3 m intervals, with additional samples taken at notable lithologic changes, to prevent sampling bias for specific rock types or exposures. Total section thickness measured was 443 m, including covered intervals at the base and top of the section.

In the lab, the samples were cut using an MK tile saw, then ground and polished with a Struers Labopol-21 two-wheel grinding apparatus. Drilling sites were determined by identifying homogeneous areas within the rocks that were not located close to veins or weathered surfaces. Analytical procedures followed are described in Kaufman et al. (1991) and Kaufman and Knoll (1995). Once drilled, 100 µg of material were acidified with 102% phosphoric acid (H_3PO_4) for 10 minutes at 90° C under vacuum. The resulting CO_2 samples were analyzed using the GV IsoPrime dual inlet gas source mass spectrometer at the University of Maryland. Eight to ten NBS-19 standards were analyzed per run and all data were subsequently reported relative to V-PDB. Uncertainties for both carbon and oxygen isotopes are less than 0.05‰.

3.3.3 Zircons

Samples of quartzite from the type localities in central Nepal were collected by Dr. Aaron Martin during the 2006 field season. Additional samples were collected from the Modi Khola valley during the 2007 field season by Dr. Martin, as well. Detrital zircon samples include type Kuncha (Sample #506078), Kushma (Sample #406102), Fagfog (Sample #506079), and Norpul/Syangia (Sample #406154) formations, as well as one sample taken from an unidentified unit in the Modi Khola (Sample #406020). One igneous sample was also collected, the Ulleri augen gneiss (Sample #507056).

Samples were crushed by hand using a stainless steel mortar and pestle, and sifted through 2 mm and 0.25 mm sieves. The resulting material was washed and panned by hand and allowed to dry overnight. Magnetic separation was accomplished using the Frantz LB-1 magnetic barrier separator, set with a 17.5° front angle and a 20° side angle. Samples were run through the Frantz at 0.5, 1, 1.5, and 2.25 (maximum) amps. Due to machine variance, maximum amp settings were as following; for sample number 406154 (2.25A), 406020 (1.97A), 507056 and 506079 (1.85A), and 406102 (1.5A). Dense liquid separation was accomplished using methylene iodide (MEI) with a density of 3.325g/ml. The samples were then hand-picked using a stereomicroscope with both transmitted and reflected light. Sample 406154, the Norpul (Syangia) type locality, did not yield any zircons and will therefore not be further evaluated. During picking, a random selection of zircon grains were chosen to prevent bias in the zircon populations of each sample based on grain morphology. With the addition of zircon standard SL-2, the zircons were mounted, polished, and taken to the University of Maryland Electron Probe Microanalyzer Laboratory. Backscatter electron and cathodoluminescent images were collected using the JEOL JXA-8900 SuperProbe (Figure 3.5a, b).

Figure 3.5a, b – Backscatter electron images (left) and cathodoluminescent images (right) of zircons from the type Kuncha Formation (Sample 506078). Red arrows indicate candidate spots for laser ablation and the red circle encompasses an inclusion which was avoided when firing the laser.

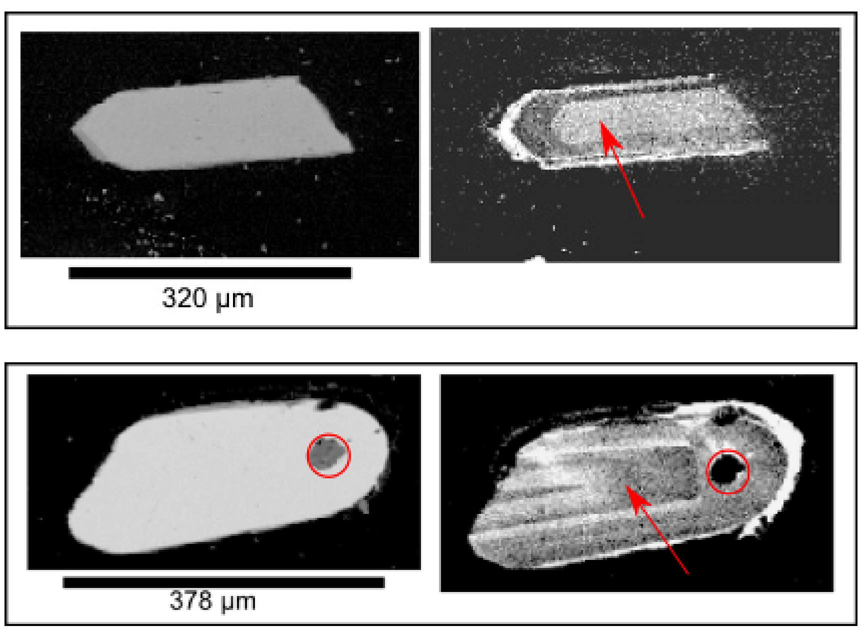

U-Pb isotopic data were collected *in-situ* from the laser ablation multicollector inductively coupled plasma mass spectrometer (LA-MC-ICPMS) at the University of Arizona LaserChron Center. The LA-ICPMS uses a New Wave/Lambda Physik DUV 193 Excimer laser, with a 193 nm wavelength. The laser is set with an 8 Hz repetition rate and a fluence of ~4 J/cm^2. Spot diameter for detrital samples was 30 µm, and for the igneous sample a spot size of 20 µm was used to allow for the collection of rim and core data from individual grains. Depth of the ablation pit is ~12-15 µm. Care was taken to avoid hitting inclusions or multiple zones within a single zircon with the laser (Fig. 3.5a, b). Ablated material was carried in a stream of helium to the plasma source and U, Th, and Pb were measured simultaneously in static mode on 10E11ohm Faraday detectors for ^{238}U, ^{232}Th, ^{208}Pb, and ^{206}Pb, a 10E12 ohm Faraday collector for ^{207}Pb, and an ion counting channel for ^{204}Pb. Examples of systematic uranium and lead changes during laser ablation can be seen in Figure 3.6a-c.

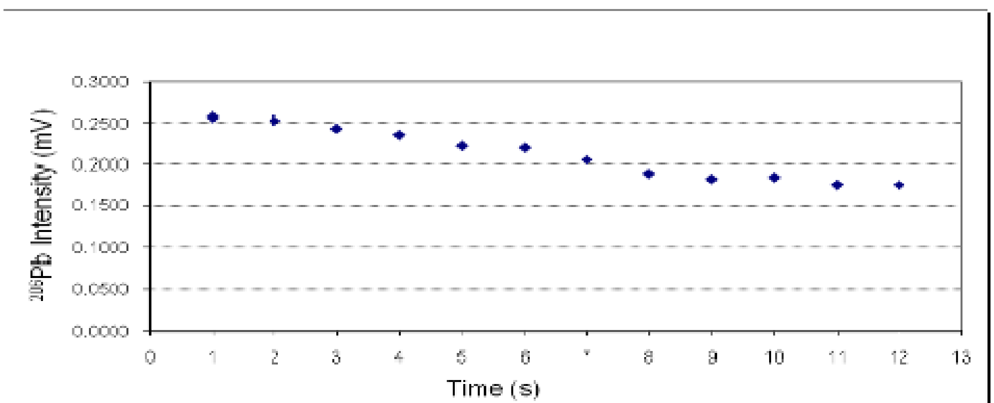

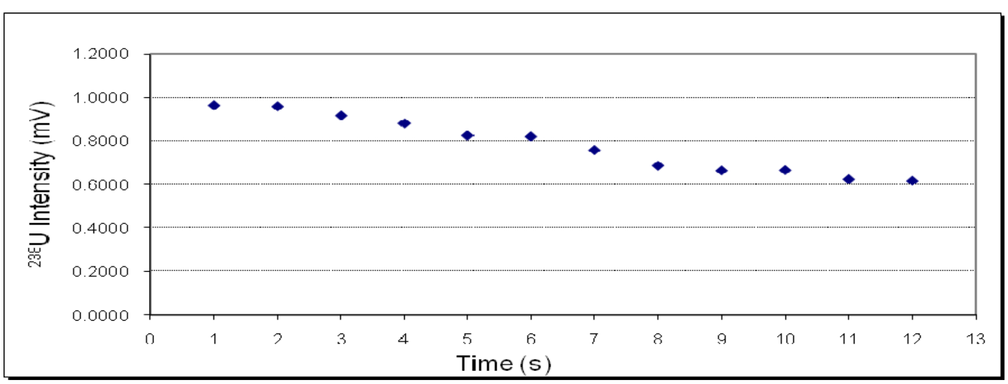

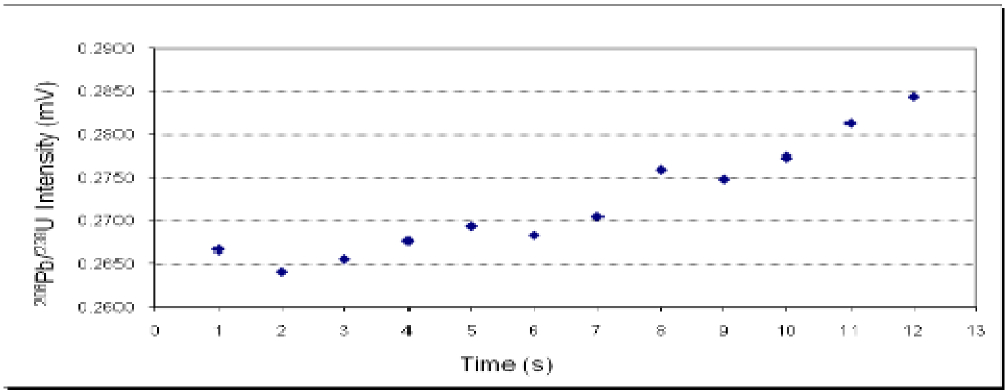

Figure 3.6a-c – Graphs of (a) ^{206}Pb intensity, (b) ^{238}U intensity, and (c) $^{206}Pb/^{238}U$ intensity changes during laser ablation. Data points are integrated over 1 second intervals.

Reduction of detrital zircon analyses was accomplished using the procedures of Gehrels et al. (2006, 2008). Three corrections were made prior to age calculation using an Excel spreadsheet supplied by the University of Arizona LaserChron Center. Depth-related fractionation was accommodated by discarding the first three seconds of data, which removes the early, typically rapidly fluctuating signal (Figure 3.7), and then extracting the nine seconds of remaining analyses as nine 1-second integrations which yield isotope ratios from the integrated intensities. A least squares regression through the remaining data to the initial ratio (fourth second of signal acquisition) was made to account for $^{206}Pb/^{238}U$ and $^{208}Pb/^{232}Th$ depth dependent changes. Correction for inter-element fractionation of $^{206}Pb/^{238}U$ and fractionation of $^{207}Pb/^{206}Pb$ was based on in-run analyses of standard SL-2 (Sri Lanka), which has an ID-TIMS age of 564 $\pm$ 4 Ma (2σ) (Gehrels et al., 2008). Inter-element fractionation of Pb/U is typically 20% and fractionation between Pb isotopes is ~2%. Uncertainties on the calibration corrections are 1-2% (2σ). The standard was analyzed after every five to seven unknowns. Unknowns were corrected using a sliding window average of the six closest standards, excluding the maximum and minimum fractionation factor values.

Common lead correction was made by measuring ^{204}Pb and assuming an initial lead composition based on the work of Stacey and Kramers (1975). Background ^{204}Hg and ^{204}Pb were measured on peaks. Uranium and thorium concentrations were also determined by comparison to the standard zircon (SL-2) which has concentrations of 518 ppm and 68 ppm, respectively, calculating the average intensity of the ^{238}U and ^{232}Th for standards used between samples and adjusting the unknowns by that factor according to their intensities. To remove detrital zircon ages without crystallization significance, e.g. an age resulting from an analyzed zircon with demonstrable lead loss, analyses with greater than 10% $^{206}Pb/^{238}U$ error, 5% $^{207}Pb/^{206}Pb$ error, 25% discordance, or 5% reverse discordance were discarded. For zircon grains older than 1,000 Ma, interpreted ages are based on $^{207}Pb/^{206}Pb$, as opposed to $^{207}Pb/^{235}U$, with an uncertainty of 1-2% (2σ).

Although the formation of "new" metamorphic zircon is rare at temperatures and pressures less than upper amphibolite or granulite facies, recrystallization of inherited zircons and growth of metamorphic rims is possible (Hoskin and Schaltegger, 2003). Therefore, in order to avoid including analyses of detrital zircons that do not reflect igneous crystallization ages, samples were evaluated for the presence of metamorphic zircon in several ways. Backscatter electron and cathodoluminescent images, which have been demonstrated to be effective methods for revealing internal crystal structure (Hanchar and Miller, 1993; Hanchar and Rudnick, 1995), were taken of all samples. Locations of cores and rims were noted for better placement of the laser during ablation, and only cores were sampled. Oscillatory zoning, which is a common characteristic of igneous zircons (Zhao et al., 2002; Hoskin and Schaltegger, 2003), was also noted in many of the zircons. Several researchers have noted that metamorphic zircons typically have higher U concentrations and higher U/Th ratios than igneous zircons (Belousova et al., 2002; Rubatto, 2002; Xian et al., 2004; Dziggel et al., 2005). Thus for each sample, outlying analyses with relatively high U concentrations or U/Th ratios compared to the sample population as a whole were discarded. No more than 5 analyses were excluded from any given sample based on the U concentration or U/Th ratio. Lastly, because only clusters of three or more analyses with overlapping ages are interpreted to have significance, the likelihood of any n>3 remaining metamorphic zircons yielding similar ages is significantly diminished.

The number of analyses discarded varied by sample. For the Kuncha type (Sample 506078) there were 39 analyses discarded out of 166 or 23% of the total analyses. From the Kushma type (Sample 406102), 53 analyses out of 178 analyses or 30% were of the total analyses were discarded. In the Fagfog type (Sample 506079) 35 analyses out of 211 analyses or 17% of the total analyses were discarded. From the unidentified quartzite in the Modi Khola (Sample 406020), 19 of 53 analyses were discarded or 36% of the total analyses.

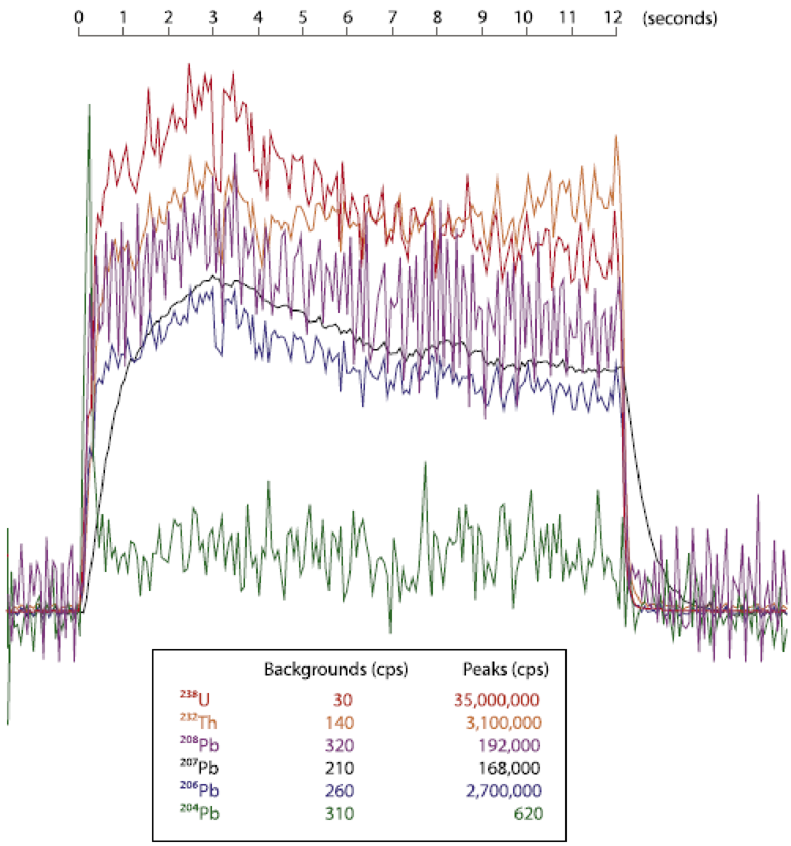

Figure 3.7 - Example of signal from ablation of a zircon using the LA-ICP-MS at the University of Arizona LaserChron Center. Laser is fired for 12 seconds, with first 3 seconds of data discarded based on rapidly fluctuating signal. Figure from Gehrels et al., 2008.

3.3.4 Justification of Detrital Zircon Method

Although accurate and precise analyses are important, the use of detrital zircons to determine a maximum depositional age for a given geologic unit is somewhat less dependent on the precision of any one individual analysis, and more focused on the number of analyses and the care with which individual zircons are selected (Anderson, 2005). Link et al. (2005) recognized detrital zircons could create a unique "barcode" of age spectra that could be used to describe a geologic unit or terrane. However, researchers need to be aware of several biases that could influence the representativeness of a given sample and take care to avoid them when possible. The abundance of (or lack of) zircon in source rocks will ultimately lead to variability in the amount of zircon produced from a given rock. Zircon is found in sedimentary, igneous, and metamorphic rocks, but its abundance is much greater in rocks with felsic or intermediate compositions than those that are mafic or ultramafic in nature (Yamashita et al., 2000, Belousova et al., 2002).

Furthermore, zircons formed in mafic rocks typically have low U concentrations, which when sampled by laser ablation can lead to a large error on the $^{206}Pb/^{238}U$ measurement (Rubatto, 2002; Hoskin and Schaltegger, 2003). The high error can result in the exclusion of those zircons and an introduction of bias into the sample. Understanding the source rocks of the detrital zircon sample and the relative quantity of mafic or ultramafic rocks that might have contributed to the sample is essential. Research on the Lesser Himalayan series indicates that the rocks consist of sediment weathered from the Indian craton and deposited on the passive margin of northern India (Gansser, 1964; DeCelles et al., 1998; Sharma, 1998; Hodges, 2000; Bollinger et al., 2004; Robinson et al., 2001, Myrow et al., 2003; Najman, 2006). The Indian subcontinent consists of six Precambrian terrains. The terrains include the Dharwar, Bastar, and Singhbhum cratons, the Southern Granulite Terrain, the Eastern Ghat Mobile Belt, and the Aravalli-Delhi Mobile Belt (including the Bundelkhand craton). The major lithologies consist of sandstones, limestones, shales, quartzites, felsic and mafic metavolcanics, granites, and gneisses along with Archean aged pillow lavas, amphibolites, and ultramafics (Divakara Rao et al., 1998; Sharma, 1998; Mishra et al., 2000;

Menon et al., 2003; Myrow et al., 2003; Leelanandam et al., 2006; Pati et al., 2007; Mall et al., 2008). Importantly, the amount of mafic or ultramafic rock of mid-Paleoproterozoic age or older in the Indian shield appears to be quite small. Therefore, it is inferred that the potential contribution of zircon from mafic or ultramafic rocks is likely restricted and the detrital samples in this study should not be unduly biased.

Surficial processes can also create natural biases in the detrital zircon record. Weathering has been shown to more easily destroy zircons or portions of zircon grains that are older, have higher U concentrations, or are metamict (Fedo et al., 2003). Distance traveled from the source will affect the concentration of zircon that is incorporated into downstream sedimentary rocks. Upriver sources may be masked by downstream inputs, especially if the lower reaches of the rivers transporting material are incised and contribute zircons from underlying units (Cawood et al., 2003; Link et al, 2005; Moecher and Samson, 2006).

While researchers have little to no control over the natural processes that bias detrital zircon populations, there are introduced biases in sampling that can be avoided. Larson and Poldervaart (1957) demonstrated that zircon breaking during crushing does not appear to be significant. However, a common grain size fraction (ex. <0.25 mm) should be used in order to avoid a grain size bias between samples (Morton et al., 1996). There is a lack of evidence to support any biases introduced by water separation on the Wilfley table or in this research, hand panning, or from the dense liquid separation of zircons (Fedo et al., 2003). Magnetic separation has the potential to cause bias in detrital zircon samples because of the positive correlations between Pb loss, U content, discordance, and magnetic susceptibility (Silver, 1963; Sircombe and Stern, 2002). It is noted that the most paramagnetic fractions of detrital zircons are typically the most unreliable (discordant) and it is suggested that a Frantz setting of 1.8 A with a 10° side angle should be an acceptable compromise between a representative sampling and analytical reliability. However, this is perhaps open to some interpretation (Sircombe and Stern, 2002).

Hand picking of the detrital zircon population has the potential to introduce a large bias into the final age population of a sample and has thus been a focus of several studies. Several researchers argue for the importance of a random sampling of grains (Dodson, 1988; Morton et al., 1996; Moecher and Samson, 2006), while others suggest picking non-random samples based on grain morphology (Ross and Villenuve, 2003), or both random and non-random samples to compare results (Anderson, 2005). Link and Fanning (2003) sampled from the the same units as Ross and Villenuve (2003) and found the same populations of zircons using a random picking method versus the previous author's selective method. They therefore maintain that picking grains based on a specific morphology is unnecessary. These arguments about random and non-random picking lead to the question: How many zircons need to be picked and analyzed to yield a statistically robust answer?

Dodson (1988) determined a sample of n=60 randomly chosen detrital zircons should detect an age population as low as 5% of a given sample at a 95% confidence interval. This assumes that any zircon in the sample has an equal opportunity of being picked. Link and Fanning (2003) found in sample sizes n>60, the smallest age populations became better defined but no new populations were detected. They also noted that one grain analysis does not constitute a population, but that a multi-grain population (n ≥ 3) was important to demonstrate the presence of any specific age group. Several other researchers use sample sizes ranging from n=35 to n=75 grains based on the work of Dodson (Morton et al., 1996; Link and Fanning, 2003; Moecher and Samson, 2006).

However, Vermeesch (2004) posits that Dodson's work does not sufficiently account for a "worst case" scenario in which there is an equal abundance of all age populations. If this were the case a sample size of n=117 would be necessary to ensure at the 95% confidence interval that an age population of 5% is not missed. If research suggests that there is *not* an equal abundance of all age populations, Anderson (2005) suggests the ideal number of analyses needed is likely somewhere between Dodson's n=60 and Vermeesch's n=117. In this study, three of the four detrital zircon samples analyzed have n >117. The remaining sample has n= 34, after much of the sample was lost during final polishing.

3.4 Results

3.4.1 Mapping

Work in the Modi Khola valley (Fig. 3.8) reveals the Kushma Formation is exposed in the southernmost and topographically lowest portion of the map area (Fig. 3.9). Outcrop near the town of Birethati (Fig. 3.10) demonstrates that the Kushma quartzite lies above the phyllitic Kuncha Formation. Moving topographically higher and northward, the Kuncha Formation is again exposed, but this time above the Kushma. The Kuncha Formation is intruded by the Ulleri augen gneiss in the valley. The repetitive sequence of Kushma and Kuncha formations is followed by exposure of another clean quartzite, also identified as the Kushma Formation.

Structurally above the quartzite are, in order, the Dhading, Benighat, and Malekhu formations of the Lakharpata Group, followed by the Gondwana and Foreland Basin sediments. Thin section photographs of the units sampled from type localities in central Nepal and from the Modi Khola can be seen in Figures 3.11a-j. These are some of the first pictures of type locality thin section to be illustrated and are included here for reference. Petrographic descriptions of the type location detrital zircon samples can be seen in Table 1. The Main Central thrust represents the structural termination of the Lesser Himalayan series and is located at the northernmost portion of the map area. Measured foliations and bedding in the Modi Khola are predominantly north (hinterland) dipping.

Figure 3.8 – View of the Modi Khola valley looking south from Ghandruk.

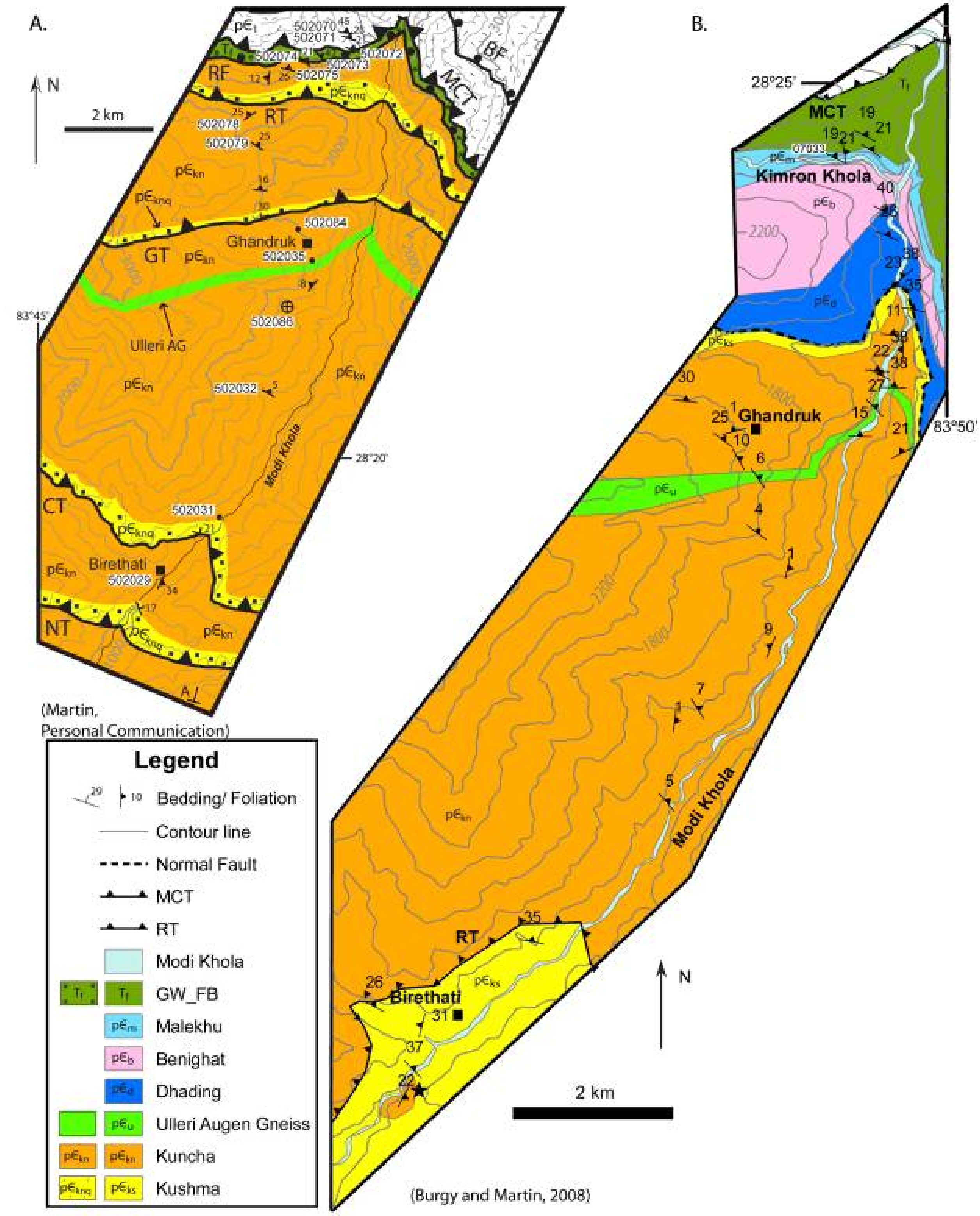

Figure 3.9 – Comparison of mapping in Modi Khola valley and surrounding region (a) completed prior to 2006 by Martin (personal communication) and (b) based on this research in 2007. CI=200 m. Black star indicates location of Figure 3.10.

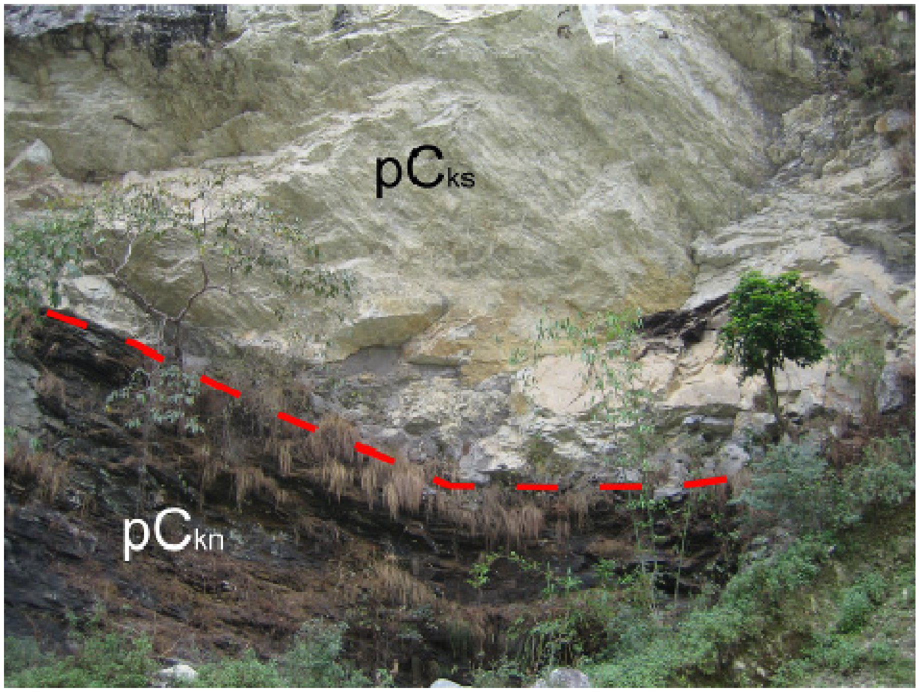

Figure 3.10 – Birethati exposure with quartzitic Kushma Formation (pC_{ks}) above phyllitic Kuncha Formation (pC_{kn}). Red dashed line denotes contact. Outcrop location in the Modi Khola valley marked by black star in Figure 3.9.

3.4.2 Malekhu Formation

Results from the analysis of the Malekhu Formation from the Trishuli River valley can be seen in Figure 3.12 and Table 2.The $\delta^{13}C$ values of the section range from -1.7 to +0.2 ‰, with a mean value of -0.9 ‰ ± 0.4 ‰ (1 s.d.), while $\delta^{18}O$ values range from -17 to -9 ‰, with a mean value of -12.4 ‰ ± 1.5 ‰. A remarkably long stratigraphic interval with limited variation about the mean can be seen in the carbon isotope data throughout the entire section, with the exceptions of a slight negative trend noted from approximately 133 m to 147 m and a somewhat larger variation is seen in the data above 387.5 m. Otherwise, there is remarkable consistency in the data over the entire 309.5 m section and across a wide variety of lithologies, including limestone, dolomite, and calcareous shale (Fig. 3.13a-d). The data for $\delta^{18}O$ reveal slightly more variability, but no significant excursions are seen. Thin sections from the Trishuli River valley reveal recrystallization and a lack of primary structures, as well as an increasing siliciclastic input near the top of the section.

A sample of the Malekhu Formation (Sample #07033) located in the Modi Khola valley (Fig. 3.9) reveals a $\delta^{13}C$ value of -0.3‰ and a $\delta^{18}O$ value of -12 ‰, which is similar to findings in the Trishuli River valley. Thin sections of the sample (Fig. 3.11 i,j) demonstrate that this unit is predominantly made up of carbonate minerals and is *not* a sandstone as suggested by previous workers (Pearson and DeCelles, 2005). Of note, the thin sections from samples in the Modi Khola valley also demonstrate a consistently larger grain size than the thin sections from the Trishuli River locality. This is expected since the Malekhu Formation in the Modi Khola valley is located within the Ramgarh thrust sheet, and experienced higher temperatures and pressures than in the Trishuli River valley.

Additionally, several samples dispersed throughout the section were drilled in multiple locations to ascertain the variability of carbon and oxygen isotope measurements on the millimeter scale. The results of this investigation demonstrate very little variability of $\delta^{13}C$ and $\delta^{18}O$ values on this scale, although there are some minor differences beyond analytical uncertainty (Fig. 3.14). The limited variation in carbon and oxygen isotopic values at the millimeter scale is also reflected in the larger, meter scale findings which demonstrate a similar tendency.

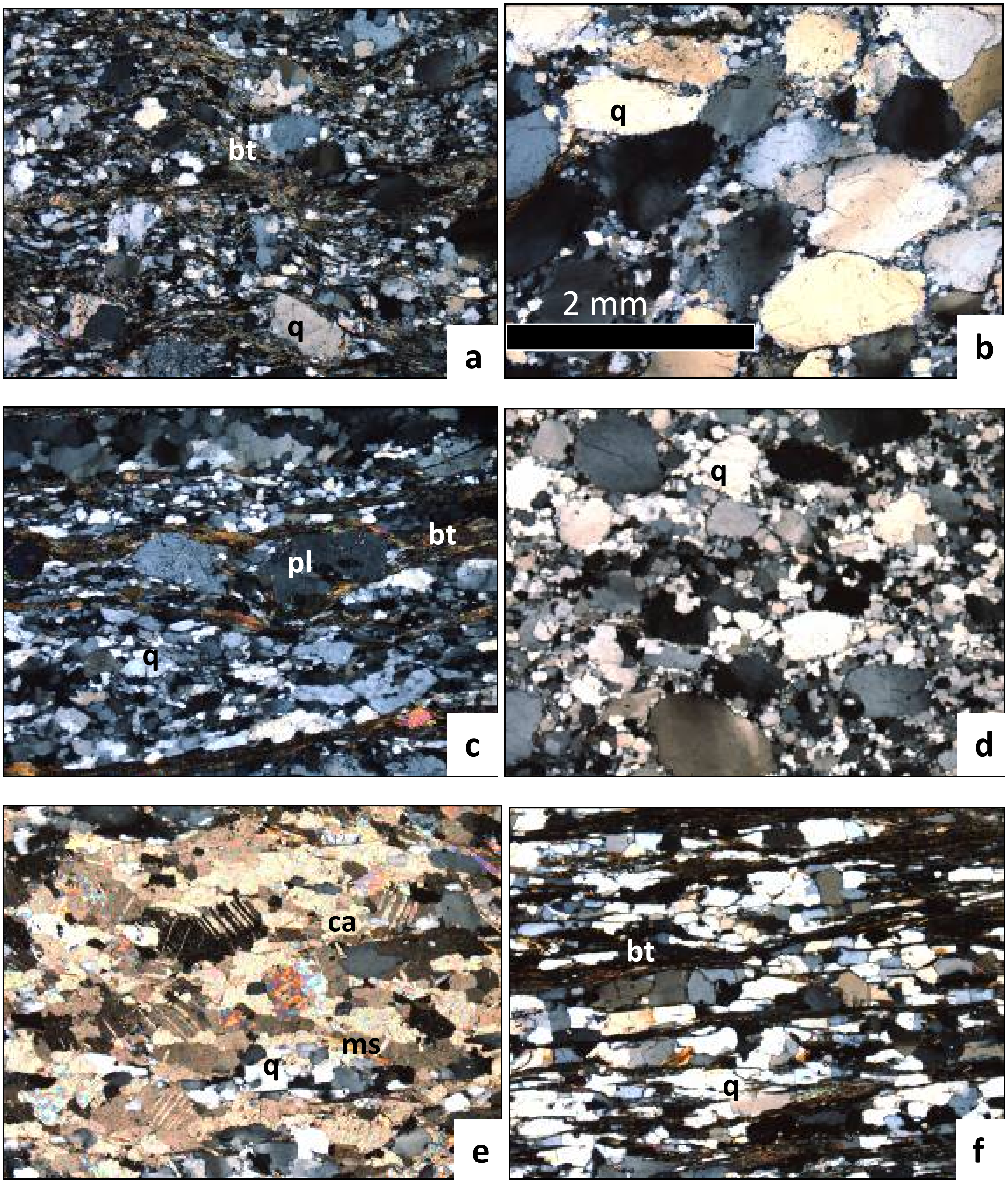

Figure 3.11a-j (and on next page). Thin sections of type localities in central Nepal and samples from the Modi Khola. Pictures (a-h) taken in cross-polar light, scale the same as in (b). (a) Kuncha Formation type locality – grey-green phyllite and phyllitic quartzite, (b) Kushma Formation type locality – coarse grained, well sorted quartzite, (c) Ulleri augen gneiss type locality, (d) Fagfog Formation type locality – medium grain, well sorted quartzite, (e) Dhading Formation – carbonate- from Modi Khola, (f) Benighat Formation – slate- from Modi Khola ,(g) Malekhu Formation – carbonate-from type locality, (h) diorite mapped in the Modi Khola, (i, j) Scale as seen in (j). Cross-polar and plane polar light respectively. Malekhu Formation from Modi Khola, which was interpreted as a sandstone by previous workers. Symbols (q) quartz, (bt) biotite, (ms) muscovite, (amp) amphibole, (ca) calcite, (pl) plagioclase feldspar.

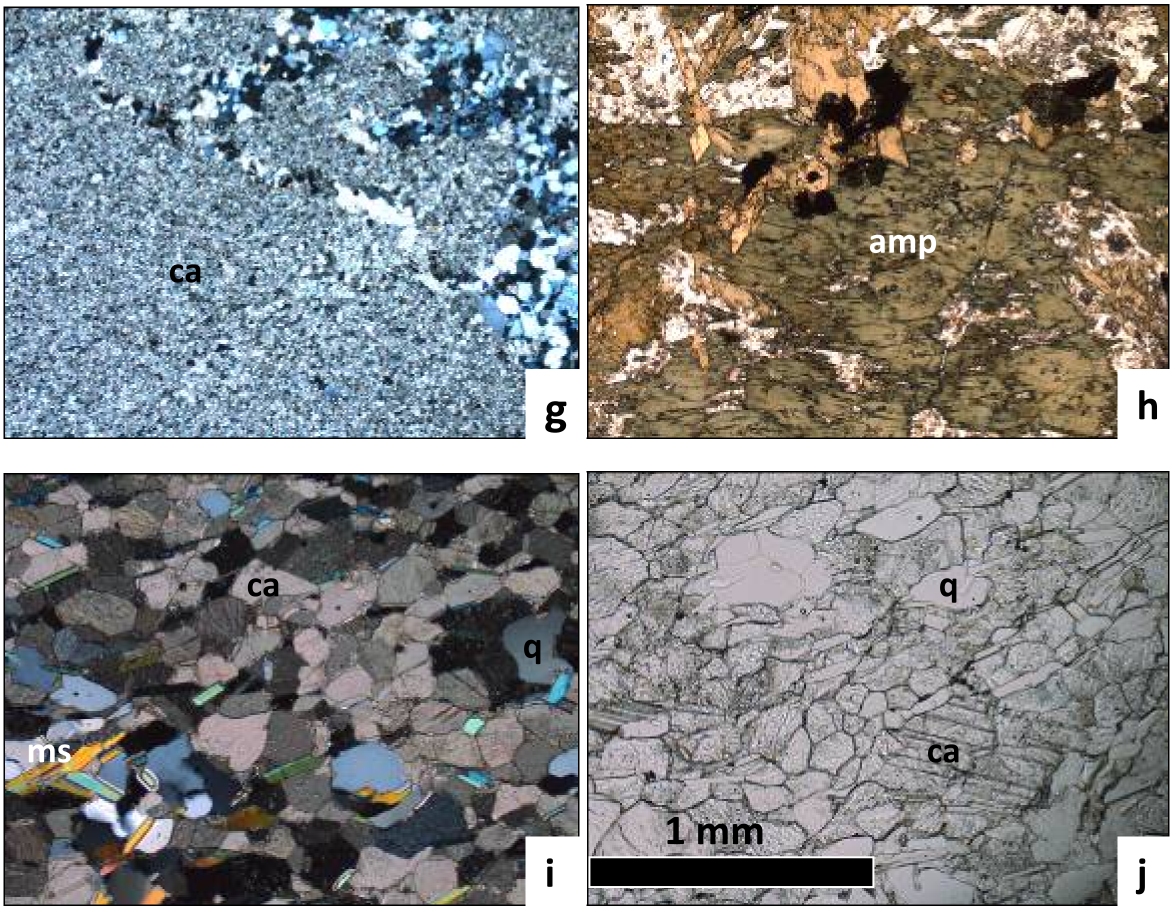

Figure 3.12 (next page) – Stratigraphic column with carbon and oxygen isotopic data for the Malekhu Limestone. Interval between base of section and 133.5m is covered, column starts at 133.5m. All values are referenced to V-PDB. Errors less than 0.05 ‰ and contained within symbols. (ca) calcite, (dol) dolomite.

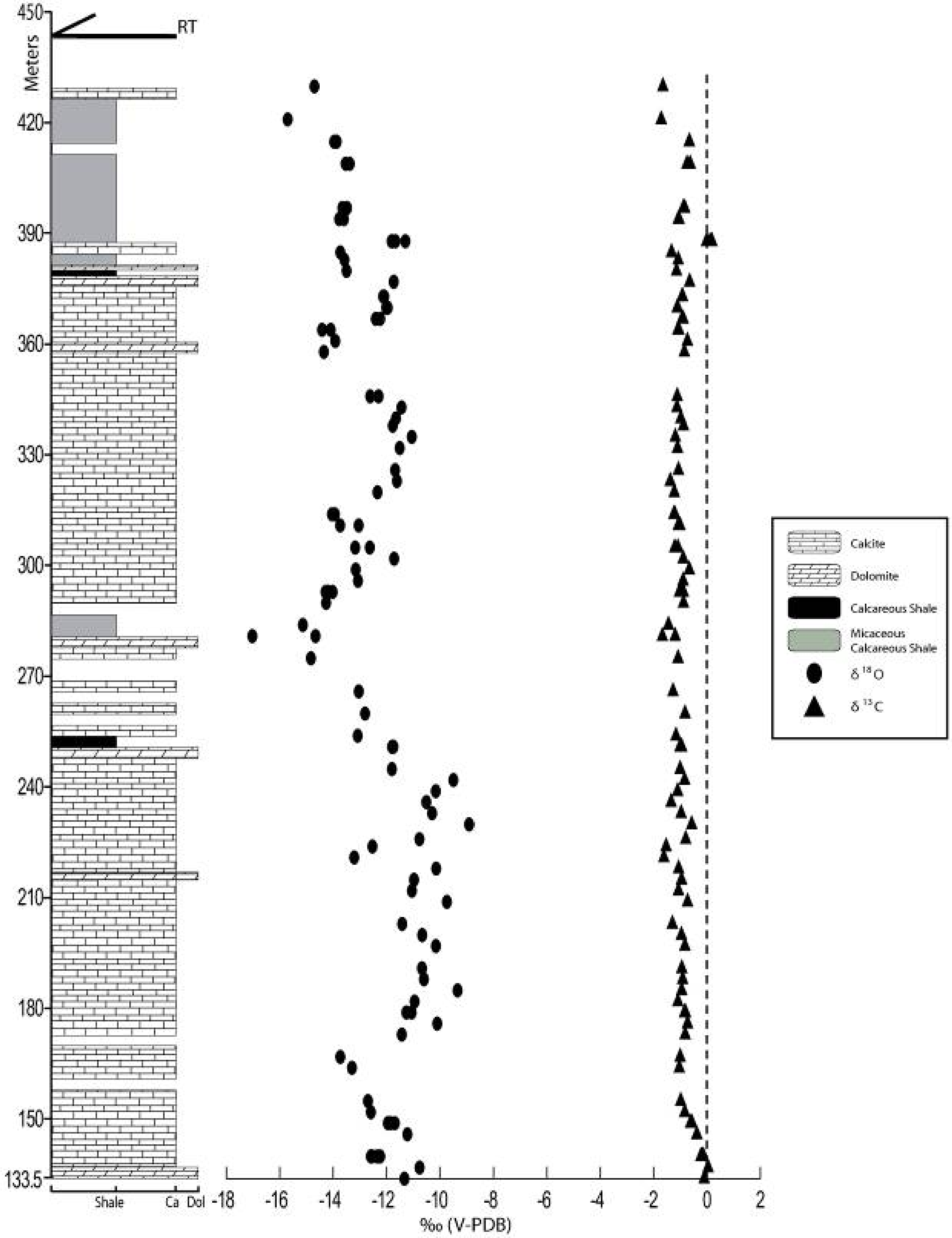

450
Meters
RT
420
390
360
330
300
270
240
210
180
150
133.5
Shale
Ca
Dol
-18
-16
-14
-12
-10
-8
-6
-4
-2
0
2
‰ (V-PDB)
Calcite
Dolomite
Calcareous Shale
Micaceous Calcareous Shale
δ 18 O
δ 13 C

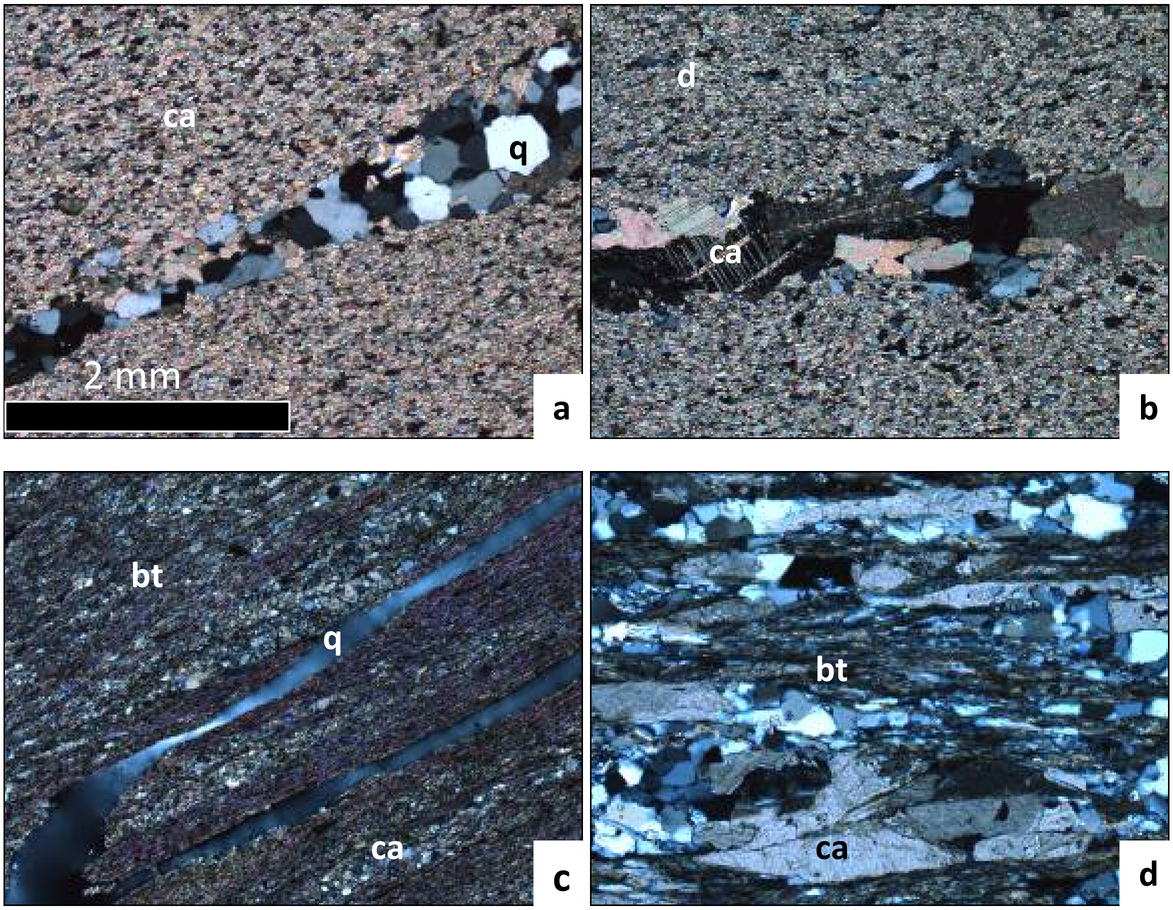

Figure 3.13a-d. – Thin sections of carbonate lithofacies present in the Malekhu Formation in the Trishuli River valley. Photos taken in cross-polar light, field of view 2 mm. (a) Crystalline carbonate – calcite with quartz vein, (b) Crystalline carbonate – dolomite with re-crystallized calcite in vein (c) Calcareous shale with quartz vein, (d) Micaceous calcareous shale.

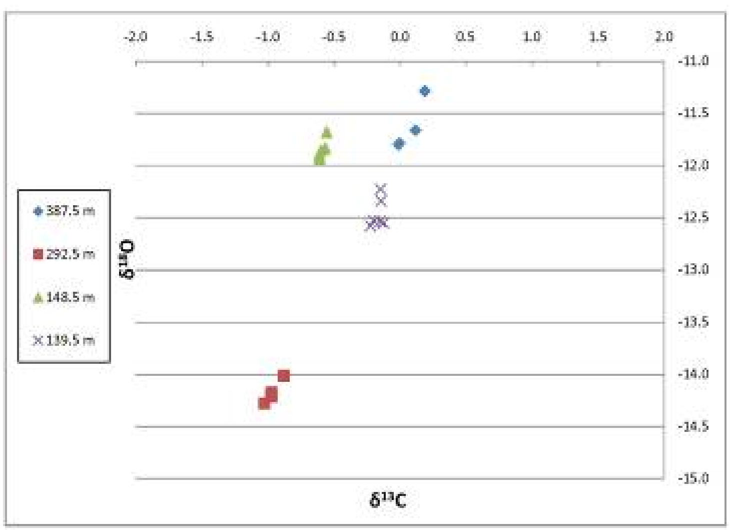

Figure 3.14 – Carbon and oxygen cross-plot of selected samples from the stratigraphic column in Fig. 3.12 demonstrate limited variablitiy of δ^{13}C and δ^{18}O values with samples on a millimeter scale. Errors contained within symbols.

3.4.3 Interpretation of Detrital Zircon Chronology

In this study detrital zircon data are presented with a combination of histograms and probability density plots. The histograms plot the number or frequency of analyses or samples on the y-axis and $^{207}Pb/^{206}Pb$ ages of samples in binned groups along the x-axis. Overlying the histogram is a probability density plot. This plot represents the ages and frequencies, as well as associated uncertainties (Vermeesch, 2004). The probability density plot is constructed by calculating a normal distribution for each analysis based on its measured age and uncertainty, then summing the probability distributions into a single curve (Gehrels et al., 2006).

Based on the premise that a geologic unit is younger than the youngest detrital zircon contained within it (law of inclusions); the youngest portion of the detrital zircon sample is of greatest interest for interpreting maximum depositional ages. While the entire age spectra of an analysis may be useful for studies of provenance, no interpretations are made regarding these ages. All interpretations focus on the youngest zircons within a given sample.

Although Vermeesch (2004) suggests that a single age analysis can be used to determine the presence of an age population, other researchers prefer to interpret only clusters of three or more analyses with overlapping ages as defining robust age populations (DeCelles et al., 2000, 2004; Gehrels et al., 2006, 2008). A single analysis is more likely to have been compromised in some way (e.g. Pb loss) and yield an erroneous age, than three or more analyses with ages that overlap. Therefore, this study does not interpret clusters of ages with less than three analyses. Furthermore, a range of ages are given for each sample and the size of the analyzed cluster is also indicated. From the range of ages, a conservative maximum depositional age, as well as a less conservative, but still robust maximum depositional age is determined for each unit.

3.4.4 Zircons

Reduction of detrital zircon analyses yield several distinct maximum depositional ages for units in the Modi Khola. For zircon grains older than 1,000 Ma, interpreted ages are based on $^{207}Pb/^{206}Pb$, as opposed to $^{207}Pb/^{235}U$, with an uncertainty of 1-2% (2σ)(Table 3). Zircons (n=127) from the type Kuncha Formation have a youngest peak on the probability density plot (Fig. 3.15a, b) of 1896 Ma, however Table 2 shows a cluster of 10 analyses with ages ranging from 1871 to 1881Ma. Therefore a conservative maximum depositional age for the Kuncha Formation is ~1896 Ma. A slightly less conservative, but still robust age for the Kuncha Formation is ~1875 Ma. The unit's depositional age is further constrained by the 1831 Ma ±17 Ma age of the Ulleri augen gneiss, which intrudes the Kuncha Formation and thus constrains the youngest possible age of deposition (DeCelles et al., 2000). Sample (507056), the Ulleri augen gneiss collected in 2007, did not yield useable ages for either cores or rims. As such, it was not included in this analysis and the published age of 1831 Ma ±17 Ma is used instead (DeCelles et al., 2000).

The maximum depositional age indicated by the youngest peak on the probability density plot for zircons (n=125) in the type Kushma Formation is 1795 Ma (Fig. 3.16a, b). Nine analyses ranging from 1771-1785 Ma suggest a less conservative, but still robust maximum depositional age of ~1780 Ma for the Kushma Formation. The maximum age of deposition peak on the probability density plot for the type Fagfog Formation (n=176) is ~1800 Ma (Fig. 3.17a, b). Seven analyses with ages ranging from 1791 to 1810 Ma also suggest a maximum depositional age of 1800 Ma for this unit. The unknown sample (n=34) taken from the Modi Khola indicates a likely maximum depositional age of ~1900 Ma, with the youngest reliable zircon population ranging between 1895 and 1908 Ma, although the sample size is much smaller than the preferred n> 60, as the majority of the sample was lost during final polishing (Fig. 3.18a, b).

3.5 Implications

3.5.1 Constraints on depositional ages

Broadly consistent with the findings of DeCelles et al. (2000), the detrital zircon analyses of this study have several interesting implications for the depositional ages of Lesser Himalayan units in central Nepal. First, the ~1875 Ma maximum depositional age of the Kuncha Formation coupled with the 1831 ± 17 Ma age of the intruded and cross-cutting Ulleri augen gneiss, provide upper and lower depositional

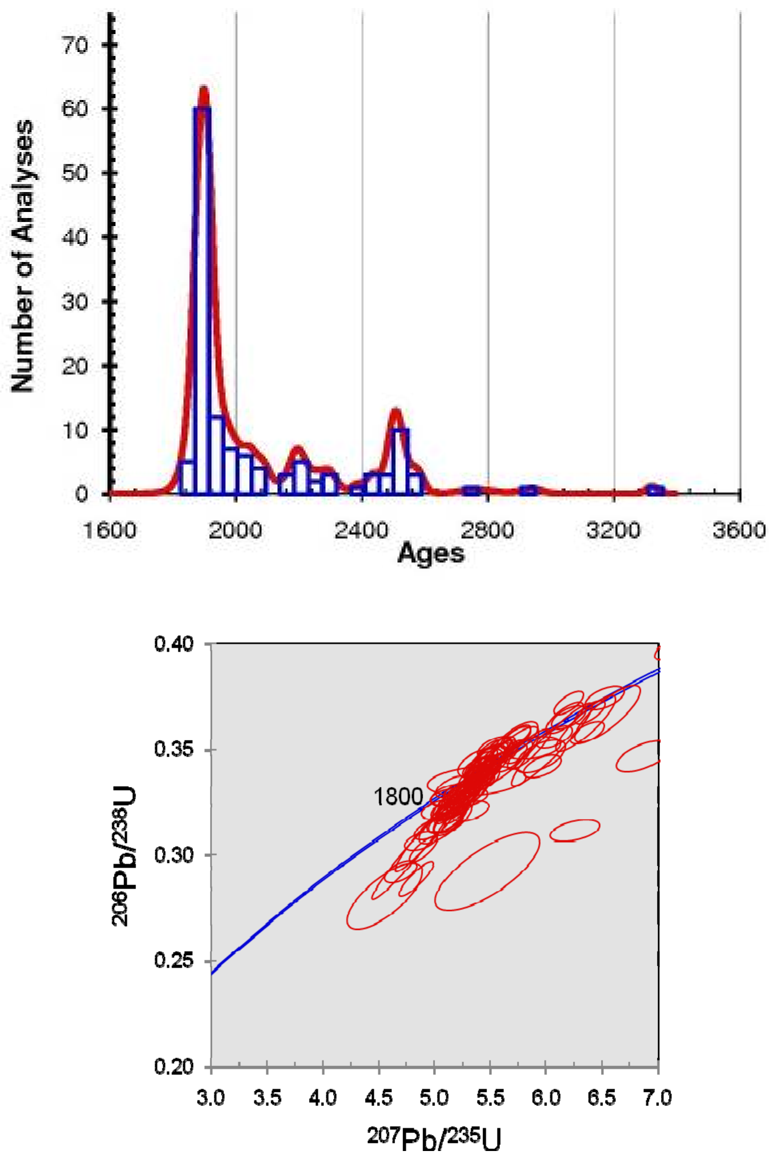

Figure 3.15a -b. – Relative probability plot of age distributions and concordia diagram of detrital zircon ages in the type Kuncha Formation (506078). Inferred depositional age is ~1875 Ma.

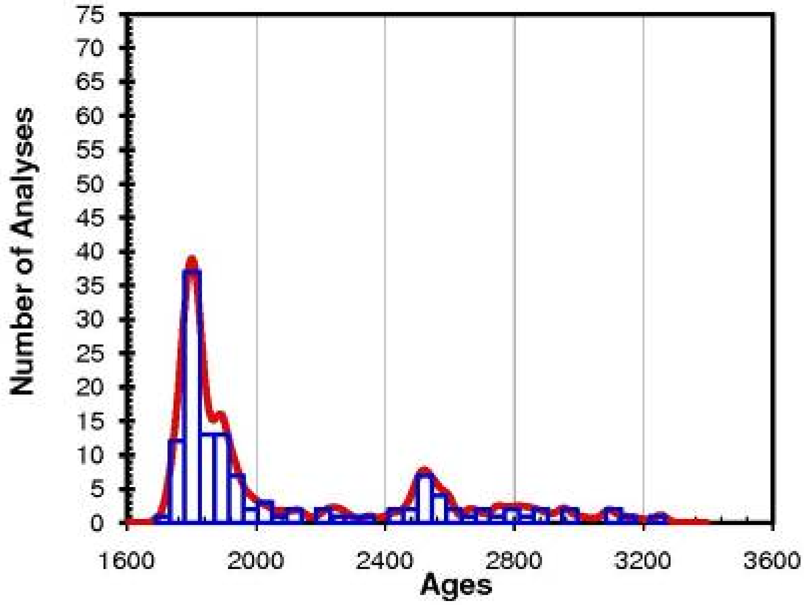

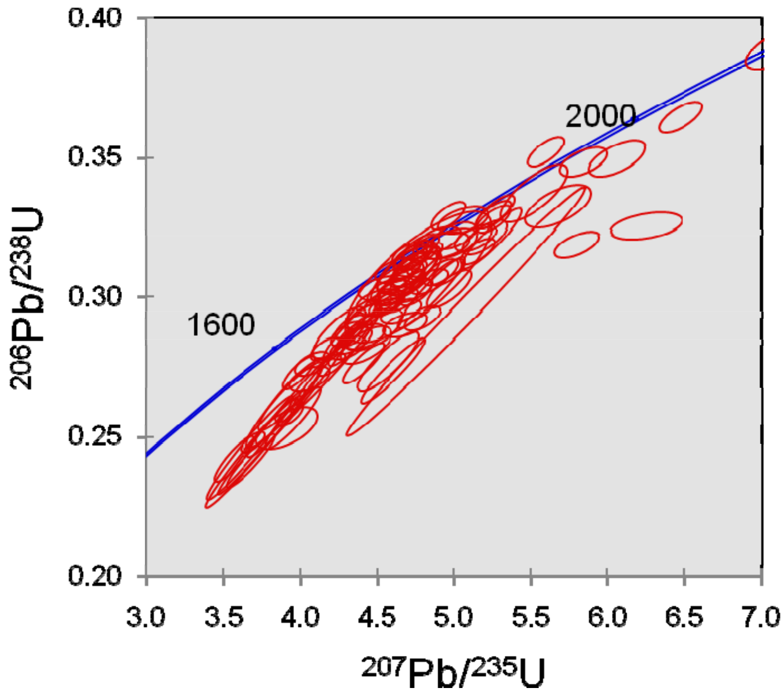

Figure 3.16a -b. – Relative probability plot of age distributions and concordia diagram of detrital zircon ages in the type Kushma Formation (406102). Inferred depositional age is ~1780 Ma.

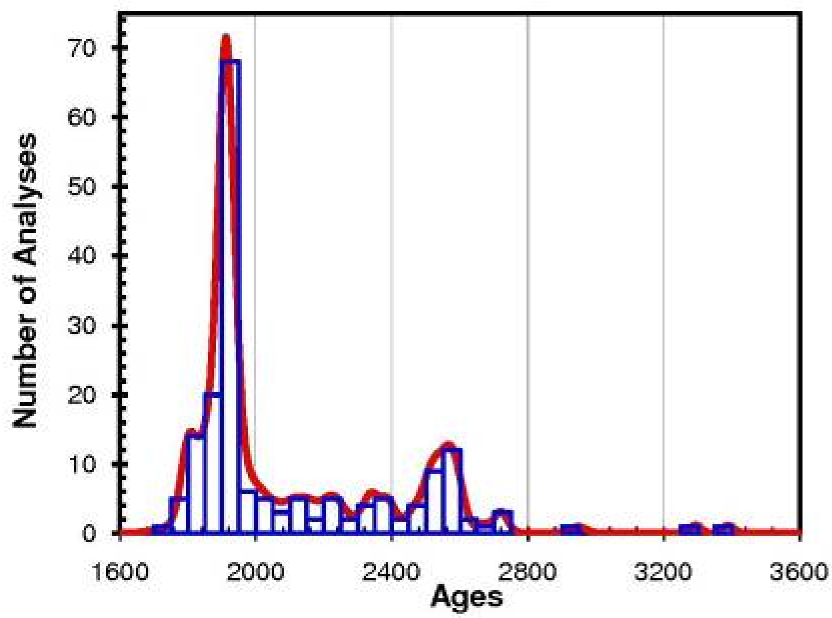

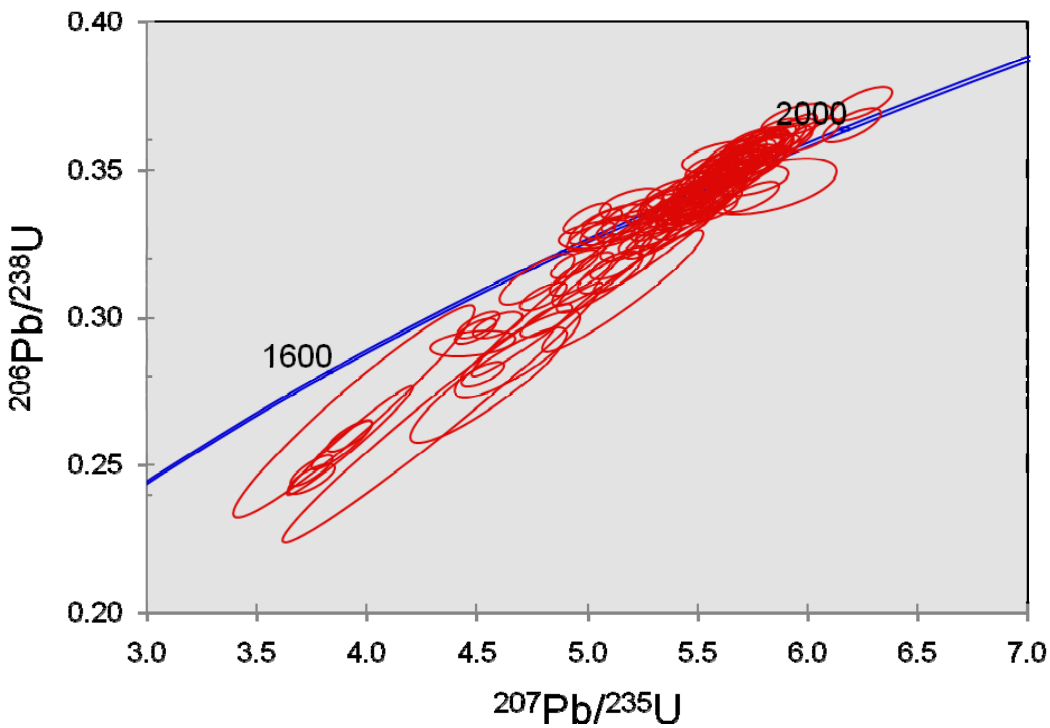

Figure 3.17a -b. – Relative probability plot of age distributions and concordia diagram of detrital zircon ages in the type Fagfog Formation (506079). Inferred depositional age is ~1800 Ma.

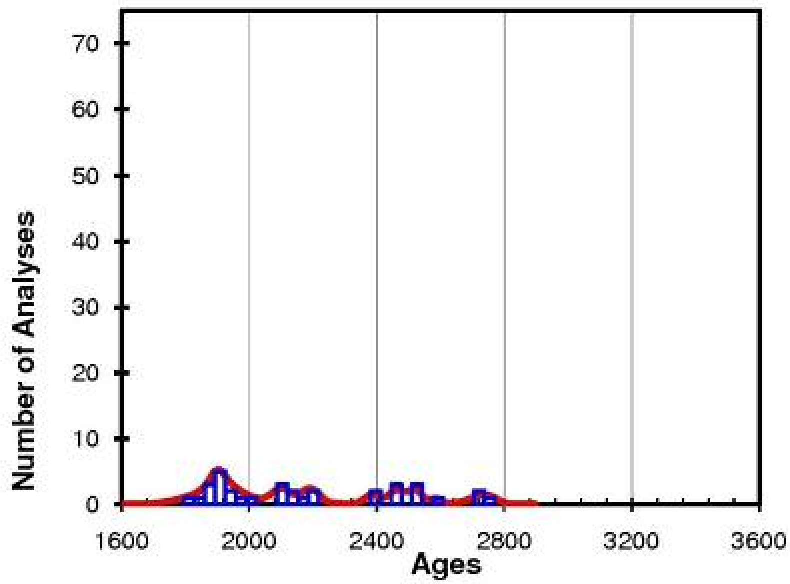

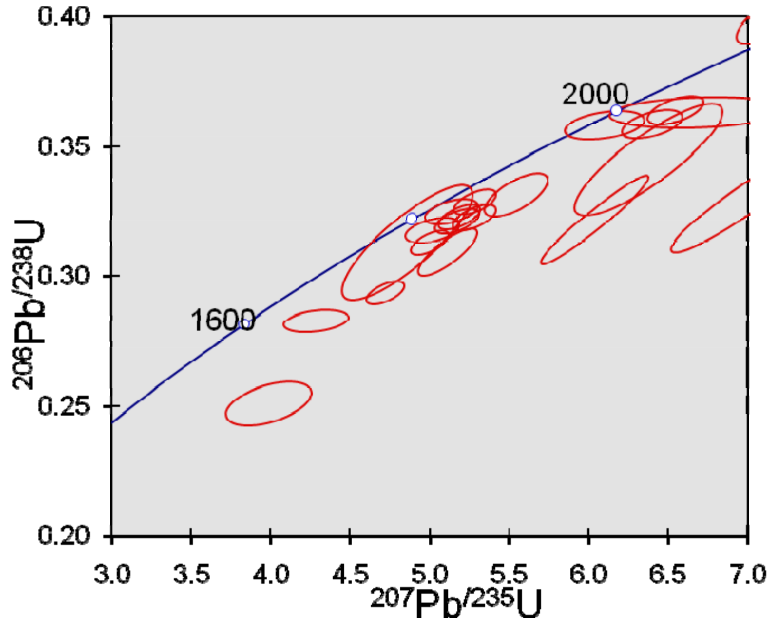

Figure 3.18a-b. – Relative probability plot of age distributions and concordia diagram of detrital zircon ages in the unknown formation in the Modi Khola (406020). Inferred depositional age is ~1900 Ma.

bounds for the unit (DeCelles et al., 2000). These data support the interpretation that the Kuncha Formation is older than the Kushma and Fagfog formations, which have maximum depositional ages that are younger than the crystallization age of the Ulleri gneiss. This finding *does not* support my earlier hypothesis (1), in which the Kushma Formation was expected to be older than the Kuncha Formation.

Second, the ~1800 Ma maximum age of deposition for the type Fagfog Formation allows the unit to have been deposited before the type Kushma Formation, but it cannot completely rule out that the unit may actually have been deposited after the deposition of the Kushma Formation. Due to the restricted sample size, the zircon population from the quartzite (406020) stratigraphically below the Lakharpata Group in the Modi Khola does not match exactly any of the type localities. However, there are similarities between the histogram profiles of the unknown and the Fagfog type locality, as well as that of the Kushma type locality. If the northernmost quartzite is the Kushma Formation, then a depositional contact between it and the underlying Kuncha Formation would be inferred. In contrast, if the northernmost quartzite is the Fagfog Formation a fault contact is required. The simplest and therefore the preferred explanation is that the northernmost quartzite is actually a repetition of the Kushma Formation and is mapped as such. Since the data cannot distinguish between the Fagfog and Kushma formations, I am unable to falsify hypothesis (2) that the northernmost quartzite is the Fagfog Formation.

Third, the trend of near 0‰ $\delta^{13}C$ values throughout the Malekhu section in Trishuli River valley *is* consistent with hypothesis (3) of a Mesoproterozoic (>1250 Ma) age of deposition. Unfortunately, the data cannot differentiate between an early Mesoproterozoic depositional age and that of a younger, relatively quiescent interval between the larger $\delta^{13}C$ shifts of the later Mesoproterozoic or Neoproterozoic. However, in practical terms, there appears to be no evidence for carbonates from a thick, Neoproterozoic aged succession with near 0‰ $\delta^{13}C$ values continuously throughout the section. Buick et al. (1995) found a comparably limited range of $\delta^{13}C$ values in the Mesoproterozoic Bangemall Group in Australia and noted that the ”flat” carbon values also existed over an approximately 2500 m thickness of strata. Knoll et al. (1995) examined Proterozoic carbonates of the 2200 m thick Anbar Massif in northwestern Siberia which span the Meso-Neoproterozoic boundary. They found $\delta^{13}C$ values of 0 to -1.9‰ in the older units (1600-1200 Ma), and slightly greater variation, -2.7 to 4.6‰, in the younger units (1200-850 Ma). Spanning a similar time rage, Kumar et al. (2002) investigated the 4300 m thick Proterozoic Vindhyan Basin in central India, in which the older, Mesoproterozoic, unit (~2100 m thick) also shows $\delta^{13}C$ values of 0‰ and the younger Neoproterozoic unit values show a range from -7.5 to 2‰. Kaufman et al. (2006) found significantly more negative and positive $\delta^{13}C$ values in the ~1400 m thick Neoproterozoic (Ediacaran Period) Krol platform in the Lesser Himalaya of northern India, as did Tewari and Sial (2007). These studies lead to a preference for an early (>1250 Ma) Mesoproterozoic age of deposition for the Malekhu Formation (Fig. 3.19).

The $\delta^{13}C$ age of the Malekhu Formation is significant because it confirms that the Lakharpata Group of central Nepal is not correlative with other carbonate successions in the Lesser Himalayan *physiographic* province in India, e.g., the Neoproterozoic Infra Krol Formation and the Krol group (Aharon et al., 1987; Kaufman et al., 2006; Tewari and Sial, 2007).

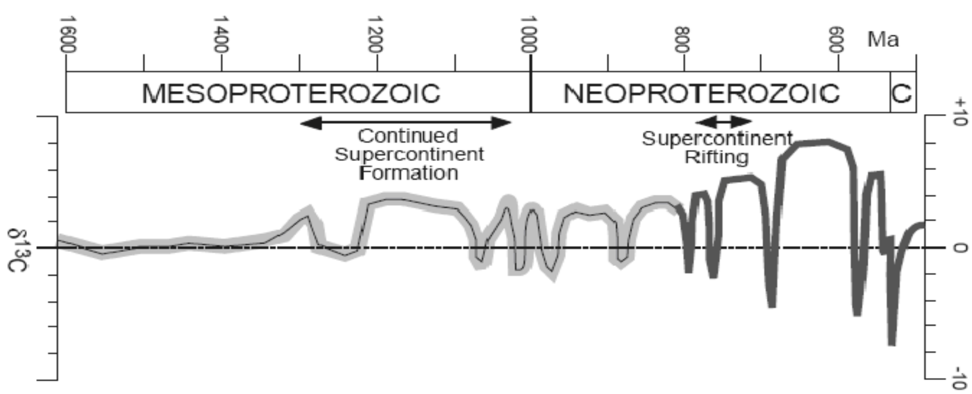

Figure 3.19 – $\delta^{13}C$ curve for Meso-and Neo-Proterozoic rocks (Kah et al., 1999).

Post-depositional diagenesis has been shown to cause $\delta^{18}O$ values to become more negative through aqueous fluid interactions, coupled with temperature increases after burial, while leaving $\delta^{13}C$ values relatively unchanged (Tucker, 1983; Banner and Hanson, 1990; Wickham and Peters, 1993; Jacobsen and Kaufman, 1999; Kah et al., 1999; Kaufman et al., 2006). The wide range of negative $\delta^{18}O$ values suggests the influence of an isotopically depleted metamorphic or meteoric fluid interaction with the rocks (Jacobsen and Kaufman, 1999; Baumgartner and Valley, 2003). The variation in oxygen values appears to be unrelated to or uncoupled from the carbon isotopes which remain unchanging throughout the section. The significant amount of veining in parts of the measured section, which can be seen in thin section (Fig. 3.13a-d), is physical evidence consistent with fluids moving through the system.

3.5.2 Stratigraphy in the Modi Khola

Based on depositional age constraints of the detrital zircons, a reorganization of the stratigraphy of central Nepal is necessary. Detrital zircons and Ulleri augen gneiss magmatic zircons constrain the Kuncha Formation as older than the Kushma, therefore the Kuncha Formation should be considered the basal unit of the Lesser Himalayan package. This is supported by field evidence in the geologic exposure south of the town of Birethati (Fig. 3.10), which clearly demonstrates the relationship of Kushma Formation overlying Kuncha Formation, as well as the larger map scale contact between the units. Furthermore, it has been noted by previous workers that exposures of the Ulleri augen gneiss exclusively intrude the Kuncha Formation, but never the Kushma Formation or younger units. If the Kushma Formation were the older unit, evidence of the Ulleri augen gneiss intruding the Kushma would be expected.

While mapping, no evidence was found to indicate the existence of the Dandagon or Syangia formations in the Modi Khola. The northernmost quartzite in the Modi Khola is likely the Kushma Formation, based on detrital zircon analyses and evaluation of field relationships. Based on this identification and from the absence of the Dandagon and Syangia formations, a significant amount of the

Lesser Himalayan series is missing/ omitted from the region, either through normal faulting or a stratigraphic hiatus. A normal fault is inferred based on the presence of the omitted units in nearby regions.

The package of rocks topographically and stratigraphically above the northernmost quartzite are likely the Dhading, Benighat, and Malekhu formations (the Lakharpata Group as recognized in western Nepal). This interpretation is supported by thin section petrography, which confirm the carbonate-shale-carbonate lithologies of the units (Fig. 3.11a-j). Furthermore, thin sections of the Malekhu Formation from the Modi Khola demonstrate a larger grain size than that of the measured section in the Trishuli River valley. This finding suggests that the rocks have experienced more recrystallization in the Modi Khola valley, which is consistent with its metamorphic history. However, the similarity in $\delta^{13}C$ and $\delta^{18}O$ values between the Modi Khola and Trishuli river valleys suggests limited diagenetic differences between the two.

Topographically above the Malekhu Formation, the Gondwana/Foreland Basin units are exposed. The Main Central thrust is structurally above the Gondwana and Foreland Basin and represents the top of the Lesser Himalayan series.

3.5.3 Structural Significance

The presence of a thrust fault is inferred from the repetition of Kuncha and Kushma units in the Modi Khola. Since the Ramgarh thrust is defined as the first major thrust fault below the MCT, the northernmost exposure of the Kuncha Formation marks the location of the Ramgarh thrust. Based on this interpretation, the location of the Ramgarh thrust is ≥10 km further south than indicated by previous mapping (Fig.3.9 and 3.20; Martin et al., 2005; Pearson and DeCelles, 2005). DeCelles et al. (2001) note that the Ramgarh thrust sheet, where currently located, is unusually thin for such a regionally extensive feature. This study's findings imply that the Ramgarh thrust does in fact carry a thick package of rock similar to, but thinner, than that of the Main Central thrust, and supports the assertion of Pearson and

DeCelles (2005) that the thrust is a kinematically important structure in the Himalayan fold and thrust belt. Furthermore, this interpretation reduces the number of thrust faults mapped below the MCT within the Modi Khola from four to one (Fig. 3.9), and would thus reduce the estimates of shortening accommodated in the region.

3.6 Conclusions

Field observations, $\delta^{13}C$ analyses, and U-Pb detrital zircon ages support the following conclusions in the central Nepal Himalaya:

(1) The Kuncha Formation is older than the Kushma Formation in central Nepal. Detrital zircons indicate a conservative maximum depositional age for the Kuncha Formation of ~1896 Ma. A slightly less conservative, but still robust age for the Kuncha Formation is ~1875 Ma. The Ulleri augen gneiss, which intrudes the Kuncha Formation, is dated at 1831±17 Ma age and constrains the youngest possible age of deposition for the unit. Detrital zircons from the Kushma Formation, which is not intruded by the Ulleri augen gneiss, indicate a maximum depositional age of the ~1795 Ma. A less conservative, but still robust maximum depositional age of ~1780 Ma for the Kushma Formation is still consistent with this conclusion.

(2) The Malekhu Limestone was likely deposited before 1250 Ma. There appears to be no evidence for a thick succession of Neoproterozoic aged carbonate rocks with consistently near 0‰ $\delta^{13}C$ values throughout the section, especially those of the Infra Krol and Krol formations in the physiographic Lesser Himalaya (Buick et al., 1995; Knoll et al., 1995; Kumar et al., 2002).

(3) Upper and lower age bounds for Lesser Himalayan rocks in central Nepal between the Kuncha and Malekhu formations are ~1875 Ma to ~1250 Ma (likely lower bound on the Malekhu Formation), indicating deposition occurred over no more than a 625 Ma time span.

(4) Based on the depositional ages determined in this study, the Ramgarh thrust is likely located farther south than previously mapped. The new location of the Ramgarh would imply that the thrust does in fact carry a thick package of rock similar to that of the Main Central thrust, and the

reduction in the number of faults mapped in the Modi Khola may reduce shortening estimates in the fold and thrust belt of central Nepal.

(5) Reevaluation of fault locations in central Nepal is called for based on the stratigraphy defined in the Modi Khola. Confirmation of this finding in other parts of Nepal is necessary, and if supported, should be reflected in balanced cross sections of the region.

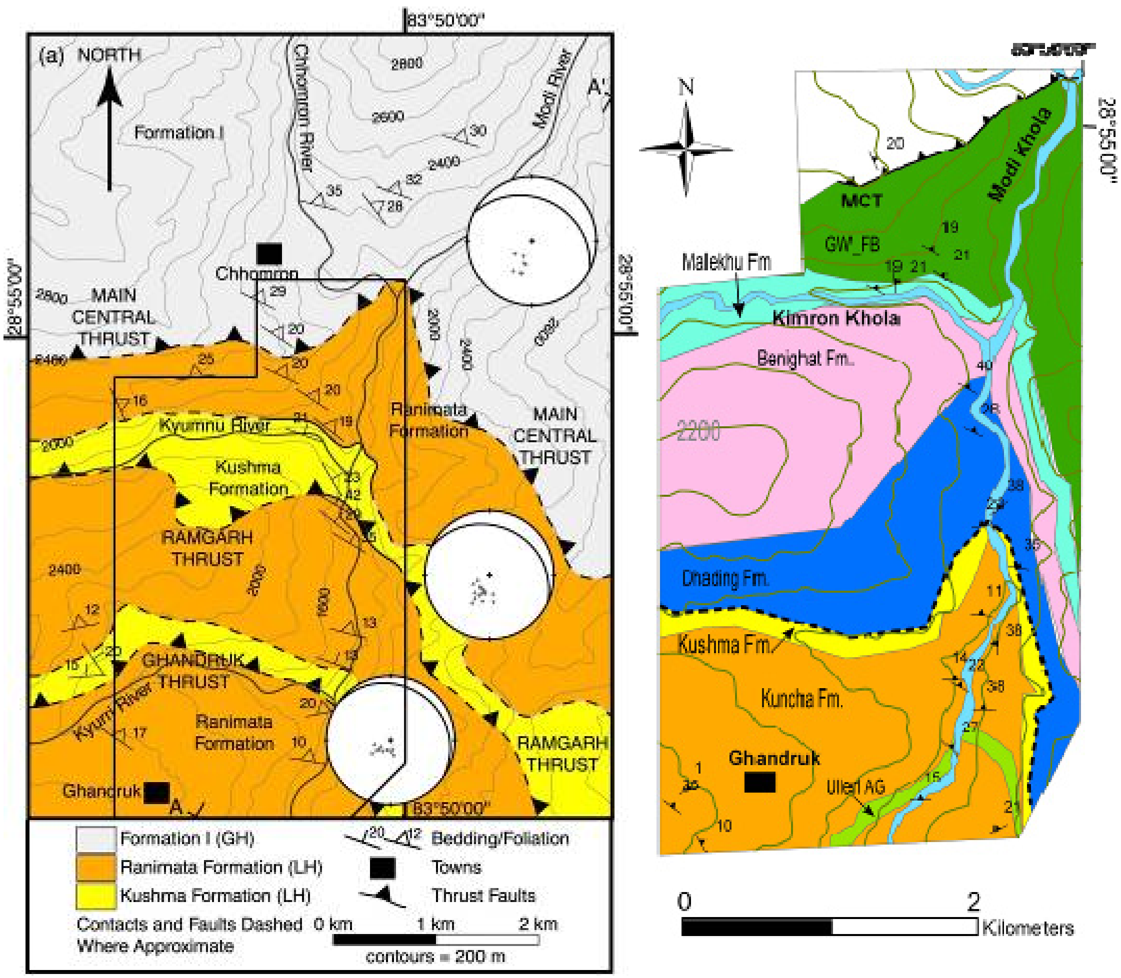

Figure 3.20 – Comparison of mapping by Pearson and DeCelles (2005) and mapping completed in this study in 2007. Lithologic units are the same as in Figure 3.9. The Ranimata Formation in Pearson and DeCelles (2005) may be the lateral equivalent of the Kuncha Formation (orange) in central Nepal. Contour interval is 200m for both maps.

Table 1 – Petrographic descriptions of detrital zircon samples in this study.

Sample Number	Sample Name	Predominant Minerals	Accessory Minerals
406020	Unknown in Modi Khola	quartz	muscovite, zircon
406102	Kushma Formation	quartz	chlorite, muscovite, sulfides, tourmaline, zircon
506078	Kuncha Formation	quartz, muscovite	hematite/magnetite, sulfides, tourmaline, zircon
506079	Fagfog Formation	quartz	muscovite, rutile, tourmaline, zircon

Table 2 – Carbon and oxygen values of the Malekhu formation. Data highlighted in color correspond to Figure 3.9.

Height above base (m)	$\delta^{13}C$	$\delta^{18}O$	Height above base (m)	$\delta^{13}C$	$\delta^{18}O$
133.5	-0.1	-11	292.5	-0.9	-14
136.5	0.0	-11	292.5	-1.0	-14
139.5	-0.1	-12	292.5	-1.0	-14
139.5	-0.1	-12	292.5	-1.0	-14
139.5	-0.2	-13	292.5	-1.0	-14
139.5	-0.2	-13	295.5	-0.9	-13
139.5	-0.2	-13	298.5	-0.7	-13
139.5	-0.1	-13	301.5	-0.9	-12
145.5	-0.4	-11	304.5	-1.1	-13
148.5	-0.6	-12	304.5	-1.2	-13
148.5	-0.6	-12	310.5	-1.0	-13
148.5	-0.6	-12	310.5	-1.1	-14
148.5	-0.6	-12	313.5	-1.2	-14
148.5	-0.6	-12	313.5	-1.2	-14
151.5	-0.8	-13	319.5	-1.2	-12
154.5	-1.0	-13	322.5	-1.4	-12
163.5	-1.0	-13	325.5	-1.1	-12
166.5	-1.0	-14	331.5	-1.1	-11
172.5	-0.8	-11	334.5	-1.2	-11
175.5	-0.7	-10	337.5	-0.9	-12
178.5	-0.8	-11	339.5	-1.0	-12
178.5	-0.8	-11	342.5	-1.1	-11
181.5	-1.1	-11	345.5	-1.1	-12
184.5	-0.9	-9	345.5	-1.1	-13
187.5	-0.9	-11	357.5	-0.8	-14
190.5	-0.9	-11	360.5	-0.7	-14
196.5	-0.8	-10	363.5	-1.1	-14
199.5	-1.0	-11	363.5	-1.1	-14
202.5	-1.3	-11	366.5	-0.9	-12
208.5	-0.7	-10	366.5	-0.9	-12
211.5	-1.1	-11	369.5	-1.1	-12
214.5	-1.0	-11	369.5	-1.1	-12
217.5	-1.1	-10	372.5	-0.9	-12
220.5	-1.6	-13	372.5	-0.9	-12
223.5	-1.5	-13	376.5	-0.6	-12
225.5	-0.8	-11	379.5	-1.1	-13
229.5	-0.6	-9	382.5	-1.1	-14
232.5	-1.0	-10	384.5	-1.3	-14
235.5	-1.3	-11	387.5	-0.0047	-12
238.5	-1.1	-10	387.5	0.1180	-12
241.5	-0.8	-9	387.5	0.1874	-11
244.5	-1.0	-12	387.5	-0.0112	-12
250.5	-1.0	-12	393.5	-1.0	-14
250.5	-0.9	-12	393.5	-1.1	-14
253.5	-1.2	-13	396.5	-0.9	-13
259.5	-0.8	-13	396.5	-0.8	-14
265.5	-1.3	-13	408.5	-0.6	-13
274.5	-1.1	-15	408.5	-0.7	-14
280.5	-1.7	-17	414.5	-0.7	-14
280.5	-1.2	-15	414.5	-0.6	-14
283.5	-1.4	-15	420.5	-1.7	-16
289.5	-0.9	-14	429.5	-1.6	-15

Table 3– U-Pb detrital zircon analyses.

U	Isotopic ratios						Apparent ages (Ma)							Ages used	
U (ppm)	$^{206}Pb/^{204}Pb$	$^{207}Pb^*/^{235}U$	± (%)	$^{206}Pb/^{238}U$	± (%)	Error Corr.	$^{206}Pb^*/^{238}U$	± (Ma)	$^{207}Pb^*/^{235}U$	± (Ma)	$^{206}Pb^*/^{207}Pb^*$	± (Ma)	Concord.	Age (Ma)	± (Ma)
Sample 506078 – Kuncha Fm. (Lat, Long = 28.12613°, 84.34905°)															
799	75325	5.14828	1.67	0.33217	1.00	0.60	1849	16	1844	14	1839	24	1.01	1839	24
290	14050	5.11838	1.90	0.32830	1.00	0.52	1830	16	1839	16	1849	29	0.99	1849	29
321	30368	5.39134	1.58	0.34242	1.22	0.77	1898	20	1883	14	1867	18	1.02	1867	18
324	32306	5.41025	2.53	0.34355	1.32	0.52	1904	22	1886	22	1868	39	1.02	1868	39
198	15979	5.43952	1.50	0.34517	1.00	0.67	1912	17	1891	13	1869	20	1.02	1869	20
836	33214	5.08251	1.42	0.32226	1.00	0.71	1801	16	1833	12	1870	18	0.96	1870	18
248	10120	5.53482	1.82	0.35062	1.00	0.55	1938	17	1906	16	1872	27	1.04	1872	27
264	19544	5.39347	1.81	0.34147	1.00	0.55	1894	16	1884	16	1873	27	1.01	1873	27
376	37490	5.40051	1.41	0.34159	1.00	0.71	1894	16	1885	12	1875	18	1.01	1875	18
256	18555	5.39259	1.41	0.34091	1.00	0.71	1891	16	1884	12	1876	18	1.01	1876	18
893	69830	5.33576	1.56	0.33687	1.00	0.64	1872	16	1875	13	1878	22	1.00	1878	22
294	21963	5.48941	1.66	0.34638	1.00	0.60	1917	17	1899	14	1879	24	1.02	1879	24
223	22910	5.23708	1.92	0.33042	1.00	0.52	1840	16	1859	16	1879	30	0.98	1879	30
653	66194	5.21299	1.59	0.32889	1.00	0.63	1833	16	1855	14	1879	22	0.98	1879	22
442	34453	5.27139	1.41	0.33219	1.00	0.71	1849	16	1864	12	1881	18	0.98	1881	18
921	75827	5.54070	1.95	0.34904	1.19	0.61	1930	20	1907	17	1882	28	1.03	1882	28
291	20731	5.36995	1.42	0.33824	1.00	0.71	1878	16	1880	12	1882	18	1.00	1882	18
207	19472	5.29985	1.41	0.33357	1.00	0.71	1856	16	1869	12	1884	18	0.99	1884	18
797	40867	4.95667	1.81	0.31190	1.00	0.55	1750	15	1812	15	1884	27	0.93	1884	27
248	18072	5.39717	1.41	0.33953	1.00	0.71	1884	16	1884	12	1884	18	1.00	1884	18
184	20669	5.15907	1.60	0.32415	1.00	0.62	1810	16	1846	14	1887	23	0.96	1887	23
364	25208	5.42230	1.87	0.34058	1.21	0.65	1889	20	1888	16	1887	26	1.00	1887	26
1021	47042	4.88344	2.01	0.30646	1.00	0.50	1723	15	1799	17	1889	31	0.91	1889	31
598	40312	4.79973	4.97	0.30105	4.83	0.97	1697	72	1785	42	1890	21	0.90	1890	21
137	8882	4.99931	4.67	0.31354	4.50	0.96	1758	69	1819	40	1890	22	0.93	1890	22
230	22802	5.22026	3.27	0.32735	1.00	0.31	1826	16	1856	28	1890	56	0.97	1890	56
220	21475	5.17269	2.39	0.32434	1.71	0.72	1811	27	1848	20	1890	30	0.96	1890	30
204	19858	5.52960	2.30	0.34672	1.74	0.76	1919	29	1905	20	1890	27	1.02	1890	27
364	22118	5.47920	2.14	0.34340	1.84	0.86	1903	30	1897	18	1891	20	1.01	1891	20
183	13296	5.12942	1.49	0.32147	1.00	0.67	1797	16	1841	13	1891	20	0.95	1891	20
382	22829	5.37802	1.49	0.33693	1.11	0.74	1872	18	1881	13	1892	18	0.99	1892	18
175	15954	5.33255	2.58	0.33383	2.38	0.92	1857	38	1874	22	1893	18	0.98	1893	18
201	22723	5.21034	1.41	0.32605	1.00	0.71	1819	16	1854	12	1894	18	0.96	1894	18
524	47243	5.12015	1.52	0.32032	1.14	0.75	1791	18	1839	13	1894	18	0.95	1894	18
555	74574	5.25434	1.41	0.32865	1.00	0.71	1832	16	1861	12	1895	18	0.97	1895	18
430	35768	5.56044	2.17	0.34766	1.00	0.46	1923	17	1910	19	1895	35	1.01	1895	35

562	41138	5.43393	1.96	0.33971	1.04	0.53	1885	17	1890	17	1896	30	0.99	1896	30
265	25997	5.21799	2.31	0.32617	1.99	0.86	1820	32	1856	20	1896	21	0.96	1896	21
565	45610	5.15678	1.84	0.32185	1.00	0.54	1799	16	1846	16	1899	28	0.95	1899	28
468	43635	5.46276	1.47	0.34093	1.00	0.68	1891	16	1895	13	1899	19	1.00	1899	19
192	20518	5.53399	1.97	0.34523	1.70	0.86	1912	28	1906	17	1899	18	1.01	1899	18
687	54206	5.37924	1.41	0.33523	1.00	0.71	1864	16	1882	12	1901	18	0.98	1901	18
185	12530	5.37782	5.40	0.33497	1.41	0.26	1862	23	1881	46	1902	94	0.98	1902	94
479	34461	5.49145	1.41	0.34205	1.00	0.71	1897	16	1899	12	1902	18	1.00	1902	18
497	35611	5.47237	1.44	0.34055	1.03	0.72	1889	17	1896	12	1904	18	0.99	1904	18
752	77232	5.43694	1.41	0.33829	1.00	0.71	1878	16	1891	12	1904	18	0.99	1904	18
824	51174	4.69642	2.03	0.29216	1.17	0.58	1652	17	1767	17	1904	30	0.87	1904	30
1035	76872	5.26111	2.11	0.32687	1.86	0.88	1823	30	1863	18	1907	18	0.96	1907	18
341	33024	5.61773	1.41	0.34901	1.00	0.71	1930	17	1919	12	1907	18	1.01	1907	18
935	95878	5.11073	2.27	0.31749	1.45	0.64	1777	23	1838	19	1907	31	0.93	1907	31
249	20051	5.73419	1.41	0.35613	1.00	0.71	1964	17	1937	12	1907	18	1.03	1907	18
258	19237	5.72667	1.53	0.35556	1.00	0.65	1961	17	1935	13	1908	21	1.03	1908	21
422	31010	5.04518	2.41	0.31322	1.67	0.69	1757	26	1827	20	1908	31	0.92	1908	31
438	29870	5.38184	1.87	0.33411	1.00	0.53	1858	16	1882	16	1908	28	0.97	1908	28
390	23517	5.18912	1.57	0.32183	1.00	0.64	1799	16	1851	13	1910	22	0.94	1910	22
294	44950	5.29166	1.41	0.32807	1.00	0.71	1829	16	1868	12	1911	18	0.96	1911	18
196	10216	5.40277	1.64	0.33494	1.10	0.67	1862	18	1885	14	1911	22	0.97	1911	22
642	35288	5.41618	1.41	0.33567	1.00	0.71	1866	16	1887	12	1911	18	0.98	1911	18
276	25714	5.53956	1.41	0.34318	1.00	0.71	1902	16	1907	12	1912	18	0.99	1912	18
541	43454	5.35886	1.41	0.33196	1.00	0.71	1848	16	1878	12	1912	18	0.97	1912	18
359	15048	5.47800	1.41	0.33927	1.00	0.71	1883	16	1897	12	1912	18	0.98	1912	18
312	18354	5.72687	2.28	0.35461	1.61	0.71	1957	27	1935	20	1913	29	1.02	1913	29
347	23579	5.29138	1.95	0.32747	1.67	0.86	1826	27	1867	17	1914	18	0.95	1914	18
226	9290	5.13442	1.77	0.31699	1.33	0.75	1775	21	1842	15	1918	21	0.93	1918	21
391	36253	5.10155	1.96	0.31491	1.00	0.51	1765	15	1836	17	1918	30	0.92	1918	30
325	13546	4.90064	1.70	0.30238	1.34	0.79	1703	20	1802	14	1919	19	0.89	1919	19
348	20288	5.34281	1.68	0.32942	1.14	0.68	1836	18	1876	14	1921	22	0.96	1921	22
552	24251	4.55454	4.92	0.28050	3.62	0.74	1594	51	1741	41	1923	60	0.83	1923	60
467	43282	5.30852	2.62	0.32687	2.42	0.92	1823	38	1870	22	1923	18	0.95	1923	18
587	47168	5.12682	1.62	0.31528	1.00	0.62	1767	15	1841	14	1925	23	0.92	1925	23
174	15392	5.46316	1.42	0.33532	1.00	0.70	1864	16	1895	12	1929	18	0.97	1929	18
505	24696	5.16365	2.16	0.31671	1.60	0.74	1774	25	1847	18	1930	26	0.92	1930	26
442	46963	5.65633	3.18	0.34681	2.64	0.83	1919	44	1925	27	1930	32	0.99	1930	32
242	26659	5.68954	1.61	0.34585	1.24	0.77	1915	21	1930	14	1946	18	0.98	1946	18
308	33397	5.74878	1.56	0.34869	1.00	0.64	1928	17	1939	14	1950	21	0.99	1950	21
942	64760	5.31715	2.04	0.32062	1.00	0.49	1793	16	1872	17	1960	32	0.91	1960	32
145	18019	6.19633	1.41	0.37196	1.00	0.71	2039	17	2004	12	1968	18	1.04	1968	18
901	48270	5.84359	2.16	0.35014	1.80	0.83	1935	30	1953	19	1972	21	0.98	1972	21
304	33614	5.88007	2.80	0.35074	1.00	0.36	1938	17	1958	24	1980	46	0.98	1980	46

431	45909	6.16332	1.80	0.36513	1.33	0.74	2006	23	1999	16	1992	22	1.01	1992	22
354	36179	6.19520	1.67	0.36524	1.00	0.60	2007	17	2004	15	2000	24	1.00	2000	24
224	20781	6.07491	1.67	0.35599	1.00	0.60	1963	17	1987	15	2011	24	0.98	2011	24
491	47683	5.94776	2.46	0.34667	1.46	0.59	1919	24	1968	21	2021	35	0.95	2021	35
389	20933	6.04941	3.93	0.35220	3.68	0.94	1945	62	1983	34	2023	25	0.96	2023	25
317	16150	6.38643	1.41	0.36774	1.00	0.71	2019	17	2030	12	2042	18	0.99	2042	18
108	9554	6.52287	1.79	0.37436	1.00	0.56	2050	18	2049	16	2048	26	1.00	2048	26
365	18342	5.96098	1.82	0.34196	1.00	0.55	1896	16	1970	16	2049	27	0.93	2049	27
225	17742	6.35210	2.78	0.36225	2.44	0.88	1993	42	2026	24	2059	23	0.97	2059	23
473	45482	6.36356	1.59	0.35797	1.00	0.63	1973	17	2027	14	2083	22	0.95	2083	22
322	27184	6.54882	2.98	0.36694	2.43	0.81	2015	42	2052	26	2090	30	0.96	2090	30
393	41451	7.11704	1.41	0.39844	1.00	0.71	2162	18	2126	13	2092	18	1.03	2092	18
1014	58632	7.33811	2.21	0.39602	1.24	0.56	2151	23	2153	20	2156	32	1.00	2156	32
684	43603	5.47820	5.63	0.29214	4.19	0.74	1652	61	1897	48	2177	65	0.76	2177	65
120	14979	7.46065	1.42	0.39745	1.00	0.71	2157	18	2168	13	2179	17	0.99	2179	17
105	10285	7.58167	2.92	0.40133	2.74	0.94	2175	51	2183	26	2190	17	0.99	2190	17
241	34075	7.43213	2.02	0.39267	1.00	0.50	2135	18	2165	18	2193	30	0.97	2193	30
175	22298	7.32228	1.56	0.38473	1.00	0.64	2098	18	2152	14	2203	21	0.95	2203	21
238	24782	7.45694	1.69	0.39070	1.36	0.81	2126	25	2168	15	2208	17	0.96	2208	17
210	24323	7.60750	1.84	0.39823	1.00	0.54	2161	18	2186	17	2209	27	0.98	2209	27
281	27386	7.67173	1.55	0.39254	1.00	0.64	2135	18	2193	14	2249	21	0.95	2249	21
434	25074	6.86762	2.33	0.34672	1.41	0.61	1919	23	2094	21	2272	32	0.84	2272	32
261	27843	8.59628	3.63	0.42922	2.71	0.75	2302	52	2296	33	2291	42	1.00	2291	42
768	33091	6.25552	2.35	0.31153	1.08	0.46	1748	17	2012	21	2295	36	0.76	2295	36
381	31978	8.19314	1.41	0.40779	1.00	0.71	2205	19	2253	13	2296	17	0.96	2296	17
670	77469	9.14145	1.41	0.43214	1.00	0.71	2315	19	2352	13	2384	17	0.97	2384	17
491	75883	8.94157	2.60	0.41168	2.40	0.92	2223	45	2332	24	2429	17	0.91	2429	17
236	18829	9.62632	1.84	0.43921	1.00	0.54	2347	20	2400	17	2445	26	0.96	2445	26
489	18634	7.97869	3.42	0.36395	2.86	0.84	2001	49	2229	31	2445	32	0.82	2445	32
120	18869	10.18803	1.41	0.45361	1.00	0.71	2411	20	2452	13	2486	17	0.97	2486	17
221	34902	9.93674	1.41	0.43974	1.00	0.71	2349	20	2429	13	2496	17	0.94	2496	17
268	20950	10.15060	1.54	0.44900	1.17	0.76	2391	23	2449	14	2497	17	0.96	2497	17
302	35691	9.75769	1.75	0.42977	1.00	0.57	2305	19	2412	16	2504	24	0.92	2504	24
67	10498	10.45692	1.59	0.45968	1.24	0.78	2438	25	2476	15	2507	17	0.97	2507	17
347	36030	10.79749	1.59	0.47443	1.00	0.63	2503	21	2506	15	2508	21	1.00	2508	21
312	30238	10.06373	1.52	0.44213	1.00	0.66	2360	20	2441	14	2508	19	0.94	2508	19
384	33354	11.36050	3.23	0.49887	2.55	0.79	2609	55	2553	30	2509	33	1.04	2509	33
401	31728	10.82332	1.41	0.47394	1.00	0.71	2501	21	2508	13	2514	17	0.99	2514	17
114	12357	11.16286	1.56	0.48739	1.00	0.64	2559	21	2537	15	2519	20	1.02	2519	20
92	13022	10.50956	2.59	0.45865	1.49	0.58	2434	30	2481	24	2520	36	0.97	2520	36
356	44131	10.74324	2.66	0.46624	2.46	0.93	2467	50	2501	25	2529	17	0.98	2529	17
204	21637	11.44159	2.77	0.49429	1.14	0.41	2589	24	2560	26	2537	42	1.02	2537	42
880	110760	11.17538	2.39	0.47892	1.02	0.43	2523	21	2538	22	2550	36	0.99	2550	36

336	58186	10.75940	1.53	0.45499	1.00	0.65	2417	20	2503	14	2572	19	0.94	2572	19
137	13726	10.19257	2.74	0.42924	2.52	0.92	2302	49	2452	25	2579	18	0.89	2579	18
82	4293	15.04288	3.96	0.56565	2.00	0.51	2890	47	2818	38	2767	56	1.04	2767	56
262	35130	16.06230	2.21	0.54393	1.00	0.45	2800	23	2881	21	2937	32	0.95	2937	32
118	23405	24.37904	1.56	0.64886	1.00	0.64	3224	25	3284	15	3320	19	0.97	3320	19

Sample 506079 – Fagfog Fm (Lat, Long = 27.85165°, 84.85856°)

453	21239	3.94169	9.21	0.26830	8.87	0.96	1532	121	1622	75	1741	46	0.88	1741	46
208	17373	4.99994	1.41	0.33379	1.00	0.71	1857	16	1819	12	1777	18	1.05	1777	18
403	24298	3.92498	1.70	0.25998	1.37	0.81	1490	18	1619	14	1791	18	0.83	1791	18
242	7933	3.88763	2.36	0.25697	2.13	0.90	1474	28	1611	19	1795	18	0.82	1795	18
1011	39800	4.51018	1.41	0.29751	1.00	0.71	1679	15	1733	12	1799	18	0.93	1799	18
665	34879	3.92561	4.82	0.25850	4.72	0.98	1482	63	1619	39	1802	18	0.82	1802	18
614	44412	5.03546	1.55	0.33097	1.19	0.77	1843	19	1825	13	1805	18	1.02	1805	18
250	13593	4.49646	1.42	0.29545	1.00	0.71	1669	15	1730	12	1806	18	0.92	1806	18
447	43076	4.77328	2.34	0.31291	1.84	0.79	1755	28	1780	20	1810	26	0.97	1810	26
509	18253	3.75043	1.90	0.24536	1.41	0.74	1414	18	1582	15	1814	23	0.78	1814	23
599	32209	5.01587	1.41	0.32763	1.00	0.71	1827	16	1822	12	1816	18	1.01	1816	18
436	36687	5.19961	1.87	0.33861	1.00	0.53	1880	16	1853	16	1822	29	1.03	1822	29
100	9582	5.05454	2.38	0.32837	1.00	0.42	1830	16	1829	20	1826	39	1.00	1826	39
189	13936	5.12215	1.93	0.33270	1.18	0.61	1851	19	1840	16	1827	28	1.01	1827	28
342	21958	4.48376	2.83	0.29123	1.00	0.35	1648	15	1728	23	1827	48	0.90	1827	48
298	16526	5.09035	1.58	0.32945	1.03	0.65	1836	16	1834	13	1833	22	1.00	1833	22
463	25384	4.59584	1.59	0.29744	1.00	0.63	1679	15	1749	13	1833	22	0.92	1833	22
455	28384	4.94158	1.42	0.31819	1.00	0.71	1781	16	1809	12	1842	18	0.97	1842	18
132	12571	5.21251	1.88	0.33461	1.23	0.66	1861	20	1855	16	1848	26	1.01	1848	26
146	12224	5.17455	1.72	0.33111	1.10	0.64	1844	18	1848	15	1854	24	0.99	1854	24
340	23228	4.80266	1.42	0.30722	1.01	0.71	1727	15	1785	12	1854	18	0.93	1854	18
688	43823	5.29792	1.56	0.33700	1.00	0.64	1872	16	1869	13	1864	22	1.00	1864	22
414	33141	4.97424	1.94	0.31496	1.54	0.79	1765	24	1815	16	1873	21	0.94	1873	21
634	64177	5.35703	1.41	0.33896	1.00	0.71	1882	16	1878	12	1874	18	1.00	1874	18
315	30235	5.60571	2.02	0.35445	1.00	0.49	1956	17	1917	17	1875	32	1.04	1875	32
175	15893	5.35631	1.59	0.33856	1.00	0.63	1880	16	1878	14	1876	22	1.00	1876	22
175	17476	5.43296	2.05	0.34237	1.00	0.49	1898	16	1890	18	1881	32	1.01	1881	32
176	14951	5.47082	1.61	0.34411	1.00	0.62	1906	17	1896	14	1885	23	1.01	1885	23
609	45214	5.52377	1.41	0.34715	1.00	0.71	1921	17	1904	12	1886	18	1.02	1886	18
278	16505	5.60621	1.85	0.35122	1.00	0.54	1940	17	1917	16	1892	28	1.03	1892	28
374	24768	5.67712	1.61	0.35556	1.00	0.62	1961	17	1928	14	1892	23	1.04	1892	23
420	16985	5.17608	1.51	0.32396	1.00	0.66	1809	16	1849	13	1894	20	0.96	1894	20
97	9760	5.54698	1.69	0.34715	1.36	0.81	1921	23	1908	15	1894	18	1.01	1894	18
228	18859	5.66053	1.61	0.35384	1.00	0.62	1953	17	1925	14	1896	23	1.03	1896	23
334	21219	5.17283	4.22	0.32323	3.91	0.93	1805	62	1848	36	1897	28	0.95	1897	28
286	21168	5.44763	2.55	0.33996	1.29	0.51	1887	21	1892	22	1899	40	0.99	1899	40

476	35737	5.38823	1.41	0.33609	1.00	0.71	1868	16	1883	12	1900	18	0.98	1900	18
194	14825	5.56936	2.20	0.34738	1.60	0.73	1922	27	1911	19	1900	27	1.01	1900	27
142	14385	5.04758	7.44	0.31479	7.29	0.98	1764	113	1827	63	1900	26	0.93	1900	26
399	35083	5.37783	2.04	0.33537	1.49	0.73	1864	24	1881	18	1900	25	0.98	1900	25
221	9742	5.31334	1.42	0.33118	1.00	0.71	1844	16	1871	12	1901	18	0.97	1901	18
216	20311	5.75861	1.65	0.35890	1.00	0.61	1977	17	1940	14	1901	24	1.04	1901	24
274	19166	5.49059	1.66	0.34213	1.33	0.80	1897	22	1899	14	1902	18	1.00	1902	18
152	12780	5.67512	1.41	0.35346	1.00	0.71	1951	17	1928	12	1902	18	1.03	1902	18
312	29445	5.65000	1.98	0.35187	1.26	0.64	1944	21	1924	17	1902	28	1.02	1902	28
278	23695	5.74208	1.64	0.35759	1.09	0.67	1971	19	1938	14	1903	22	1.04	1903	22
416	32624	5.47085	1.41	0.34055	1.00	0.71	1889	16	1896	12	1903	18	0.99	1903	18
328	34676	5.45839	1.57	0.33948	1.21	0.77	1884	20	1894	13	1905	18	0.99	1905	18
403	35290	5.50084	1.43	0.34202	1.00	0.70	1896	16	1901	12	1905	18	1.00	1905	18
286	25640	5.51823	1.41	0.34307	1.00	0.71	1901	16	1903	12	1906	18	1.00	1906	18
745	43661	4.81380	1.61	0.29906	1.26	0.78	1687	19	1787	14	1907	18	0.88	1907	18
339	30022	5.66664	1.41	0.35202	1.00	0.71	1944	17	1926	12	1907	18	1.02	1907	18
227	22437	5.57425	1.42	0.34621	1.00	0.71	1916	17	1912	12	1907	18	1.00	1907	18
501	33006	5.25583	1.44	0.32637	1.00	0.70	1821	16	1862	12	1908	19	0.95	1908	19
519	45834	5.64544	1.43	0.35053	1.00	0.70	1937	17	1923	12	1908	18	1.02	1908	18
189	18283	5.60327	1.58	0.34790	1.00	0.63	1925	17	1917	14	1908	22	1.01	1908	22
504	45074	5.72532	1.50	0.35531	1.00	0.67	1960	17	1935	13	1909	20	1.03	1909	20
571	39502	5.12461	1.46	0.31775	1.00	0.69	1779	16	1840	12	1910	19	0.93	1910	19
200	19858	5.52905	1.64	0.34278	1.19	0.72	1900	20	1905	14	1911	20	0.99	1911	20
341	29656	5.58306	1.41	0.34612	1.00	0.71	1916	17	1913	12	1911	18	1.00	1911	18
199	19646	5.83880	1.42	0.36194	1.00	0.71	1991	17	1952	12	1911	18	1.04	1911	18
457	40317	5.61243	1.41	0.34774	1.00	0.71	1924	17	1918	12	1912	18	1.01	1912	18
246	16782	5.48689	1.85	0.33990	1.00	0.54	1886	16	1899	16	1912	28	0.99	1912	28
407	27628	5.68313	1.41	0.35197	1.00	0.71	1944	17	1929	12	1912	18	1.02	1912	18
115	9166	5.78962	1.42	0.35838	1.00	0.70	1974	17	1945	12	1913	18	1.03	1913	18
212	18860	5.74132	1.67	0.35534	1.34	0.80	1960	23	1938	14	1914	18	1.02	1914	18
473	35637	5.67523	1.69	0.35124	1.00	0.59	1941	17	1928	15	1914	24	1.01	1914	24
585	35144	5.46652	2.08	0.33819	1.24	0.60	1878	20	1895	18	1914	30	0.98	1914	30
975	80405	5.55378	2.11	0.34355	1.73	0.82	1904	29	1909	18	1915	22	0.99	1915	22
828	62572	5.67947	1.41	0.35125	1.00	0.71	1941	17	1928	12	1915	18	1.01	1915	18
341	38412	5.71902	2.51	0.35367	1.76	0.70	1952	30	1934	22	1915	32	1.02	1915	32
407	26937	5.45092	1.47	0.33707	1.00	0.68	1873	16	1893	13	1915	19	0.98	1915	19
705	51992	5.58856	1.41	0.34554	1.00	0.71	1913	17	1914	12	1915	18	1.00	1915	18
276	19230	5.75485	2.17	0.35560	1.81	0.83	1961	31	1940	19	1917	22	1.02	1917	22
609	32048	5.48230	3.21	0.33873	2.87	0.89	1881	47	1898	28	1917	26	0.98	1917	26
214	18233	5.65798	1.45	0.34938	1.00	0.69	1932	17	1925	13	1918	19	1.01	1918	19
637	36945	5.43625	1.41	0.33558	1.00	0.71	1865	16	1891	12	1918	18	0.97	1918	18
598	32869	5.43971	1.57	0.33567	1.17	0.74	1866	19	1891	13	1919	19	0.97	1919	19
289	29840	5.68174	1.71	0.35058	1.39	0.81	1937	23	1929	15	1919	18	1.01	1919	18

1023	46134	4.34357	11.00	0.26791	10.82	0.98	1530	147	1702	91	1920	36	0.80	1920	36
270	26641	5.94655	1.78	0.36677	1.00	0.56	2014	17	1968	15	1920	26	1.05	1920	26
580	49404	5.76550	1.41	0.35558	1.00	0.71	1961	17	1941	12	1920	18	1.02	1920	18
972	52736	5.05853	2.57	0.31196	2.20	0.86	1750	34	1829	22	1920	24	0.91	1920	24
123	9252	5.46362	1.42	0.33690	1.00	0.71	1872	16	1895	12	1920	18	0.97	1920	18
451	29658	5.72789	1.93	0.35313	1.00	0.52	1950	17	1936	17	1921	30	1.02	1921	30
521	38051	5.13031	2.24	0.31614	1.66	0.74	1771	26	1841	19	1922	27	0.92	1922	27
521	35654	5.29774	1.61	0.32630	1.26	0.78	1820	20	1868	14	1922	18	0.95	1922	18
350	20311	5.48871	1.56	0.33801	1.00	0.64	1877	16	1899	13	1923	22	0.98	1923	22
694	39403	5.52498	2.11	0.34006	1.00	0.47	1887	16	1904	18	1924	33	0.98	1924	33
288	24658	5.78060	1.71	0.35567	1.27	0.74	1962	21	1944	15	1924	21	1.02	1924	21
470	38098	5.44224	1.55	0.33438	1.00	0.65	1860	16	1892	13	1927	21	0.97	1927	21
254	21652	5.84415	1.64	0.35889	1.30	0.79	1977	22	1953	14	1928	18	1.03	1928	18
476	29063	5.64058	2.51	0.34579	2.20	0.88	1914	36	1922	22	1931	22	0.99	1931	22
334	24153	5.76147	3.22	0.35313	2.94	0.91	1950	49	1941	28	1931	24	1.01	1931	24
929	71581	5.90616	1.47	0.36189	1.00	0.68	1991	17	1962	13	1932	19	1.03	1932	19
386	17267	5.82923	1.58	0.35666	1.00	0.63	1966	17	1951	14	1934	22	1.02	1934	22
346	27937	5.88072	1.56	0.35977	1.00	0.64	1981	17	1958	14	1934	21	1.02	1934	21
316	18551	5.47917	2.96	0.33512	2.79	0.94	1863	45	1897	25	1935	18	0.96	1935	18
272	14026	5.39750	4.48	0.32994	4.32	0.97	1838	69	1884	38	1936	21	0.95	1936	21
653	42195	5.52216	1.90	0.33731	1.00	0.53	1874	16	1904	16	1937	29	0.97	1937	29
732	44321	5.42583	1.55	0.33135	1.00	0.64	1845	16	1889	13	1938	21	0.95	1938	21
485	42949	5.73825	1.41	0.35025	1.00	0.71	1936	17	1937	12	1939	18	1.00	1939	18
191	13256	5.77188	1.48	0.35143	1.09	0.74	1941	18	1942	13	1943	18	1.00	1943	18
200	11424	4.55435	5.13	0.27720	4.61	0.90	1577	65	1741	43	1944	40	0.81	1944	40
302	25399	5.73173	2.13	0.34641	1.00	0.47	1917	17	1936	18	1956	34	0.98	1956	34
454	45746	6.01775	1.41	0.36174	1.00	0.71	1990	17	1978	12	1966	18	1.01	1966	18
729	25483	5.16099	4.68	0.30907	4.42	0.94	1736	67	1846	40	1973	27	0.88	1973	27
449	45616	6.24842	1.46	0.37230	1.00	0.69	2040	17	2011	13	1982	19	1.03	1982	19
540	39741	5.74426	1.41	0.34092	1.00	0.71	1891	16	1938	12	1989	18	0.95	1989	18
221	20071	5.83401	3.40	0.34477	1.81	0.53	1910	30	1951	30	1996	51	0.96	1996	51
562	45033	6.20229	1.41	0.36511	1.00	0.71	2006	17	2005	12	2003	18	1.00	2003	18
108	6978	5.74012	1.47	0.33639	1.06	0.72	1869	17	1937	13	2011	18	0.93	2011	18
227	15618	6.29533	1.52	0.36547	1.00	0.66	2008	17	2018	13	2028	20	0.99	2028	20
316	32921	6.50273	1.41	0.37689	1.00	0.71	2062	18	2046	12	2031	18	1.02	2031	18
315	26069	6.64897	1.93	0.38150	1.00	0.52	2083	18	2066	17	2049	29	1.02	2049	29
196	19604	6.64987	1.42	0.37914	1.00	0.71	2072	18	2066	12	2060	18	1.01	2060	18
486	33279	6.19572	1.70	0.34854	1.00	0.59	1928	17	2004	15	2083	24	0.93	2083	24
589	34343	5.92447	6.52	0.33250	4.01	0.62	1851	65	1965	57	2087	90	0.89	2087	90
275	18532	6.36796	2.18	0.35294	1.67	0.77	1949	28	2028	19	2109	25	0.92	2109	25
316	26592	6.94728	2.80	0.38177	1.00	0.36	2085	18	2105	25	2124	46	0.98	2124	46
736	44712	5.70417	5.96	0.31305	5.51	0.93	1756	85	1932	51	2127	40	0.83	2127	40
357	28324	6.90652	2.21	0.37850	1.00	0.45	2069	18	2099	20	2129	34	0.97	2129	34

361	40498	6.93259	2.07	0.37870	1.00	0.48	2070	18	2103	18	2135	32	0.97	2135	32
434	25260	5.85780	2.21	0.31443	1.60	0.72	1762	25	1955	19	2166	27	0.81	2166	27
257	26767	7.57592	3.15	0.40208	1.55	0.49	2179	29	2182	28	2185	48	1.00	2185	48
433	22221	7.85162	2.38	0.41221	1.34	0.56	2225	25	2214	21	2204	34	1.01	2204	34
338	20833	7.05794	2.41	0.36943	1.06	0.44	2027	18	2119	21	2209	38	0.92	2209	38
124	14381	8.10867	1.49	0.42197	1.00	0.67	2269	19	2243	14	2219	19	1.02	2219	19
196	17758	7.68770	2.58	0.39757	2.08	0.81	2158	38	2195	23	2230	27	0.97	2230	27
102	13091	8.30100	1.58	0.42493	1.00	0.63	2283	19	2264	14	2248	21	1.02	2248	21
402	35361	7.93988	3.12	0.40425	1.03	0.33	2189	19	2224	28	2257	51	0.97	2257	51
747	64328	8.88887	3.93	0.44503	3.11	0.79	2373	62	2327	36	2286	41	1.04	2286	41
483	41119	8.49440	1.88	0.41864	1.38	0.74	2254	26	2285	17	2313	22	0.97	2313	22
236	22065	7.80004	1.43	0.37986	1.02	0.71	2076	18	2208	13	2334	17	0.89	2334	17
336	35156	8.89805	1.85	0.43115	1.43	0.77	2311	28	2328	17	2342	20	0.99	2342	20
241	22653	9.35810	1.41	0.44950	1.00	0.71	2393	20	2374	13	2357	17	1.02	2357	17
467	49695	8.91830	1.46	0.42440	1.00	0.68	2280	19	2330	13	2373	18	0.96	2373	18
538	47593	9.24269	3.90	0.43896	2.02	0.52	2346	40	2362	36	2377	57	0.99	2377	57
124	17176	9.78670	1.41	0.46172	1.00	0.71	2447	20	2415	13	2388	17	1.02	2388	17
104	13087	9.96281	1.94	0.46925	1.66	0.86	2480	34	2431	18	2391	17	1.04	2391	17
783	88452	9.84823	1.80	0.45874	1.00	0.55	2434	20	2421	17	2409	25	1.01	2409	25
693	42007	8.33071	4.81	0.38040	1.00	0.21	2078	18	2268	44	2443	80	0.85	2443	80
76	7890	9.93253	1.42	0.44787	1.00	0.70	2386	20	2429	13	2465	17	0.97	2465	17
477	61435	10.59911	2.41	0.47146	1.43	0.59	2490	30	2489	22	2488	33	1.00	2488	33
356	38856	10.39074	2.51	0.45951	1.00	0.40	2437	20	2470	23	2497	39	0.98	2497	39
589	49758	9.87460	2.76	0.43636	2.08	0.75	2334	41	2423	25	2499	31	0.93	2499	31
516	54977	10.55048	1.82	0.46492	1.52	0.84	2461	31	2484	17	2503	17	0.98	2503	17
438	50835	11.02207	1.62	0.48569	1.16	0.72	2552	24	2525	15	2503	19	1.02	2503	19
228	20199	10.70599	1.63	0.46745	1.11	0.68	2472	23	2498	15	2519	20	0.98	2519	20
782	52763	10.69395	3.31	0.46552	3.01	0.91	2464	62	2497	31	2524	23	0.98	2524	23
932	80239	11.05779	1.92	0.48108	1.32	0.69	2532	28	2528	18	2525	24	1.00	2525	24
280	25492	10.46292	1.44	0.45403	1.00	0.70	2413	20	2477	13	2529	17	0.95	2529	17
396	37176	10.58262	1.72	0.45770	1.00	0.58	2429	20	2487	16	2535	23	0.96	2535	23
307	29780	10.86399	2.53	0.46884	1.68	0.66	2478	35	2512	24	2538	32	0.98	2538	32
246	30945	11.70167	1.73	0.50399	1.41	0.82	2631	30	2581	16	2542	17	1.04	2542	17
110	11753	10.91751	5.65	0.46672	5.50	0.97	2469	113	2516	53	2554	22	0.97	2554	22
76	12191	11.88819	1.75	0.50679	1.24	0.71	2643	27	2596	16	2559	21	1.03	2559	21
141	19370	11.88210	1.41	0.50537	1.00	0.71	2637	22	2595	13	2563	17	1.03	2563	17
565	45260	10.38622	1.91	0.44148	1.39	0.73	2357	27	2470	18	2564	22	0.92	2564	22
374	43758	11.66867	1.49	0.49444	1.00	0.67	2590	21	2578	14	2569	19	1.01	2569	19
398	43350	11.01575	3.38	0.46526	2.98	0.88	2463	61	2524	31	2574	27	0.96	2574	27
333	25457	11.38063	1.63	0.48009	1.15	0.70	2528	24	2555	15	2576	19	0.98	2576	19
380	34169	11.32346	1.65	0.47754	1.31	0.79	2517	27	2550	15	2577	17	0.98	2577	17
155	14182	9.80210	2.24	0.41315	1.57	0.70	2229	30	2416	21	2578	27	0.86	2578	27
72	9435	11.69598	1.49	0.49041	1.10	0.74	2572	23	2580	14	2587	17	0.99	2587	17

404	41781	12.33962	3.05	0.51658	1.76	0.58	2685	39	2631	29	2589	42	1.04	2589	42
418	42983	12.28759	1.54	0.51117	1.00	0.65	2662	22	2627	14	2600	20	1.02	2600	20
213	29871	12.03874	1.68	0.50026	1.00	0.60	2615	21	2607	16	2602	23	1.01	2602	23
97	8106	10.51285	1.50	0.43679	1.04	0.69	2336	20	2481	14	2602	18	0.90	2602	18
135	19859	13.18117	2.41	0.52587	2.19	0.91	2724	49	2693	23	2669	17	1.02	2669	17
524	70357	13.87237	2.03	0.53719	1.56	0.77	2772	35	2741	19	2719	21	1.02	2719	21
241	34540	13.75199	1.80	0.53245	1.50	0.83	2752	34	2733	17	2719	16	1.01	2719	16
504	53437	13.62567	1.81	0.52655	1.00	0.55	2727	22	2724	17	2722	25	1.00	2722	25
258	45679	17.91657	1.81	0.60354	1.00	0.55	3044	24	2985	17	2946	24	1.03	2946	24
464	55045	22.86169	1.97	0.61891	1.70	0.86	3106	42	3221	19	3294	16	0.94	3294	16
518	82235	26.87348	1.48	0.68445	1.00	0.68	3361	26	3379	14	3389	17	0.99	3389	17

Sample 406102 – Kushma Fm (Lat, Long = 28.23082°, 83.68118°)

185	7504	3.99509	1.77	0.27293	1.45	0.82	1556	20	1633	14	1735	19	0.90	1735	19
702	18520	3.57136	2.44	0.24204	2.18	0.89	1397	27	1543	19	1749	20	0.80	1749	20
183	14152	4.07971	1.77	0.27609	1.00	0.56	1572	14	1650	14	1752	27	0.90	1752	27
351	32252	4.25295	2.66	0.28736	2.10	0.79	1628	30	1684	22	1755	30	0.93	1755	30
356	12787	4.16873	1.62	0.28147	1.01	0.63	1599	14	1668	13	1756	23	0.91	1756	23
563	37554	3.94270	3.52	0.26512	3.25	0.92	1516	44	1622	29	1764	25	0.86	1764	25
963	49448	3.69448	1.41	0.24809	1.00	0.71	1429	13	1570	11	1766	18	0.81	1766	18
740	27759	3.67196	5.09	0.24590	4.95	0.97	1417	63	1565	41	1771	22	0.80	1771	22
758	23460	3.90341	4.21	0.26133	3.92	0.93	1497	52	1614	34	1772	28	0.84	1772	28
345	28018	4.32199	1.43	0.28908	1.00	0.70	1637	14	1698	12	1773	19	0.92	1773	19
279	9603	4.63653	2.08	0.30936	1.00	0.48	1738	15	1756	17	1778	33	0.98	1778	33
801	37514	4.05965	2.11	0.27054	1.12	0.53	1544	15	1646	17	1780	33	0.87	1780	33
463	41638	4.40820	1.75	0.29376	1.18	0.67	1660	17	1714	14	1780	24	0.93	1780	24
819	49993	4.30500	1.58	0.28672	1.00	0.63	1625	14	1694	13	1781	22	0.91	1781	22
576	26173	4.31714	2.57	0.28727	2.37	0.92	1628	34	1697	21	1783	18	0.91	1783	18
329	16693	4.74969	2.02	0.31558	1.00	0.50	1768	15	1776	17	1785	32	0.99	1785	32
230	23540	4.73214	1.69	0.31422	1.00	0.59	1761	15	1773	14	1786	25	0.99	1786	25
213	23420	4.73452	1.73	0.31426	1.25	0.72	1762	19	1773	15	1787	22	0.99	1787	22
260	14316	4.56332	2.64	0.30289	1.00	0.38	1706	15	1743	22	1787	44	0.95	1787	44
125	14424	4.79172	1.55	0.31802	1.00	0.64	1780	16	1783	13	1787	22	1.00	1787	22
247	18381	4.64407	2.63	0.30804	2.19	0.83	1731	33	1757	22	1788	26	0.97	1788	26
380	19305	4.61506	1.70	0.30603	1.00	0.59	1721	15	1752	14	1789	25	0.96	1789	25
191	7725	4.41570	1.64	0.29274	1.00	0.61	1655	15	1715	14	1789	24	0.93	1789	24
192	14886	4.96671	1.45	0.32910	1.00	0.69	1834	16	1814	12	1790	19	1.02	1790	19
445	18194	3.83488	2.99	0.25367	2.82	0.94	1457	37	1600	24	1793	18	0.81	1793	18
683	39891	3.88028	7.05	0.25655	6.98	0.99	1472	92	1610	57	1794	18	0.82	1794	18
358	8850	3.92576	1.42	0.25944	1.00	0.70	1487	13	1619	11	1795	18	0.83	1795	18
169	14933	4.70962	1.42	0.31121	1.00	0.71	1747	15	1769	12	1795	18	0.97	1795	18
310	13558	4.56422	1.88	0.30159	1.00	0.53	1699	15	1743	16	1795	29	0.95	1795	29
265	19902	4.52185	2.25	0.29811	1.00	0.45	1682	15	1735	19	1800	37	0.93	1800	37

329	29875	4.70442	2.79	0.30948	1.85	0.66	1738	28	1768	23	1803	38	0.96	1803	38
827	39597	3.67812	2.82	0.24145	2.64	0.94	1394	33	1567	23	1807	18	0.77	1807	18
601	25329	4.32514	2.15	0.28346	1.90	0.88	1609	27	1698	18	1810	18	0.89	1810	18
609	45994	4.23812	4.60	0.27762	4.49	0.98	1579	63	1681	38	1811	18	0.87	1811	18
233	18602	4.54823	1.91	0.29780	1.00	0.52	1680	15	1740	16	1812	30	0.93	1812	30
280	13880	4.69912	1.55	0.30763	1.00	0.64	1729	15	1767	13	1812	22	0.95	1812	22
166	19265	4.89824	1.93	0.32056	1.03	0.53	1792	16	1802	16	1813	30	0.99	1813	30
363	16283	4.34767	1.77	0.28449	1.10	0.62	1614	16	1702	15	1813	25	0.89	1813	25
951	28356	3.93803	1.41	0.25766	1.00	0.71	1478	13	1622	11	1813	18	0.81	1813	18
277	15622	4.30911	1.78	0.28193	1.00	0.56	1601	14	1695	15	1813	27	0.88	1813	27
422	22577	4.60584	1.71	0.30118	1.00	0.58	1697	15	1750	14	1814	25	0.94	1814	25
406	34021	4.71752	1.55	0.30822	1.00	0.65	1732	15	1770	13	1816	21	0.95	1816	21
211	13491	4.74295	2.06	0.30977	1.36	0.66	1740	21	1775	17	1817	28	0.96	1817	28
628	20422	4.55078	1.55	0.29718	1.00	0.65	1677	15	1740	13	1817	21	0.92	1817	21
582	46600	4.71254	2.80	0.30746	2.33	0.83	1728	35	1769	23	1819	28	0.95	1819	28
517	48208	4.81391	1.59	0.31370	1.24	0.78	1759	19	1787	13	1821	18	0.97	1821	18
357	20458	4.68253	1.90	0.30508	1.00	0.53	1716	15	1764	16	1821	29	0.94	1821	29
790	28313	3.95354	3.05	0.25659	2.82	0.92	1472	37	1625	25	1828	21	0.81	1828	21
391	12893	4.75162	2.36	0.30767	1.82	0.77	1729	28	1776	20	1832	27	0.94	1832	27
455	30306	4.92036	2.42	0.31842	1.00	0.41	1782	16	1806	20	1833	40	0.97	1833	40
336	13517	5.06443	2.13	0.32772	1.00	0.47	1827	16	1830	18	1833	34	1.00	1833	34
1022	32716	4.42412	1.97	0.28585	1.09	0.55	1621	16	1717	16	1836	30	0.88	1836	30
617	15517	3.91601	3.35	0.25290	1.95	0.58	1453	25	1617	27	1837	49	0.79	1837	49
199	17659	4.68096	2.52	0.30226	1.02	0.40	1702	15	1764	21	1837	42	0.93	1837	42
496	18161	4.63598	1.96	0.29896	1.00	0.51	1686	15	1756	16	1840	30	0.92	1840	30
802	26874	4.77141	6.57	0.30735	5.08	0.77	1728	77	1780	55	1842	75	0.94	1842	75
231	7164	4.48075	2.82	0.28853	1.71	0.61	1634	25	1727	23	1842	41	0.89	1842	41
179	22196	5.00367	1.88	0.32193	1.00	0.53	1799	16	1820	16	1844	29	0.98	1844	29
414	25411	4.97921	2.27	0.31897	1.16	0.51	1785	18	1816	19	1852	35	0.96	1852	35
792	37687	4.43254	2.49	0.28284	1.55	0.62	1606	22	1718	21	1859	35	0.86	1859	35
543	18915	4.75875	1.47	0.30155	1.00	0.68	1699	15	1778	12	1871	19	0.91	1871	19
244	12013	4.65777	1.88	0.29469	1.00	0.53	1665	15	1760	16	1874	29	0.89	1874	29
283	11929	4.84100	1.67	0.30544	1.00	0.60	1718	15	1792	14	1879	24	0.91	1879	24
248	18222	5.59661	1.41	0.35181	1.00	0.71	1943	17	1916	12	1886	18	1.03	1886	18
608	58236	4.91793	1.53	0.30873	1.00	0.65	1734	15	1805	13	1888	21	0.92	1888	21
310	23863	5.26897	1.54	0.33056	1.17	0.76	1841	19	1864	13	1889	18	0.97	1889	18
387	47605	5.25551	1.41	0.32946	1.00	0.71	1836	16	1862	12	1891	18	0.97	1891	18
274	13449	4.41425	2.01	0.27639	1.74	0.87	1573	24	1715	17	1893	18	0.83	1893	18
130	13088	5.13824	1.71	0.32126	1.00	0.58	1796	16	1842	15	1895	25	0.95	1895	25
284	13672	5.25798	1.42	0.32796	1.00	0.71	1828	16	1862	12	1900	18	0.96	1900	18
583	17701	4.96598	1.41	0.30875	1.00	0.71	1735	15	1814	12	1906	18	0.91	1906	18
229	12301	4.85388	2.94	0.30156	2.76	0.94	1699	41	1794	25	1907	18	0.89	1907	18
692	32868	4.68083	2.05	0.29013	1.00	0.49	1642	14	1764	17	1911	32	0.86	1911	32

386	37021	5.20243	1.85	0.32138	1.29	0.70	1796	20	1853	16	1917	24	0.94	1917	24
388	27421	5.15771	1.41	0.31625	1.00	0.71	1771	15	1846	12	1930	18	0.92	1930	18
659	31468	5.24594	2.48	0.32093	2.27	0.92	1794	36	1860	21	1935	18	0.93	1935	18
245	24480	5.52233	2.60	0.33719	1.96	0.75	1873	32	1904	22	1938	30	0.97	1938	30
351	13978	4.97112	1.89	0.30279	1.45	0.77	1705	22	1814	16	1942	22	0.88	1942	22
583	24448	4.80202	1.59	0.29244	1.00	0.63	1654	15	1785	13	1943	22	0.85	1943	22
336	11124	4.57250	2.93	0.27689	2.53	0.86	1576	35	1744	24	1953	26	0.81	1953	26
329	18402	5.84084	1.74	0.34823	1.00	0.58	1926	17	1952	15	1981	25	0.97	1981	25
642	17007	4.60406	2.99	0.27366	2.82	0.94	1559	39	1750	25	1986	18	0.79	1986	18
425	42199	5.67492	2.49	0.33267	1.50	0.60	1851	24	1928	22	2011	35	0.92	2011	35
881	43557	5.07487	10.08	0.29484	10.00	0.99	1666	147	1832	86	2026	23	0.82	2026	23
148	8115	6.05948	2.03	0.34939	1.24	0.61	1932	21	1984	18	2040	28	0.95	2040	28
237	10304	6.47044	1.44	0.36429	1.00	0.69	2002	17	2042	13	2082	18	0.96	2082	18
295	10830	5.80291	1.65	0.31874	1.00	0.61	1784	16	1947	14	2125	23	0.84	2125	23
302	20350	7.10673	1.98	0.38919	1.31	0.66	2119	24	2125	18	2131	26	0.99	2131	26
368	27076	6.25070	2.47	0.32568	1.00	0.40	1817	16	2012	22	2217	39	0.82	2217	39
387	37889	7.33722	1.93	0.38204	1.47	0.76	2086	26	2153	17	2218	22	0.94	2218	22
123	9053	7.29063	2.05	0.37255	1.61	0.79	2041	28	2148	18	2251	22	0.91	2251	22
911	52374	7.94134	1.77	0.39906	1.00	0.57	2165	18	2224	16	2280	25	0.95	2280	25
343	31158	8.18101	1.64	0.39463	1.00	0.61	2144	18	2251	15	2350	22	0.91	2350	22
595	39802	9.44799	1.84	0.43936	1.21	0.66	2348	24	2383	17	2412	23	0.97	2412	23
465	33900	8.76030	2.01	0.39807	1.24	0.62	2160	23	2313	18	2451	27	0.88	2451	27
270	24911	10.10751	2.02	0.44799	1.47	0.73	2386	29	2445	19	2494	23	0.96	2494	23
559	35729	9.43780	1.90	0.41786	1.00	0.53	2251	19	2382	17	2495	27	0.90	2495	27
156	11343	9.23105	2.86	0.40652	2.40	0.84	2199	45	2361	26	2504	26	0.88	2504	26
420	27023	9.87075	3.48	0.43466	3.30	0.95	2327	64	2423	32	2505	18	0.93	2505	18
689	32722	8.46825	1.94	0.37056	1.39	0.72	2032	24	2283	18	2515	23	0.81	2515	23
547	24740	8.86558	3.53	0.38653	1.48	0.42	2107	27	2324	32	2521	54	0.84	2521	54
243	28930	11.13003	2.00	0.48477	1.73	0.87	2548	36	2534	19	2523	17	1.01	2523	17
335	43585	11.13759	1.90	0.47902	1.00	0.53	2523	21	2535	18	2544	27	0.99	2544	27
181	10794	9.95865	1.98	0.42814	1.00	0.50	2297	19	2431	18	2545	29	0.90	2545	29
159	18792	11.01834	2.31	0.47284	1.55	0.67	2496	32	2525	21	2548	29	0.98	2548	29
113	4921	9.97476	2.45	0.42745	1.00	0.41	2294	19	2432	23	2550	38	0.90	2550	38
218	22871	11.32644	1.74	0.48322	1.00	0.58	2541	21	2550	16	2558	24	0.99	2558	24
616	31558	10.87973	1.90	0.46169	1.03	0.54	2447	21	2513	18	2567	27	0.95	2567	27
359	36683	11.54088	1.47	0.48074	1.07	0.73	2530	22	2568	14	2598	17	0.97	2598	17
289	18468	11.01828	1.41	0.45848	1.00	0.71	2433	20	2525	13	2599	17	0.94	2599	17
63	12414	12.27508	1.42	0.49298	1.00	0.71	2584	21	2626	13	2658	17	0.97	2658	17
258	17974	11.69858	1.67	0.46248	1.00	0.60	2451	20	2581	16	2684	22	0.91	2684	22
678	33847	11.11985	5.24	0.43116	1.00	0.19	2311	19	2533	49	2716	85	0.85	2716	85
341	22083	12.92678	1.47	0.49243	1.00	0.68	2581	21	2674	14	2746	18	0.94	2746	18
278	41158	12.47589	3.33	0.46278	2.31	0.69	2452	47	2641	31	2789	39	0.88	2789	39
173	24233	13.62468	2.95	0.50499	1.00	0.34	2635	22	2724	28	2790	45	0.94	2790	45

303	37463	14.63241	2.76	0.52206	1.00	0.36	2708	22	2792	26	2853	42	0.95	2853	42
221	11445	12.86812	4.12	0.45530	1.03	0.25	2419	21	2670	39	2866	65	0.84	2866	65
202	21364	15.04269	4.40	0.52224	2.21	0.50	2709	49	2818	42	2897	62	0.93	2897	62
799	123872	16.49168	1.43	0.55313	1.00	0.70	2838	23	2906	14	2953	16	0.96	2953	16
217	13346	15.86391	2.42	0.51988	1.00	0.41	2699	22	2869	23	2990	35	0.90	2990	35
402	22745	14.60165	7.85	0.44958	7.28	0.93	2393	146	2790	75	3090	47	0.77	3090	47
272	35260	19.81526	1.41	0.60890	1.00	0.71	3066	24	3082	14	3093	16	0.99	3093	16
187	25411	20.59891	4.35	0.60533	3.32	0.76	3051	81	3120	42	3164	45	0.96	3164	45
541	79400	23.01154	2.39	0.63930	2.08	0.87	3186	52	3227	23	3253	19	0.98	3253	19

Sample 406020 – Unidentified sample (Lat, Long = 28.38187°, 83.80073°)

617	23248	4.28844	3.15	0.28279	1.00	0.32	1605	14	1691	26	1799	54	0.89	1799	54
63	6768	4.85940	5.58	0.31303	4.67	0.84	1756	72	1795	47	1842	55	0.95	1842	55
334	22828	5.13569	2.14	0.32500	1.00	0.47	1814	16	1842	18	1874	34	0.97	1874	34
316	17533	5.02149	2.25	0.31757	1.00	0.45	1778	16	1823	19	1875	36	0.95	1875	36
1191	30436	3.98662	4.47	0.25088	2.19	0.49	1443	28	1631	36	1884	70	0.77	1884	70
1005	26602	5.00331	1.57	0.31286	1.00	0.64	1755	15	1820	13	1895	22	0.93	1895	22
586	32183	5.18701	1.66	0.32298	1.00	0.60	1804	16	1850	14	1903	24	0.95	1903	24
427	29994	5.28227	1.66	0.32877	1.00	0.60	1832	16	1866	14	1904	24	0.96	1904	24
481	20472	4.72198	1.65	0.29350	1.00	0.61	1659	15	1771	14	1906	24	0.87	1906	24
771	46531	5.17165	1.75	0.32116	1.00	0.57	1795	16	1848	15	1908	26	0.94	1908	26
375	22937	5.28125	1.67	0.32277	1.00	0.60	1803	16	1866	14	1936	24	0.93	1936	24
387	15720	5.11488	2.42	0.30936	1.98	0.82	1738	30	1839	21	1955	25	0.89	1955	25
502	25032	5.54236	2.39	0.33140	1.64	0.69	1845	26	1907	21	1975	31	0.93	1975	31
184	8168	6.09649	2.68	0.35818	1.00	0.37	1974	17	1990	23	2007	44	0.98	2007	44
469	30798	6.39960	1.96	0.35855	1.00	0.51	1975	17	2032	17	2090	30	0.94	2090	30
43	6973	7.19554	2.47	0.40135	1.93	0.78	2175	36	2136	22	2098	27	1.04	2098	27
425	27362	6.54321	1.75	0.36382	1.00	0.57	2000	17	2052	15	2104	25	0.95	2104	25
436	24482	6.68588	5.49	0.36305	1.07	0.20	1997	18	2071	48	2145	94	0.93	2145	94
468	21485	6.37485	4.81	0.34496	4.12	0.86	1910	68	2029	42	2151	43	0.89	2151	43
398	21951	6.03807	3.66	0.32162	3.52	0.96	1798	55	1981	32	2179	17	0.82	2179	17
157	17146	7.70224	1.63	0.40649	1.00	0.61	2199	19	2197	15	2195	22	1.00	2195	22
206	10299	7.51050	1.47	0.39293	1.00	0.68	2136	18	2174	13	2210	19	0.97	2210	19
411	29052	9.00424	1.67	0.42619	1.00	0.60	2289	19	2338	15	2382	23	0.96	2382	23
314	14477	6.94502	4.01	0.32781	3.75	0.93	1828	60	2104	36	2387	24	0.77	2387	24
1353	75914	8.56405	3.28	0.38792	2.87	0.87	2113	52	2293	30	2457	27	0.86	2457	27
785	59391	9.83780	1.53	0.44446	1.00	0.65	2371	20	2420	14	2461	20	0.96	2461	20
457	38351	9.78517	2.39	0.44013	1.00	0.42	2351	20	2415	22	2469	37	0.95	2469	37
70	8122	10.96234	3.13	0.48103	2.29	0.73	2532	48	2520	29	2510	36	1.01	2510	36
214	18883	10.86886	1.50	0.47416	1.00	0.67	2502	21	2512	14	2520	19	0.99	2520	19
470	30679	10.22232	1.67	0.44488	1.00	0.60	2372	20	2455	15	2524	23	0.94	2524	23
504	44632	11.68696	1.44	0.48998	1.00	0.69	2571	21	2580	13	2587	17	0.99	2587	17
235	25125	12.65721	2.74	0.49362	1.18	0.43	2586	25	2654	26	2707	41	0.96	2707	41

400	30642	13.27228	2.31	0.51182	1.45	0.63	2664	32	2699	22	2725	30	0.98	2725	30
364	36858	13.87242	1.77	0.52393	1.00	0.57	2716	22	2741	17	2760	24	0.98	2760	24

* = radiogenic Pb. All errors are reported at the 1-sigma level.

U concentration has an uncertainty of ~ 25%.

References

Achache, J., Courtillot, V., and Xiu, Y., 1984, Paleogeographic and tectonic evolution of southern Tibet since middle Cretaceous time: New paleomagnetic data and synthesis: Journal of Geophysical Research, v. 89, p. 10,311–10,339.

Aharon, P., Schidlowski, M., Singh, I.B., 1987, Chronostratigraphic markers in the end-Precambrian carbon isotope record of the Lesser Himalaya: Nature, v. 327, p. 699–702.

Alley, R.B. and Cuffey, K.M., 2001, Oxygen- and Hydrogen- Isotopic Ratios of Water in Precipitation: Beyond Paleothermometry *in* Valley, J.W. and Cole, D.R., eds. Stable Isotope Geochemistry: Reviews in Mineralogy and Geochemistry, v. 43, p. 527-553.

Anbar, A.D., and Knoll, A.H., 2002, Proterozoic ocean chemistry and evolution: A bioinorganic bridge?: Science, v. 297, p. 1137-1142.

Anderson, T., 2005, Detrital zircons as tracers of sedimentary provenance: limiting conditions from statistics and numerical simulation: Chemical Geology, v. 216, p. 249-270.

Arita, K., 1983, Origin of the inverted metamorphism of the Lower Himalayas, central Nepal: Tectonophysics, v. 95, p. 43-60.

Armstrong, F.C., and Oriel, S.S., 1965, Tectonic development of Idaho-Wyoming thrust belt: AAPG Bulletin, v, 71, p.1847-1866.

Bally, A.W., Gordy, P.L., and Stewart, G.A., 1966, Structure, seismic data, and orogenic evolution of the southern Canadian Rocky Mountains: Can. J. Pet. Geol., v. 14, p. 337-381.

Banner, J.L. and Hanson, G.N., 1990, Calculation of simultaneous isotopic and trace element variations during water-rock interaction with applications to carbonate diagenesis: Geochimica et Cosmochemica Acta, v. 54, p. 3123-3137.

Baumgartner, L.P., and Valley, J.W., 2003, Stable isotope transport and contact metamorphic fluid flow *in* Valley, J.W. and Cole, D.R., eds. Stable Isotope Geochemistry: Reviews in Mineralogy and Geochemistry, v. 43, p. 415-467.

Beaumont, C., Jamieson, R.A., Nyugen, M.H., and Lee, B., 2001, Himalayan tectonics explained by extrusion of a low-viscosity crustal channel coupled to focused surface denudation: Nature, v.

414, p. 738-742.

Belousova, E.A., Griffin, W.L., O'Reilly, S.Y., and Fisher, N.I., 2002, Igneous zircon: trace element composition as an indicator of source rock type: Contrib. Mineral. Petr., v.143, p.602-622.

Berner, R.A., 2001, Modeling atmospheric O2 over Phanerozoic time: Geochim. Cosmochim. Acta, v. 65, p. 685–694.

Besse, J., and Courtillot, V., 1988, Paleogeographic maps of the continents bordering the Indian Ocean since the Early Jurassic: Journal of Geophysical Research, v. 93, p. 11,791–11,808.

Besse, J., Courtillot, V., Pozzi, J.P., Westphal, M., and Zhou, Y.X., 1984, Palaeomagnetic estimates of crustal shortening in the Himalayan thrusts and Zangbo Suture: Nature, v. 311, p. 621–626, doi: 10.1038/311621a0.

Beyssac, O., Bollinger, L., Avouac, J.-P., and Goffe, B., 2004, Thermal metamorphism in the Lesser Himalaya of Nepal determined from Raman spectroscopy of carbonaceous material: Earth and Planetary Science Letters, v. 225, p. 233-241.

Bigelesien, J., 1965, Chemistry of Isotopes: Science, v. 147, p. 463-471.

Bilham, R., Larson, D., and Freymuller, J., 1997, Indo-Asian convergence rates in the Nepal Himalaya: Nature, v. 386, p. 61–64, doi: 10.1038/386061a0.

Bollinger, L., Henry. P., and Avouac, J.P., 2006, Mountain building in the Nepal Himalaya: Thermal and kinematic model: Earth and Planetary Science Letters, v. 244, p.58–71.

Bollinger, L., Avouac, J.-P., Beyssac, O., Catlos, E. J., Harrison, T. M., Grove, M., Goffe, B., and Sapkota, S., 2004, Thermal structure and exhumation history of the Lesser Himalaya in central Nepal: Tectonics, v. 23, TC5015.

Bombolakis, E. G., 1986, Thrust-fault mechanics and origin of a frontal ramp: Journal of Structural Geology, v. 8, p. 281-290.

Broeker, W.S., 1970, A boundary condition on the evolution of atmospheric oxygen: Journal of Geophysical Research, v. 75, p. 3553-3557.

Buick, R., Des Marais, D.J., and Knoll, A.H., 1995, Stable isotopic compositions of carbonates from the Mesoproterozoic Bangemall Group, northwestern Australia: Chemical Geology, v. 123, p. 153-

171.

Burdett, J.W., Grotzinger, J.P., and Arthur, M.A., 1990, Did major changes in the stable isotope composition of Proterozoic seawater occur?: Geology, v. 18, p. 227–230.

Butler, R.W.H., 1987, Thrust sequences: Journal of the Geological Society, London, v. 144, pp. 619-634.

Carson, C.J., Ague, J.J., Grove, M., Coath, C.D., and Harrison, T.M., 2002a, U-Pb isotopic behaviour of zircon during upper-amphibolite facies fluid infiltration in the Napier Complex, east Antarctica: Earth and Planetary Science Letters, v. 199, p. 287-310.

Carson, C.J., Ague, J.J., and Coath, C. D., 2002b, U-Pb geochronology from Tonagh Island, East Antarctica: implications for the timing of ultra-high temperature metamorphism of the Napier Complex: Precambrian Research, v.116, p. 237-263.

Catlos, E. J., Harrison, T. M., Kohn, M. J., Grove, M., Ryerson, F. J., Manning, C. E., and Upreti, B. N., 2001, Geochronologic and thermobarometric constraints on the evolution of the Main Central Thrust, central Nepal Himalaya: Journal of Geophysical Research, B, Solid Earth and Planets, v. 106, p. 16,177-16,204.

Cawood, P.A., Nemchin, A.A., Freeman, M., and Sircombe, K., 2003, Linking source and sedimentary basin: Detrital zircon record of sediment flux along a modern river system and implications for provenance studies: Earth and Planetary Science Letters, v. 210, p. 259-268.

Chapple, W.M., 1978, Mechanics of thin-skinned fold-and-thrust belts: GSA Bulletin, v. 89, p. 1189-1198.

Cherniak, D.J., and Watson, E.B., 2001, Pb diffusion in zircon: Chemical Geology, v. 172, p. 5–24.

Coward, M. P., and Butler, R. W. H., 1985, Thrust tectonics and the deep structure of the Pakistan Himalaya: Geology, v. 13, p. 417 – 420.

Dahl, P.S., 1997, A crystal-chemical basis for Pb retention and fission-track annealing systematics in U-bearing minerals, with implications for geochronology: Earth and Planetary Science Letters, v. 150, p. 277-290.

Dahlen, F.A., Suppe, J., and Davis, D., 1984, Mechanics of Fold-and-Thrust Belts and Accretionary Wedges:Cohesive Coulomb Theory: Journal of Geophysical Research, v. 89, p. 10,087-10,101.

Dahlstrom, C.D.A., 1970, Structural geology in the eastern margin of the Canadian Rocky Mountains: Bull. Can. Pet. Geol., v. 18, p. 332-406.

Davis, D., Suppe, J., and Dahlen, F.A., 1983, Mechanics of fold-and-thrust belts and accretionary wedges: Journal of Geophysical Research, v. 88, p. 1153-1172.

DeCelles, P. G., and Mitra, G., 1995, History of the Sevier orogenic wedge in terms of critical taper models, northeast Utah and southwest Wyoming: GSA Bulletin, v. 107, p. 454-462.

DeCelles, P. G., Gehrels, G. E., Quade, J., LaReau, B., and Spurlin, M., 2000, Tectonic implications of U-Pb zircon ages of the Himalayan orogenic belt in Nepal, Science, 288, 497 – 499.

DeCelles, P.G., Robinson, D.M., Quade, J., Ojha, T.P., Garzione, C.N., Copeland, P., and Upreti, B.N., 2001, Stratigraphy, structure, and tectonic evolution of the Himalayan fold-thrust belt in western Nepal: Tectonics, v. 20, p. 487-509.

DeCelles, P.G., Robinson, D.M., and Zandt, G., 2002, Implications of shortening in the Himalayan fold-thrust belt for uplift of the Tibetan Plateau: Tectonics, v. 21, p. 1062–1087, doi: 10.1029/2001TC001322.

DeCelles, P.G., Gehrels, G.E., Najman, Y., Martin, A.J., Carter, A., and Garzanti, E., 2004, Detrital geochronology and geochemistry of Cretaceous–Early Miocene strata of Nepal: implications for timing and diachroneity of initial Himalayan orogenesis: Earth and Planetary Science Letters, v. 227, p. 313-330.

DeCelles, P. G., Gehrels, G. E., Quade, J., Kapp, P. A., Ojha, T. P., and Upreti, B. N., 1998, Neogene foreland basin deposits, erosional unroofing, and the kinematic history of the Himalayan fold-thrust belt, western Nepal: Geol. Soc. Am. Bull., v. 110, p. 2 – 21.

Derry, L.A., Kaufman, A.J., and Jacobsen, S.B., 1992, Sedimentary cycling and environmental change in the Late Proterozoic: evidence from stable and radiogenic isotopes. Geochim. Cosmochim. Acta, v. 59, p. 1317–1329.

Des Marais, D.J., 1997, Isotopic evolution of the biogeochemical carbon cycle during the Proterozoic eon: Organic Chemistry, v. 27, p. 185-193.

Divakara Rao, V., Gupta, H.K., Gupta, S.B., Mall, D.M., Mishra, D.C., Murty, P.R.K., Narayana, B.L., Reddy, P.R., and Tewari, H.C., 1998. Geotransect in the Central Indian shield, across Narmada–Son Lineament and the Central Indian Suture: Int. Geol. Rev., v. 40, p. 1021–1037.

Dodson M. H., Compston W., Williams I. S., and Wilson J. F., 1988, A search for ancient detrital zircons in Zimbabwean sediments: Journal of the Geological Society of London, v. 145, p. 977-983.

Dziggel, A., Armstrong, R.A., Stevens, G., and Nasdala, L., 2005, Growth of zircon and titanite during metamorphism in the granitoid-gneiss terrane south of the Barberton greenstone belt, South Africa: Mineralogical Magazine, v. 69, p. 1019-1036.

Elliott, D., 1976a, The motion of thrust sheets: Journal of Geophysical Research, v. 81, p. 949-963.

Elliott, D., 1976b, The energy balance and deformation mechanisms of thrust sheets: Philosophical Transactions of the Royal Society of London, v. 283, p. 289-312.

Emiliani, C., 1955, Pleistocene temperatures: Journal of Geology, v. 63, p. 538-578.

Farquhar, G.D., Ehleringer, J.R., and Hubick, K.T., 1989, Carbon isotope discrimination and photosynthesis: Annual Rev. Plant Physiol Plant Mol Biol, v. 40, p. 503-537.

Fedo, C.M., Sircombe, K.N., and Rainbird, R.H., 2003, Detrital Zircon Analysis of the Sedimentary Record *in* Hanchar, J.M. and Hoskin, P.W.O., eds., Zircon: Reviews in Mineralogy and Geochemistry, v. 53, p. 277-303.

Finch, R.J. and Hanchar, J.M., 2003, Structure and Chemistry of Zircon and Zircon-Group Minerals *in* Hanchar, J.M. and Hoskin, P.W.O., eds., Zircon: Reviews in Mineralogy and Geochemistry, v. 53, p. 1-25.

Fiorentini, G., Lissia, M., and Mantovani, F., 2007, Geo-neutrinos and earth's interior: Physics Reports, v. 453, p. 117 – 172.

Gansser, A., 1964, Geology of the Himalayas: London, Wiley Interscience, 289 p.

Gehrels, G.E., Valencia, V.A., and Pullen, A., 2006, Detrital zircon geochronology by Laser-Ablation Multicollector ICPMS at the Arizona LaserChron Center, *in* Geochronology: Emerging Opportunities, Paper 12, ed. T. Loszewski and W. Huff, p. 67-76, Paleo. Soc., Washington, D.C.

Gehrels, G.E., Valencia, V.A., and Ruiz, J., 2008, Enhanced precision accuracy, efficiency, and spatial resolution of U-Pb ages by laser ablation-multicollector-inductively coupled plasma-mass spectrometry: Geochemistry Geophysics Geosystems, v. 9, p.1-13; doi:10.1029/2007GC001805.

Goff, D.F., and Wiltschko, D.V., 1992, Stresses beneath a ramping thrust sheet: Journal of Structural Geology, v. 14, p. 437-449.

Guillot, S., Garzanti, E., Baratoux, D., Marquer, D., Maheo, G., and de Sigoyer, J., 2003, Reconstructing the total shortening history of the NW Himalaya: Geochemistry, Geophysics, Geosystems, v. 4, p. 1-22.

Hanchar, J.M. and Miller, CF., 1993, Zircon zonation patterns as revealed by cathodoluminescence and back-scattered electron images: Implications for interpretation of complex crustal histories: Chemical Geology, v. 110, p. l-13.

Hanchar, J.M. and Rudnick, R.L., 1995, Revealing hidden structures: The application of cathodoluminescence and back-scattered electron imaging to dating zircons from lower crustal xenoliths: Lithos, v. 36, p. 289-303.

Hauck, M. L., Nelson, K. D., Brown, L. D., Zhao, W., and Ross, A. R., 1998, Crustal structure of the Himalayan orogen at ~90° east longitude from Project INDEPTH deep reflection profiles: Tectonics, v. 17, p. 481–500.

Hawkins, D.P., and Bowring, S.A., 1997, U-Pb systematics of monazite and xenotime: Case studies from the Paleoproterozoic of the Grand Canyon, Arizona: Contributions to Mineralogy and Petrology, v. 127, p. 87–103.

Hayes, J.M., 1983, Practice and Principles of Isotopic Measurements in Organic Geochemistry *in* Meinschein, W.G., ed., Organic Geochemistry of Contemporaneous and Ancient Sediments: Great Lakes Section, Society of Economic Paleontologists and Mineralogists, p. 5.1-5.31.

Hayes, J.M., 1983, Geochemical evidence bearing on the origin of aerobiosis, a speculative hypothesis *in* Schopf, J.W., ed., Earth's Earliest Biosphere: It's Origin and Evolution: Princeton, Princeton University Press, p.291-301.

Heim, A., and Gansser, A., 1939, Central Himalaya: Geological observations of the Swiss expedition 1936: Memoirs of the Swiss Society of Natural Sciences, v. 73, 245 p.

Hodges, K.V., 2000, Overview: Tectonics of the Himalaya and southern Tibet from two perspectives:

GSA Bulletin, v. 112, p. 324-350.

Hodges, K.V., Parrish, R.R., and Searle, M.P., 1996, Tectonic evolution of the central Annapurna Range, Nepalese Himalayas: Tectonics, v. 15, p. 1264-1291.

Hoefs, J., 2004, Stable Isotope Geochemistry, 5th edition, Springer-Verlag Berlin Heidelberg New York, 244 p.

Hole, M.J., 1998, Stratigraphical Applications of Radiogenic Isotope Geochemistry in Doyle, P. and Bennett, M.R., eds., Unlocking the Stratigraphical Record: John Wiley and Sons Ltd, UK, 532 p.

Horton, B.K., 1999, Erosional control on the geometry and kinematics of thrust belt development in the central Andes: Tectonics, v. 18, p. 1292-1304.

Hoskin, P.W.O., and Schaltegger, U., 2003, The composition of zircon and igneous and metamorphic petrogenesis *in* Hanchar, J.M. and Hoskin, P.W.O., eds., Zircon: Reviews in Mineralogy and Geochemistry, v. 53, p.27-62.

Hudson, J.D., 1977, Stable isotopes and limestone lithification: Journal of the Geological Society of London, v. 133, p. 637–660.

Jacobsen, S.B., and Kaufman, A.J., 1999, The Sr, C and O isotopic evolution of Neoproterozoic seawater: Chemical Geology, v. 161, p. 37-57.

Jamieson, R.A., Beaumont, C., Medvedev, S., and Nguyen, M.H., 2004, Crustal channel flows: 2. Numerical models with implications for metamorphism in the Himalayan-Tibetan orogen: Journal of Geophysical Research, v. 109, B06407.

Kah, L.C., Sherman, A.G., Narbonne, G.M., Knoll, A.H., and Kaufman, A.J., 1999, $\delta^{13}C$ stratigraphy of the Proterozoic Bylot Supergroup, Baffin Island, Canada: implications for regional lithostratigraphic correlations: Can. J. Earth Sci. v. 36, p. 313–332.

Karhu, J.A., and Holland, H.D., 1996, Carbon isotopes and the rise of atmospheric oxygen: Geology, v. 24, p. 867–870.

Kaufman, A.J., and Knoll, A.H. 1995, Neoproterozoic variations in the carbon isotopic composition of seawater: stratigraphic and biogeochemical implications: Precambrian Research, v. 73: p. 27–49.

Kaufman, A.J., Knoll, A.H., Narbonne, G.M., 1997. Isotopes, ice ages, and terminal Proterozoic Earth history: Proc. Natl. Acad. Sci., v. 94, p. 6600–6605.

Kaufman, A.J., Corsetti, F.A., and Varni, M.A., 2007, The effect of rising atmospheric oxygen on carbon and sulfur isotope anomalies in the Neoproterozoic Johnnie Formation, Death Valley, USA: Chemical Geology, v. 237, p. 47–63

Kaufman, A.J., Hayes, J. M., Knoll, A. H., and Germs, G. J. B., 1991, Isotopic compositions of carbonates and organic carbon from upper Proterozoic successions in Namibia; stratigraphic variation and the effects of diagenesis and metamorphism: Precambrian Research, v. 49: p. 301-327.

Kaufman, A.J., Jiang, G., Christie-Blick, N., Banerjee, D.M., and Rai, V., 2006, Stable isotope record of the Neoproterozoic Krol platform in the Lesser Himalayas of northern India: Precambrian Research, v. 147, p. 156-185.

Knoll, A.H., Kaufman, A.J., and Semikhatov, M.A., 1995, The carbon-isotopic composition of Proterozoic carbonates: Riphean successions from northwestern Siberia (Anabar Massif, Turukhansk Uplift): American Journal of Science, v. 295, p. 823-850.

Kohn, M.J., 2008, P-T-t data from central Nepal support critical taper and repudiate large-scale channel flow of the Greater Himalayan Sequence: GSA Bulletin, v. 120, p. 259-273.

Kohn, M.J., and Valley, J.W., 1994, Oxygen isotope constraints on metamorphic fluid flow, Townshend Dam, Vermont USA: Geochim Cosmochim Acta, v. 58, p. 5551-5566.

Kumar, B., Das Sharma, S., Sreenivas, B., Dayal, A.M., Rao, M.N., Dubey, N., and Chawla, B.R., 2002, Carbon, oxygen and strontium isotope geochemistry of Proterozoic carbonate rocks of the Vindhyan Basin, central India: Precambrian Research, v. 113, p. 43-63.

Larson, L.H., and Poldervaart, A., 1957, Measurement and distribution of zircons in some granitic rocks of magmatic origin: Mineral Mag, v. 31, p. 544-564.

Larson, K.M., Burgmann, R., Bilham, R., and Freymueller, J.T., 1999, Kinematics of the India-Eurasia collision zone from GPS measurements: Journal of Geophysical Research, v. 104, p. 1077–1093, doi: 10.1029/1998JB900043.

Lavé, J., and Avouac, J.-P., 2000, Active folding of fluvial terraces across the Siwaliks Hills, Himalayas of central Nepal: Journal of Geophysical Research, v. 105, p. 5735–5770, doi: 10.1029/1999JB900292.

Lee, J.K.W., Williams, I.S., and Ellis, D.J., 1997, Pb, U and Th diffusion in natural zircon: Nature, v. 390, p. 159–162.

Leech, M.L., Singh, S., and Jain, A.K., 2007, Continuous Metamorphic Zircon Growth and Interpretation of U-Pb SHRIMP Dating: An Example from the Western Himalaya: International Geology Review, v. 49, p. 313-328.

Leech, M.L., Singh, S., Jain, A.K., Klemperer, S.L., and Manickavasagam, R.M., 2005, The onset of India–Asia continental collision: Early, steep subduction required by the timing of UHP metamorphism in the western Himalaya: Earth and Planetary Science Letters, v. 234, p. 83– 97.

Leelanandam, C., Burke, K., Ashwal, L.D., and Webb, S.J., 2006, Proterozoic mountain building in Peninsular India: an analysis based primarily on alkaline rock distribution: Geol. Mag., v. 143, p. 195–212.

Lillie, R.J., Johnson, G.D., Yousuf, M., Zamin, A.S.H., and Yeats, R.S., 1987, Structural development within the Himalayan foreland fold-and-thrust belt of Pakistan, *in* Beaumont, C., and Tankard, A.J., eds., Sedimentary basins and basin forming mechanisms: Memoirs of the Canadian Society of Petroleum Geology, v. 12, p. 379–392.

Lindsay, J. F., and Brasier, M.D., 2002, Did global tectonics drive early biosphere evolution? Carbon isotope record from 2.6 to 1.9 Ga carbonates of Western Australian basins: Precambrian Research, v. 114, p. 1–34.

Link, P.K., and Fanning, C.M., 2003, Detrital zircon ages from from the Yellowjacket, Apple Creek, and Gunsight Formations, Blackbird Mining District, Salmon River Mountains, central Idaho: Northwest Geology, v. 32, p. 206-207.

Link, P.K., Fanning, C.M., and Beranek, L.P., 2005, Reliability and longitudinal change of detrital-zircon age spectra in the Snake River system, Idaho and Wyoming: An example of reproducing the bumpy barcode: Sedimentary Geology, v. 182, p. 101-142.

Lyon-Caen, H., and Molnar, P., 1985, Gravity anomalies, flexure of the Indian plate, and the structure, support and evolution of the Himalaya and Ganga Basin: Tectonics, v. 4, p. 513–538.

Mall, D.M., Reddy, P.R., and Mooney, W.D., 2008, Collision tectonics of the Central Indian Suture zone as inferred from a deep seismic sounding study: Tectonophysics, v. 460, p.116–123.

Makel, G., and Walters, J., 1993, Finite-element analysis of thrust tectonics - Computer simulation of detachment phase and development of thrust faults: Tectonophysics, v. 226, p. 167-185.

Martin, A.J., 2005, Tectonics of the Southern Annapurna Range, Central Nepal Himalaya [Ph.D. dissert.]: Tucson, University of Arizona.

Martin, A.J., DeCelles, P.G., Gehrels, G.E., Patchett, P.J., and Isachsen, C., 2005, Isotopic and structural constraints on the location of the Main Central thrust in the Annapurna Range, central Nepal Himalaya: GSA Bulletin, v. 117, p. 926-944.

Mattinson, J.M., Graubard, C.M., Parkinson, D.L., and McClelland, W.C., 1996, U-Pb reverse discordance in zircons: the role of fine-scale oscillatory zoning and sub-micron transport of Pb *in* Basu, A. and Hart S., eds., Earth Processes: Reading the Isotopic Code: Geophysical Monograph, v. 95, p. 355-376.

Menon, R., Kumar, P.S., Reddy, G.K., and Srinivasan, R., 2003, Radiogenic heat production of Late Archaean Bundelkhand granite and some Proterozoic gneisses and granitoids of central India: Current Science, v. 85, p. 634-638.

Mezger, K. and Krogstad, E.J., 1997, Interpretation of discordant U-Pb zircon ages: An evaluation: Journal of Metamorphic Geology, v. 15, p. 127-140.

Mishra, D. C., Singh, B., Tiwari, V. M., Gupta, S. B. and Rao, M. B. S. V., 2000, Two cases of continental collisions and related tectonics during the Proterozoic period in India – insights from gravity modelling constrained by seismic and magnetotelluric studies: Precambrian Research, v. 99, p. 149–169.

Moecher, D.P. and Samson, S.D., 2006, Differential zircon fertility of source terranes and natural bias in the detrital zircon record: Implications for sedimentary provenance analysis: Earth and Planetary Science Letters, v. 247, p. 252-266.

Morton A., Clauoe-Long J. C., and Berge C., 1996, SHRIMP constraints on sediment provenance and transport history in the Mesozoic Statfjord Formation, North Sea: Journal of the Geological Society of London, v. 153, p. 915–929.

Myrow, P.M., Hughes, N.C., Paulsen, T.S., William, I.S., Parcha, S.K., Thompson, K.R., Bowring, S.A., Peng, S.-C., and Ahluwalia, A.D., 2003, Integrated tectonostratigraphic analysis of the Himalaya and implications for its tectonic reconstruction: Earth and Planetary Science Letters, v. 212, p. 433-441.

Najman, Y., 2006, The detrital record of orogenesis: A review of approaches and techniques used in the Himalayan sedimentary basins: Earth-Science Reviews, v. 74, p. 1 –72.

O'Leary, M.H., 1981, Carbon isotope fractionation in plants: Phytochemistry, v. 20. p. 553-567.

Panian, J., and Wiltschko, D., 2007, Ramp initiation and spacing in a homogeneous thrust wedge: Journal of Geophysical Research, v. 112, B05417.

Pati, J.K., Patel, S.C., Pruseth, K.L., Malviya, V.P., Arima, M., Raju, S., Pati, P., and Prakash, K., 2007, Geology and geochemistry of giant quartz veins from the Bundelkhand Craton, central India and their implications: J. Earth Syst. Sci., v. 116, p. 497–510.

Patriat, P., and Achache, J., 1984, Indian-Asia collision chronology has implications for crustal shortening and driving mechanisms of plates: Nature, v. 311, p. 615–621, doi: 10.1038/311615a0.

Paudel, L. P., and Arita, K., 2000, Tectonic and polymetamorphic history of the Lesser Himalaya in central Nepal: Journal of Asian Earth Sciences, v. 18, no. 5, p. 561-584.

Pearson, O. N. and DeCelles, P.G., 2005, Structural geology and regional tectonic significance of the Ramgarh thrust, Himalayan fold-thrust belt of Nepal: Tectonics, v. 24, p. 1-26.

Pêcher, A.,1978, Deformations et metamorphisme associes a une zone de cisaillement: Exemple du grand chevauchement central Hiamalayan (MCT), 354p., D.Sc. thesis, Univ. Grenoble, France.

Pidgeon, R. T., and Wilde, S. A., 1998, The interpretation of complex zircon U-Pb systems in Archaean granitoids and gneisses from the Jack Hills, Narryer Gneiss Terrane, Western Australia: Precambrian Research, Volume 91, p. 309-332.

Powers, P.M., Lillie, R.J., and Yeates, R.S., 1998, Structure and shortening of the Kangra and Dehra Dun reentrants, Sub-Himalaya, India: Geological Society of America Bulletin, v.110, p. 1010–1027, doi:10.1130/0016-7606(1998)110<1010:SASOTK>2.3.CO;2.

Prothero, D.R. and Schwab, F., 2004, Sedimentary Geology, 2^{nd} edition, W.H. Freeman and Company, 557 p.

Ripperdan, R.L., 2001, Stratigraphic Variation in Marine Carbonate Carbon Isotope Ratios *in* Valley, J.W. and Cole, D.R., eds. Stable Isotope Geochemistry: Reviews in Mineralogy and Geochemistry, v. 43, p. 637-662.

Robinson, D.M., 2008, Forward modeling the kinematic sequence of the central Himalayan thrust belt, western Nepal: Geosphere, v. 4, p. 785-801.

Robinson, D.M., DeCelles, P.G., and Copeland, P., 2006, Tectonic evolution of the Himalayan thrust belt in western Nepal: Implications for channel flow models: GSA Bulletin, v. 118, p. 865-885.

Robinson, D.M, DeCelles, P.G., Patchett, P.J. and Garzione, C.N., 2001, The kinematic evolution of the Nepalese Himalaya interpreted from Nd isotopes: Earth and Planetary Science Letters, v. 192, p. 507-521.

Romer, R.L., 2003, Alpha-recoil in U–Pb geochronology: effective sample size matters: Contributions to Mineralogy and Petrology, v. 145, p. 481-491.

Ross, G.M., and Villenuve, M., 2003, Provenance of the Mesoproterozoic (1.45 Ga) Belt Basin (Western North America): another piece of the pre-Rodinia paleogeographic puzzle: GSA Bulletin, v. 115, p. 1191-1217.

Rowley, D.B., 1996, Age of initiation of collision between India and Asia: A review of stratigraphic data: Earth and Planetary Science Letters, v. 145, p. 1 – 13.

Rubatto, D., 2002, Zircon trace element geochemistry: partitioning with garnet and the link between U–Pb ages and metamorphism: Chemical Geology, v. 184, p. 123–138.

Schelling, D., 1992, The tectonostratigraphy and structure of the eastern Nepal Himalaya: Tectonics, v. 11, p. 925–943.

Schelling, D., and K. Arita, 1991, Thrust tectonics, crustal shortening, and the structure of the far-eastern Nepal Himalaya: Tectonics, v. 10, p. 851 – 862.

Schidlowski, M., Hayes, J.M., and Kaplan, I.R., 1983, Isotopic inferences of ancient biochemistries:

Carbon, sulfur, hydrogen, and nitrogen *in* Schopf, J.W., ed., Earth's Earliest Biosphere: It's Origin and Evolution: Princeton, Princeton University Press, p. 149-186.

Schmitz, M.D., and Bowring, S.A., 2003, Ultrahigh-temperature metamorphism in the lower crust during Neoarchean Ventersdorp rifting and magmatism, Kaapvaal Craton, southern Africa: GSA Bulletin, v.115, p. 533-548.

Sharma, K.K., 1998, Geologic and tectonic evolution of the Himalaya before and after the India-Asia collision: Proc. Indian Acad. Sci. (Earth and Planet. Sci.), v. 107, p. 265-282.

Silver, L., 1963, The relation between radioactivity and discordance in zircons: National Academy of Sciences – National Research Council Publication, v. 1075, p. 34-52.

Sircombe, K.N., and Stern, R. A., 2002, An investigation of artificial biasing in detrital zircon U-Pb geochronology due to magnetic separation in sample preparation: Geochimica et Cosmochimica Acta, v. 66, p. 2379-2397.

Srivastava, P., and Mitra, G., 1994, Thrust geometries and deep structure of the outer and lesser Himalaya, Kumaon and Garhwal (India): Implication for evolution of the Himalayan fold-and-thrust belt: Tectonics, v. 13, p. 89–109, doi: 10.1029/93TC01130.

Stacey, J. and Kramers, J., 1975, Approximation of terrestrial lead isotope evolution by a two-stage model: Earth Planet. Sci. Letters, v. 26, p. 207-221.

Strayer, L.M., Hudelston, P.J., and Lorig, L.J., 2001, A numerical model of deformation and fluid-flow in an evolving thrust wedge: Tectonophysics, v. 335, p. 121-145.

Tewari, V.C., and Sial, A.N., 2007, Neoproterozoic –Early Cambrian isotopic variation and chemostratigraphy of the Lesser Himalaya, India, Eastern Gondwana: Chemical Geology, v. 237, p.64-88.

Tucker, M.E., 1983, Sedimentation of organic-rich limestones in the late Precambrian of southern Norway: Precambrian Research, v. 22, p. 293-315.

Upreti, B.N., 1996, Stratigraphy of the western Nepal Lesser Himalaya: A synthesis: Journal of the Nepal Geological Society, v. 13, p. 11-28.

Urey, H.C., 1947, The Thermodynamic properties of isotopic substances: J Chem Soc 1947, p.562.

Valley, J.W., 1996, Stable isotope geochemistry of metamorphic rocks *in* Valley, J.W., Taylor, H.P., and O'Neil., J.R., eds., Stable isotopes in high temperature geological processes: Rev Mineral, v. 16, p. 445-489.

Vermeesch, P., 2004, How many grains are needed for a provenance study?: Earth and Planetary Science Letters, v. 224, p. 441-451.

Veizer, J., Ala, D., Azmy, K., Bruckschen, P., Buhl, Dieter, Bruhn, F., Carden, G.A.F., Diener, A., Ebneth, S., Godderis, Y., Jasper, T., Korte, C., Pawellek, F., Podlaha, O.G., and Strauss, H., 1999, $^{87}Sr/^{86}Sr$, $\delta^{13}C$ and $\delta^{18}O$ evolution of Phanerozoic seawater: Chem. Geol., v. 161, p. 59–88.

Wickham, S.M. and Peters, M.T., 1993, High $\delta^{13}C$ Neoproterozoic carbonate rocks in western North America: Geology, v. 21, p.165-168.

Xian, W. S., Sun, M., Malpas, J., Zhao, G. C., Zhou, M. F., Ye, K., Liu, J. B., and Phillips, D. L., 2004, Application of Raman Spectroscopy to Distinguish Metamorphic and Igneous Zircons: Analytical Letters, v. 37, p. 119-130.

Yamashita, K., Creaser, R.A., and Villeneuve, M.E., 2000, Integrated Nd isotopic and U^Pb detrital zircon systematics of clastic sedimentary rocks from the Slave Province, Canada: evidence for extensive crustal reworking in the early- to mid-Archean: Earth and Planetary Science Letters, v. 174, p. 283-299.

Zachos, J., Pagani, M., Sloan, L., Thomas, E., and Billups, K., 2001, Trends, rhythms, and aberrations in global climate 65 Ma to present: Science, v. 292, p. 686-693.

Zhao, G.C., 2002, SHRIMP U–Pb zircon ages of the Fuping complex: implications for late Archean to Paleoproterozoic accretion and assembly of the north China Craton: Am. J. Sci., v. 302, p. 191-226.